SBIR- 08.02-8591
release date- 5/16/88 ✓

FINAL REPORT

SBIR 83-1 PHASE II

millitech®

Millimeter and Submillimeter Components, Instruments, Subsystems

FINAL REPORT

SBIR 83-1 PHASE II

Presented to: P.M. Tackney
Chief, Procurement Branch
M/S 180-805
NASA Resident Office -- JPL
Jet Propulsion Laboratory
4800 Oak Grove Drive
Pasadena, CA 91109

Contract: NAS7-933

Presented by: G.R. Huguenin
Millitech Corporation
South Deerfield Research Park
Post Office Box 109
South Deerfield, MA 01373

Millitech Job A125

January 14, 1987

ORIGINAL PAGE
BLACK AND WHITE PHOTOGRAPH

A125 Final Report

Table of Contents

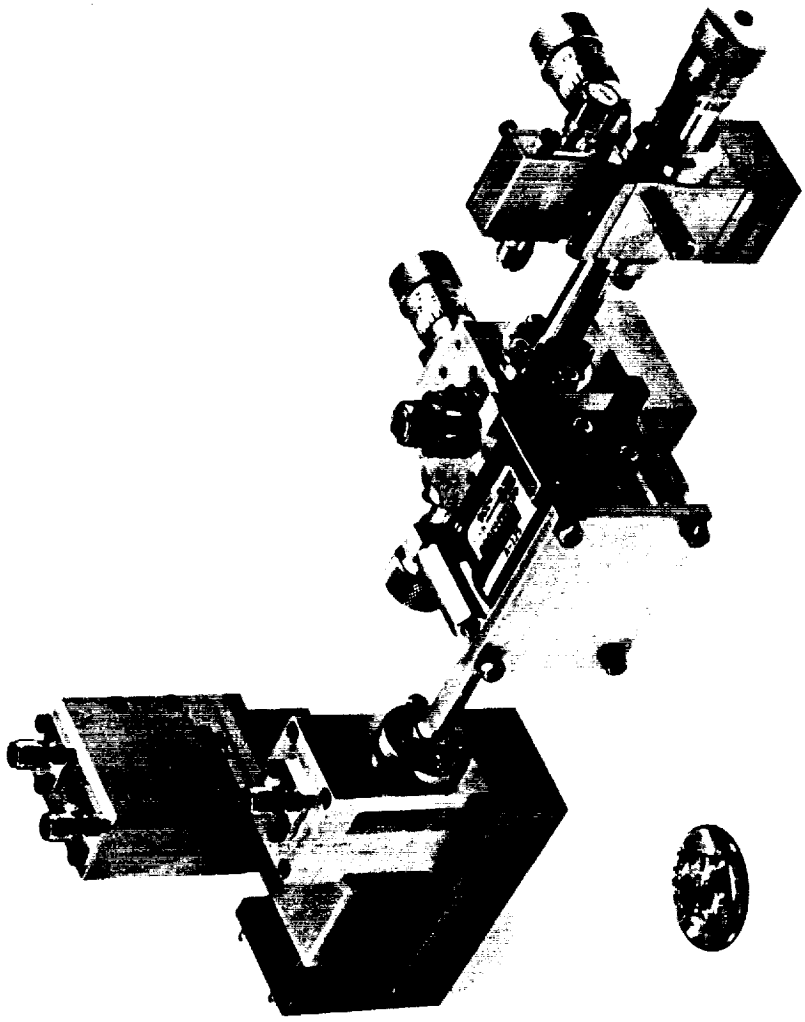

PROJECT SUMMARY

The purpose of this research was to develop a reliable submillimeter wave spectrometer for space-borne high frequency spectral line work. The emphasis was on improving the efficiency of frequency multipliers to limit the system components to rugged, low power consumption solid-state devices. This research has allowed Millitech to develop increased efficiency and performance in Millitech's existing line of submillimeter components and systems.

Millitech has fabricated and tested a complete solid-state spectrometer front end for use at 560 GHz (the 1_{10} to 1_{01} transition of water vapor). The spectrometer was designed with the rigors of flight conditions in mind. The spectrometer uses a phase-locked, solid-state Gunn diode oscillator as the local oscillator, employing a tripler to produce about 3 mW of power at 285 GHz, and a low noise second harmonic waveguide mixer which requires <2 mW of LO power. The LO (and the signal) is injected into the mixer by means of a quasioptical diplexer. The measured system noise temperature is 2800 K (DSB) over 400 MHz. The whole spectrometer front end is compact (21 cm by 21 cm by 24 cm), light (7.4 kg), and has a power consumption of <8 W. Other topics explored in this work include compact frequency agile phase lock loops, optical filters, and InP Gunn oscillators for low noise applications.

As a result of this research, the improvement in the design of multipliers and harmonic mixers will allow their use as the LO power for a variety of satellite-borne receivers operating in the 200 to 600 GHz frequency range.

1.0 SYSTEM OVERVIEW/INTRODUCTION

1.1 DEVELOPMENT OBJECTIVES

For NASA's SBIR Program Phase II, Millitech proposed to design, develop, and build a solid-state submillimeter receiver, with the inherent ability to be space qualified (see Appendix 1). Constraining the package size to a 20 cm cube and low power consumption were also considered important goals for aerospace applications.

Although no system performance specification was called out, the design was targeted at the following performance levels:

- System center frequency 557 GHz; tunability should be +10 GHz with a minimum number of adjustments. (This frequency range covers a number of interesting spectral lines including H2O 2(1,1) to 2(0,2) transition.)
- System noise temperature of <3000 K (DSB) over 500 MHz bandwidth, with increased instantaneous bandwidth (> 1 GHz) as a goal.
- All solid-state system; power consumption < 10 W.
- Mass < 5 kg.
- Compact: system to fit in 20 cm by 20 cm by 20 cm volume.
- High reliability and ruggedness: system should survive temperature, vibration, and humidity extremes characteristic of shuttle launch and space operation.

Based on previous experience from a University of Massachusetts/Lincoln Labs cooperation, a harmonic mixer approach for a frequency of 557 GHz seemed feasible. In this work a klystron LO pumped a tripler which in turn pumped a harmonic mixer for 557 GHz. The IF amplifier was a 1.4 GHz low noise FET amp, and the overall receiver noise temperature at the

best frequencies (near 560 GHz) was 3900 K DSB. Since this mixer was not optimized it seemed reasonable to expect better results with a more advanced design.

With the advent of high power diodes, an adequate output at 92.7 GHz is now quite feasible using a Gunn oscillator to replace the klystron LO. At the beginning of this work only GaAs Gunn devices were available producing 50 mW at 92.7 GHz. As work progressed, Millitech's in-house oscillator facility produced oscillators using InP diodes with even more power.

In previous work under Phase I of this contract, a study of tripler efficiency was undertaken to optimize the output power at millimeter wave frequencies. As an outgrowth of this work, a tripler pump was developed for 278 GHz with an output power which proved quite adequate for the system application.

The harmonic mixer required the most study. The mixer was developed using both computer studies of theoretical harmonic mixer noise, and model studies of actual mixer structures. An additional constraint was an IF bandwidth of 400 MHz which required use of a microwave design program to optimize the IF port impedances. The mixer that was built appears to validate the design concepts and in fact is a substantial improvement on the previous work.

1.2 RESULTS

In building the 550 GHz radiometer, Millitech has solved a major problem confronting submillimeter heterodyne systems, that of having sufficient local oscillator power supplied by a rugged solid-state device with low power requirements. Historically, carcinotrons (BWO's), lasers, or klystrons have (when available) provided the local oscillator for high frequency systems. Such sources must be supported by power/control units that are very large, exceedingly heavy, and require high voltages (~2 kV) and currents (~30 mA), which render them inappropriate for

spaceflight applications. By using a second harmonic mixer with low LO drive requirements and a multiplied Gunn oscillator source (2.5 W DC required power), the radiometer power consumption is < 8 Watts, the majority of which is required by the phase-lock loop electronics. The radiometer box is compact (21 cm by 21 cm by 24 cm) and relatively light in weight (7.4 kg), and could be made even lighter and slightly more compact if necessary.

A summary of the system test results are as follows:

System Noise Temperature Versus IF Frequency

IF Frequency (GHz)	Y (dB)	T_{SYS} (DSB °K)
1.1	0.22	4055
1.2	0.285	3091
1.3	0.29	3036
1.4	0.295	2991
1.5	0.30	2927
1.6	0.295	2991
1.7	0.29	3036
1.8	0.24	3692

For optimum system noise temperature, see Figure 3.2-4 in Section 3.2.

The system block diagram (Figure 1.1) illustrates the position of major system components detailed in the following report. In the corresponding report section, the design, development, and implementation of each subsystem and major component is described. Also included are other devices that were explored under this contract but not installed in the final radiometer.

FIGURE 1.1 -- Radiometer Block Diagram

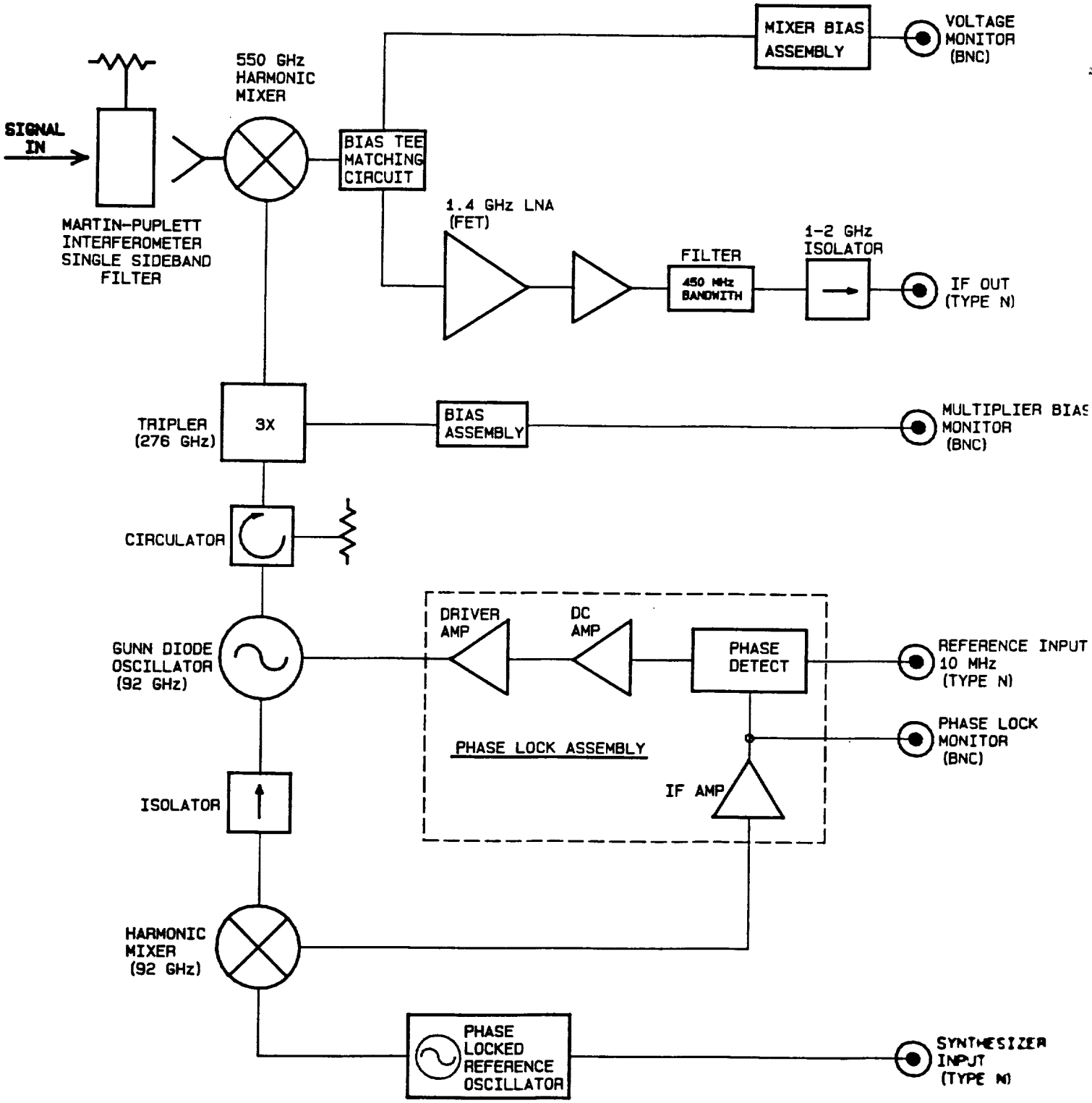

2.0 INPUT OPTICS

2.1 CONFOCAL RESONATOR FILTER

Filters play an important role in many types of microwave and millimeter wave systems. In the context of heterodyne radiometric systems, uses include:

(1) local oscillator filtering to reduce LO noise
(2) single sideband filtering to select one input sideband of a mixer
(3) diplexers to provide combined signal and local oscillator to a single-ended mixer.

At microwave frequencies, different types of filters have been developed for the various transmission media which are employed. Microstrip circuits often employ coupled line and dielectric resonator filters. Cavity filters are widely used in waveguide systems. The low loss of waveguide at wavelengths $\gtrsim$3mm results in these filters having high Q and low absorption.

At shorter millimeter frequencies, single mode waveguide has been the dominant transmission medium, but increasing loss at higher frequencies limits the performance of filter circuits. Resonant ring filters for local oscillator/signal diplexing work very well up to ~100 GHz (loss $\lesssim$0.4 dB for signal), but performance in the 120 to 170 GHz range is noticeably worse (~0.75 dB). Thus, alternatives to waveguide filters are needed. Since the transmission medium gaining increasing acceptance at short millimeter and submillimeter wavelengths is quasioptical transmission, and as filter design is relatively less developed at these high frequencies, it is appropriate to investigate new quasioptical filter designs.

Different types of quasioptical filters have been developed, most of which derive from designs previously used in guided wave media at longer wavelengths. These will be briefly considered below.

The dual beam interferometer exists in various realizations including amplitude division (Mach-Zehnder) and polarization rotating (Martin-Puplett) versions[1]. These devices are designed to have a sinusoidal response, which is produced by the difference between the paths traveled by the two parts of the beam. The minima and maxima of response can be very close to zero and unity for an optimized design, but the bandwidth is directly related to the periodicity of the response through the sinusoidal form of the transmission function. (More complex variations have been devised which partially overcome this limitation[2].) The dual beam interferometer is an exact analog of the circuit formed by connecting together two waveguide hybrid tees with two different lengths of waveguide, as shown in Figure 2.1-1.

Filters employing the concept of multiple reflections between mirrors are generally referred to as "Fabry-Perot filters" in optics and both this and the designation "multiple beam interferometer" are used for quasioptical versions of this device. Two partially reflecting surfaces are used, but many different configurations are used to overcome problems of walkoff. This problem arises when the beam is at non-normal incidence. Waveguide filters using multiple reflections are widely used; the reflections can be produced by posts or irises in the waveguide, as shown in Figure 2.1-2. Most such devices employ more than two reflections in order to adjust the response of the filter; this technique has been extended to quasioptical multiple beam interferometers but has not been widely used in practice. Some methods of changing the impedance level in quasioptical and waveguide filter sections are shown in Figure 2.1-3. Dielectric filling lowers the impedance level in all cases ((a) through (c)). Waveguide sections can change Z by varying height (d) and/or width of guide (e). Quasioptical filters can obtain $Z>Z_o$ by employing a section with thin metal plates parallel to the electric field. The impedance of this device will necessarily be relatively frequency dependent as are impedances in waveguides. This is a distinct disadvantage compared to the frequency independent impedances in quasioptical filter sections based solely on

FIGURE 2.1-1 - COMPARISON OF QUASIOPTICAL AND WAVEGUIDE DUAL BEAM INTERFEROMETERS

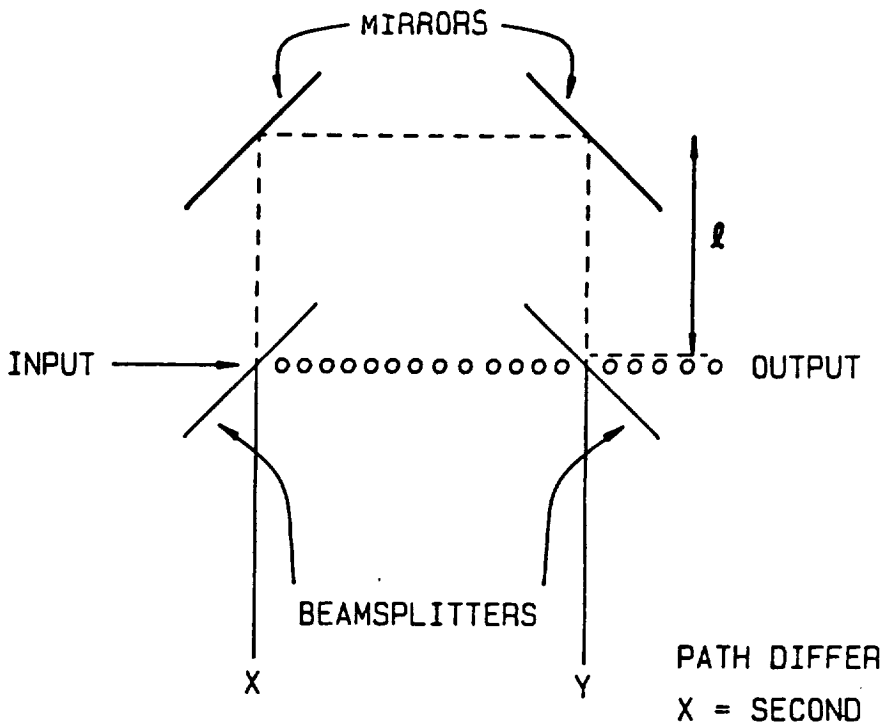

PATH DIFFERENCE = 2ℓ

X = SECOND INPUT
Y = SECOND OUTPUT

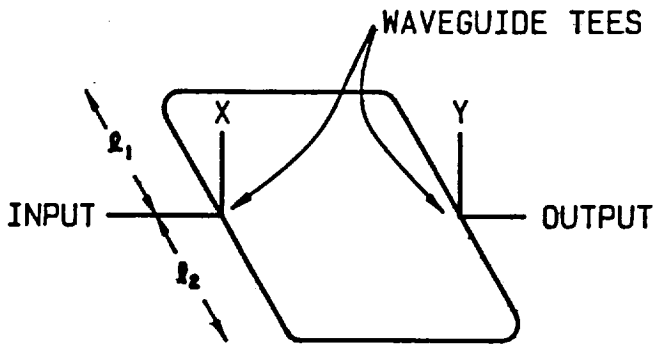

PATH DIFFERENCE = $2(\ell_2 - \ell_1)$

X = SECOND INPUT
Y = SECOND OUTPUT

FIGURE 2.1-2 - COMPARISON OF QUASIOPTICAL MULTIPLE BEAM INTERFEROMETERS AND WAVEGUIDE FILTERS

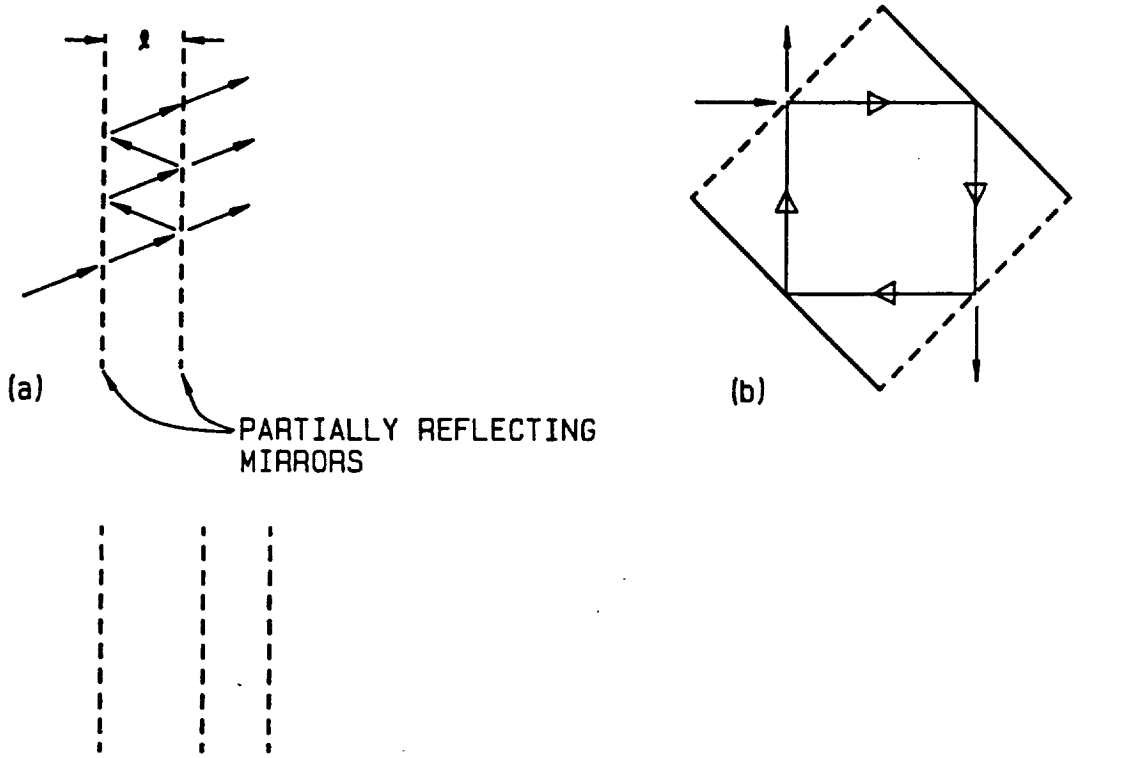

FIGURE 2.1-3 - SOME METHODS OF CHANGING IMPEDANCE LEVELS IN QUASIOPTICAL AND WAVEGUIDE FILTERS

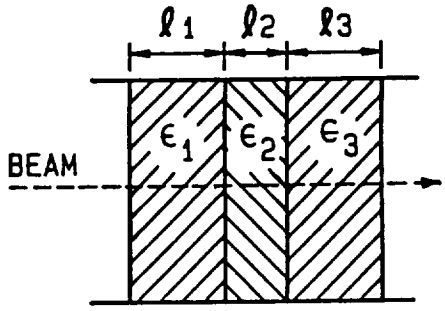

(a)

$$Z_i = \frac{Z_o}{\sqrt{\epsilon_i}}$$

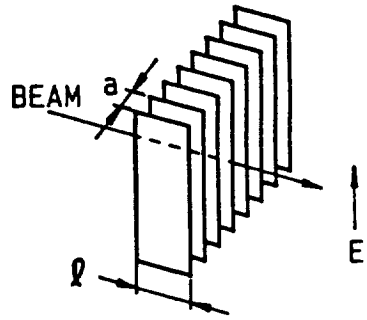

Z > Zo

(b)

QUASIOPTICAL

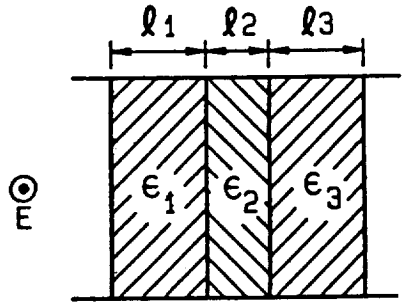

(c)

$$Z_i = \frac{Z_{go}}{\sqrt{\epsilon_i}}$$

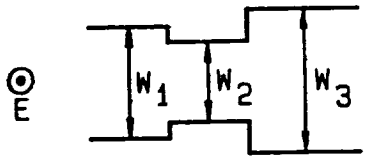

(e)

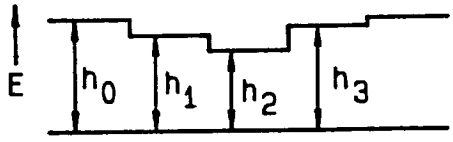

(d)

$$Z_i = Z_{go}\left(\frac{h_0}{h_i}\right)$$

WAVEGUIDE

dielectrics. However, since the latter produce only $Z<Z_o$, the filter designs using only dielectrics are necessarily somewhat restricted.

A major problem with quasioptical filters is the effect of diffraction. For a Gaussian beam, this can be expressed in terms of the growth of the beam radius away from the beam waist, where the beam radius W has its minimum value W_o. The relationship is given by

$$W = W_o \left[1 + \left(\frac{\lambda Z}{\pi W_o^2} \right)^2 \right]^{\frac{1}{2}}$$

where Z is the distance along the axis of propagation from the beam waist, and λ is the wavelength. The effect of diffraction is not simply to enlarge the beam (which could be dealt with by transformation using a lens or mirror), but since quasioptical filters employ beams which have traveled <u>different</u> distances, the degree of interference is reduced if the radii (and curvatures) of the beams are not identical. This has been analyzed for dual beam interferometers[1] and for Fabry-Perot interferometers[3]. For the latter devices, it has been found that a device filled completely with material of index of refraction n has diffraction loss approximately a factor n^4 smaller than a device with similar response characteristics but in free space[4]. This method of reducing losses due to diffraction has been used in systems at millimeter wavelengths[5]. It is, however, limited in its effectiveness by absorption loss in the dielectric material.

It has been recognized for some time that diffraction loss can also be reduced by refocusing the beam after each pass through a Fabry-Perot interferometer. Such devices are generally called resonators. Coupling energy in and out of resonators can be accomplished by small diameter irises if waveguides are the external transmission medium, but achieving proper coupling and reasonable transmission through the resonator is difficult[6]. Certain types of resonators can be effectively coupled to propagating Gaussian beams by partially reflecting mirrors[7],[8], which are illustrated in Figure 2.1-4.

FIGURE 2.1-4 - QUASIOPTICAL RESONATORS

(a) GOLDSMITH AND SCHLOSSBERG, 1980

(b) PICKETT AND CHIOU, 1983

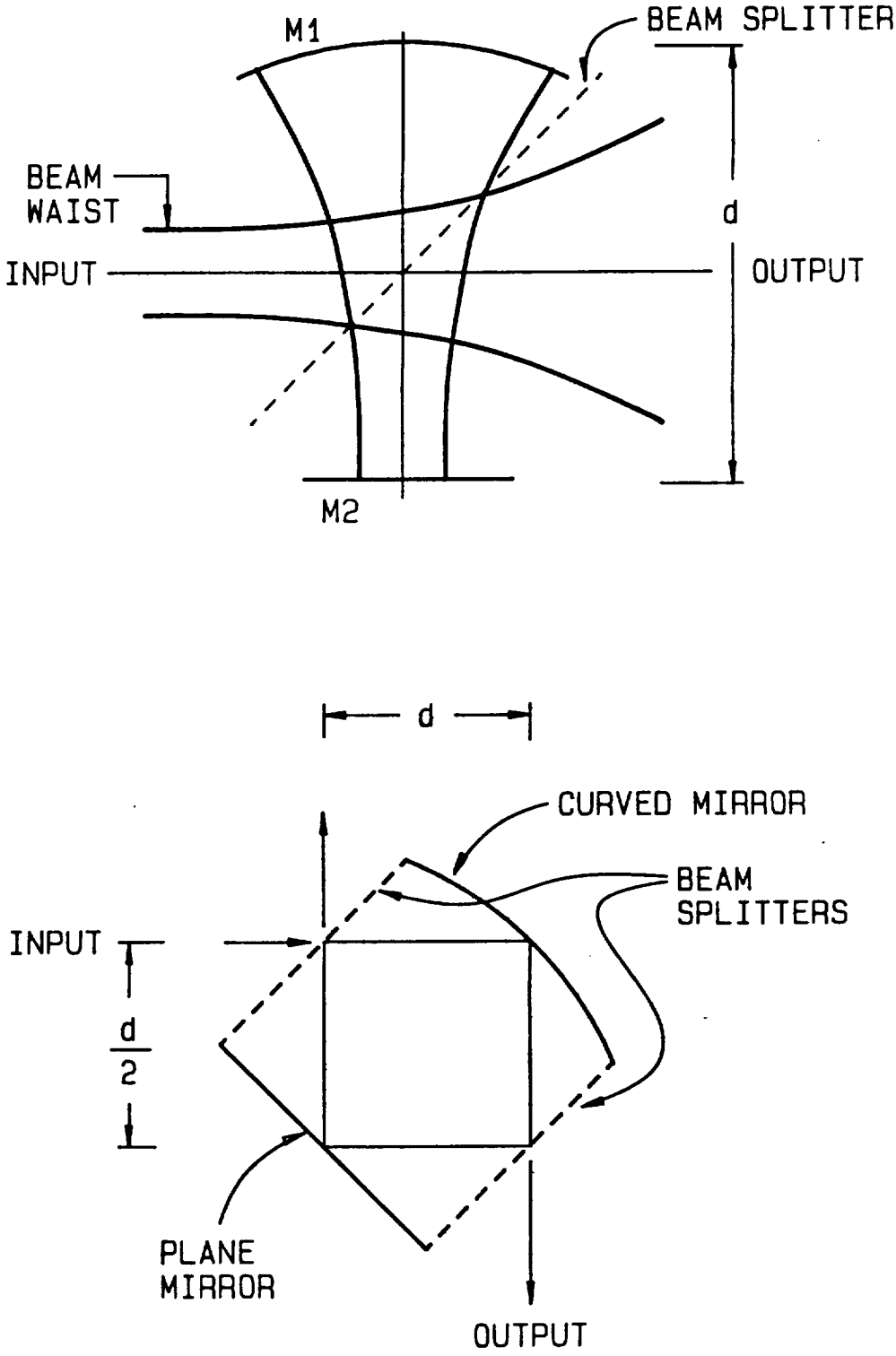

These resonators do have greatly reduced diffraction loss as expected, since the resonant wave is refocused after each pass and returns to the original mode. Ideally, the unwanted loss per pass is only due to the spillover and to absorption in mirrors. Unfortunately, there is a serious drawback to both of these designs, which is that the mirror spacing d cannot be made arbitrarily small in comparison to the mirror size, and hence with respect to the beam diameter. This means that for a reasonable level of spillover loss, the free spectral range (= spacing between resonances = c/2d) has a lower limit. This can be a serious problem if one wants to avoid spurious responses over a relatively large frequency range.

To overcome this drawback while retaining the low diffraction loss advantage of the resonator structure, we have investigated the design shown in Figure 2.1-5. The resonator is of the semi-confocal type, with one plane and one flat mirror. The radius of curvature R_M of the spherical mirror is equal to twice the mirror spacing, d = 2.46 cm. In this situation the resonant frequencies are given by

$$f = \frac{c}{2d}\left(q + \frac{5}{4}\right)$$

where q is an integer, and the beam waist radius is

$$W_o = \left(\frac{\lambda R_M}{2\pi}\right)^{\frac{1}{2}} = 0.50 \text{ cm}$$

at a wavelength of 0.32 cm. The diffraction loss per pass is given by

$$\frac{P_L}{P_{INC}} = \exp\ -2\left(\frac{D_M}{2W}\right)^2$$

where D_M is the diameter of the mirror, and W is the beam radius which is equal to W_o at the flat mirror (where the waist is located) and $W_o\sqrt{2}$ at the curved mirror.

The innovative feature of our design is that we use the two resonator mirrors themselves as the partially reflective surfaces for coupling the radiation into and out of the resonator. This is done using metal mesh,

FIGURE 2.1-5 - QUASIOPTICAL RESONATORS USING CURVED AND FLAT PARTIAL REFLECTORS

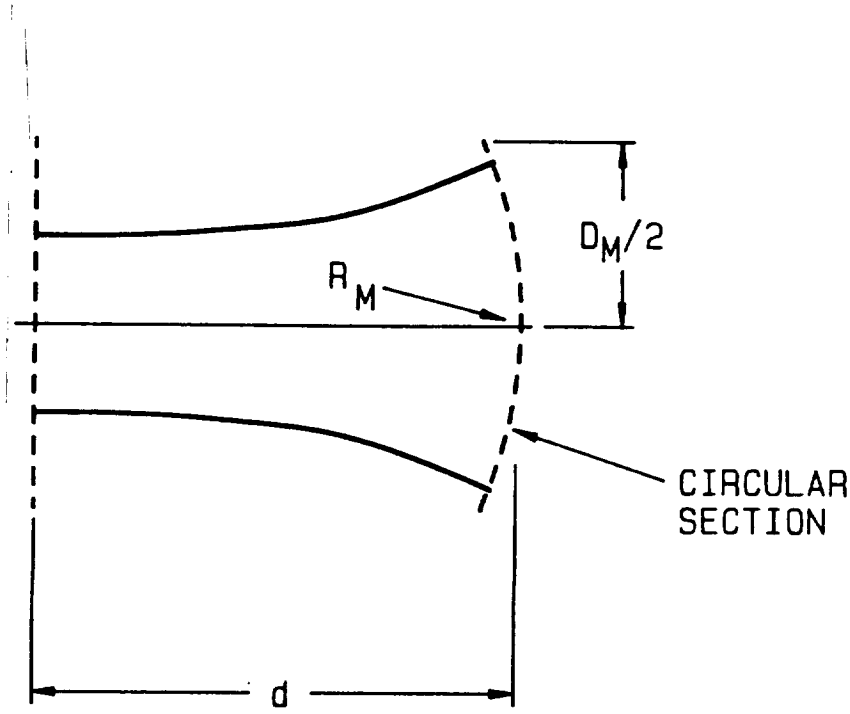

which acts as a partial reflector. The flat mirror is straightforward, but we have also found that the mesh can be glued to a curved surface and that the resulting mirror works very well. This allows us to analyze the resonator as a "normal" Fabry-Perot interferometer with essentially zero diffraction loss. We also have the option to make the plate spacing arbitrarily small (if a large free spectral range is required) and still have a mirror diameter large enough compared to the waist radius so that diffraction loss is very small.

The resonator built to verify this concept, as discussed above, was designed for operation at a wavelength of 0.32 cm. The mirror diameters are 3.75 cm so that at the curved mirror, where W = 0.707 cm, the diffraction loss is 8×10^{-7}. Thus, the response should be entirely dominated by the mirror reflectivity. For mirrors having fractional power reflection R, the resonator transmission is given by

$$|t|^2 = \frac{1}{1+H \sin^2(a)}$$

where $H = 4R/(1-R)^2$ and

a = one-half the round trip phase delay.

Resonances occur for a equal to a multiple of π, and the theoretical maximum transmission is unity. The minima occur for odd multiples of $\pi/2$ and are equal to $(1 + H)^{-1}$.

The mirrors are made by gluing rectangular copper mesh (made by Buckbee Mears Co.) onto rexolite disks; the disk thickness is chosen to be resonant at the nominal operating wavelength. The mesh had a nominal 50 lines per inch spacing, with a grid period of 0.051 cm and aperture size of 0.045 cm. Mounted on a rexolite holder, the insertion loss of a single grid is 9 dB, corresponding to R = 0.874. The theoretical value of H is then 221 and the minimum transmission 0.0045 (-23 dB).

The coupling to the resonator is effected by lenses which match the beams produced by scalar feedhorns to the size and location of the

resonator waist. The design of the system is shown in Figures 2.1-6 and 2.1-7.

Data were obtained with a BWO sweep oscillator and detector attached to the feedhorns. In Figure 2.1-8 we show a transmission curve. The minimum loss is less than a few tenths of a dB, indicating very low mirror absorption. The minimum transmission is approximately -24 dB which agrees very well with that predicted from the mirror reflectivity. The resonances are quite clean, indicating that higher order modes are not being excited. This is not always the case; as shown in Figure 2.1-9, if a small (few mm) lateral misalignment of one of the feedhorns occurs, other modes do enter, the basic response of the resonator is not appreciably changed.

We conclude that the semi-confocal resonator with only 2 mirrors, which are the coupling mirrors, has attractive features for millimeter and submillimeter applications. It can work effectively as a LO or SSB filter, and the availability of a large free-spectral range combined with low loss and compact size are valuable attributes.

REFERENCES

1. P.F. Goldsmith, "Quasi-Optical Techniques at Millimeter and Submillimeter Wavelengths," Infrared and Millimeter Waves Vol. 6, K.J. Button, ed, 277-343. New York: Academic, 1982.

2. N.R. Erickson, "A Directional Filter Diplexer Using Optical Techniques for Millimeter to Submillimeter Wavelengths," IEEE Trans. Microwave Theory Tech., MTT-25, 865-866, 1977.

3. J.A. Arnaud, A.A.M. Saleh, and J.T. Ruscio, "Walk-Off Effects in Fabry-Perot Diplexers," IEEE Trans. Microwave Theory Tech., MTT-22, 486-493, 1974.

4. P.F. Goldsmith, "Diffraction Loss in Dielectric-Filled Fabry-Perot Interferometers," IEEE Trans. Microwave Theory Tech., MTT-30, 820-823, 1982.

FIGURE 2.1-6 - SEMI-CONFOCAL RESONATOR

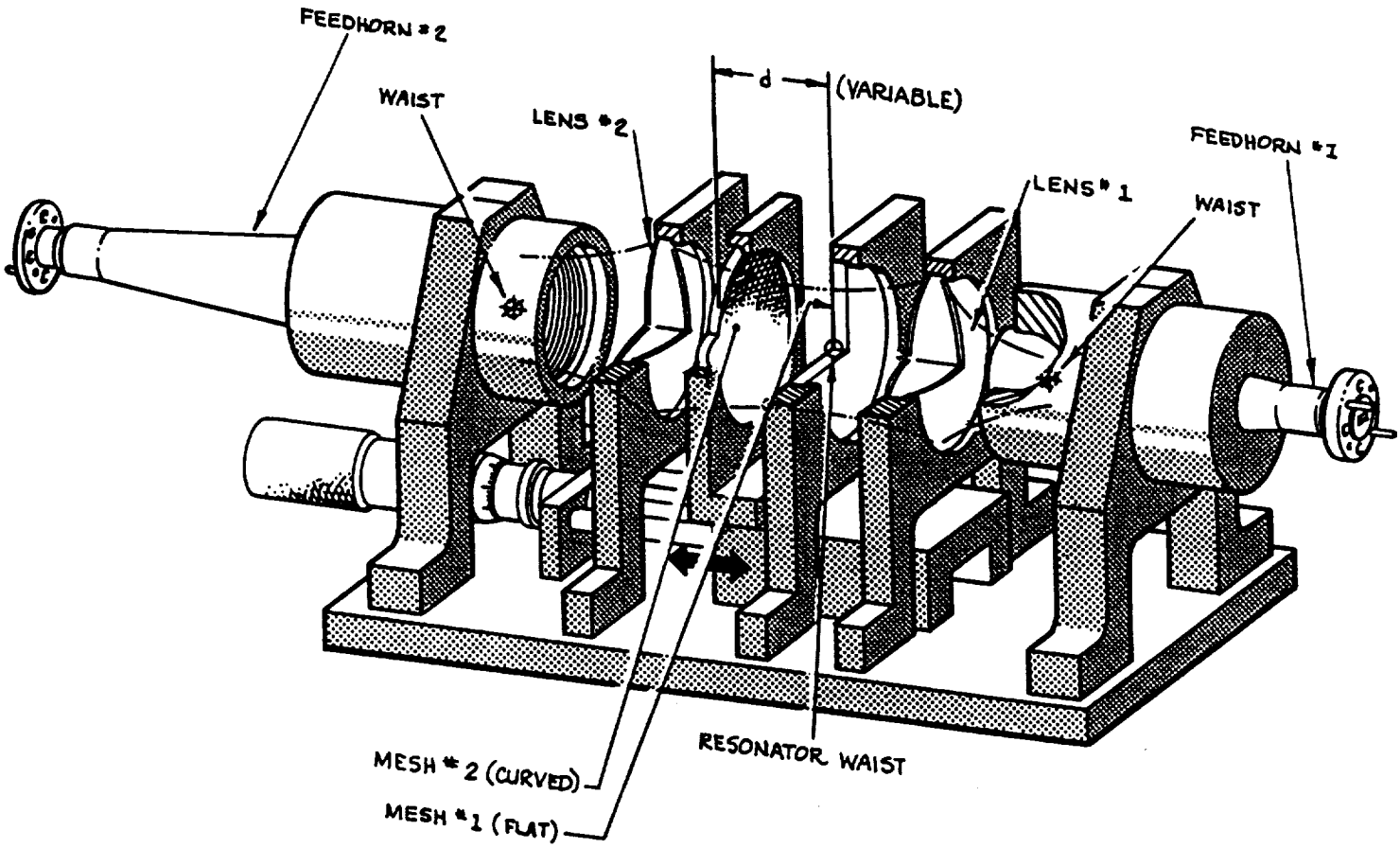

FIGURE 2.1-7 - SEMI-CONFOCAL RESONATOR

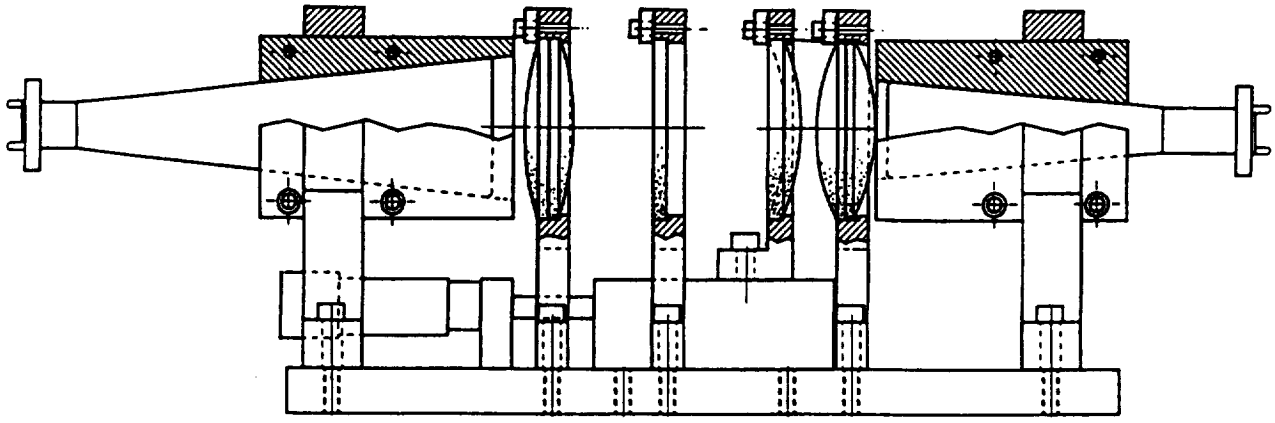

FIGURE 2.1-8

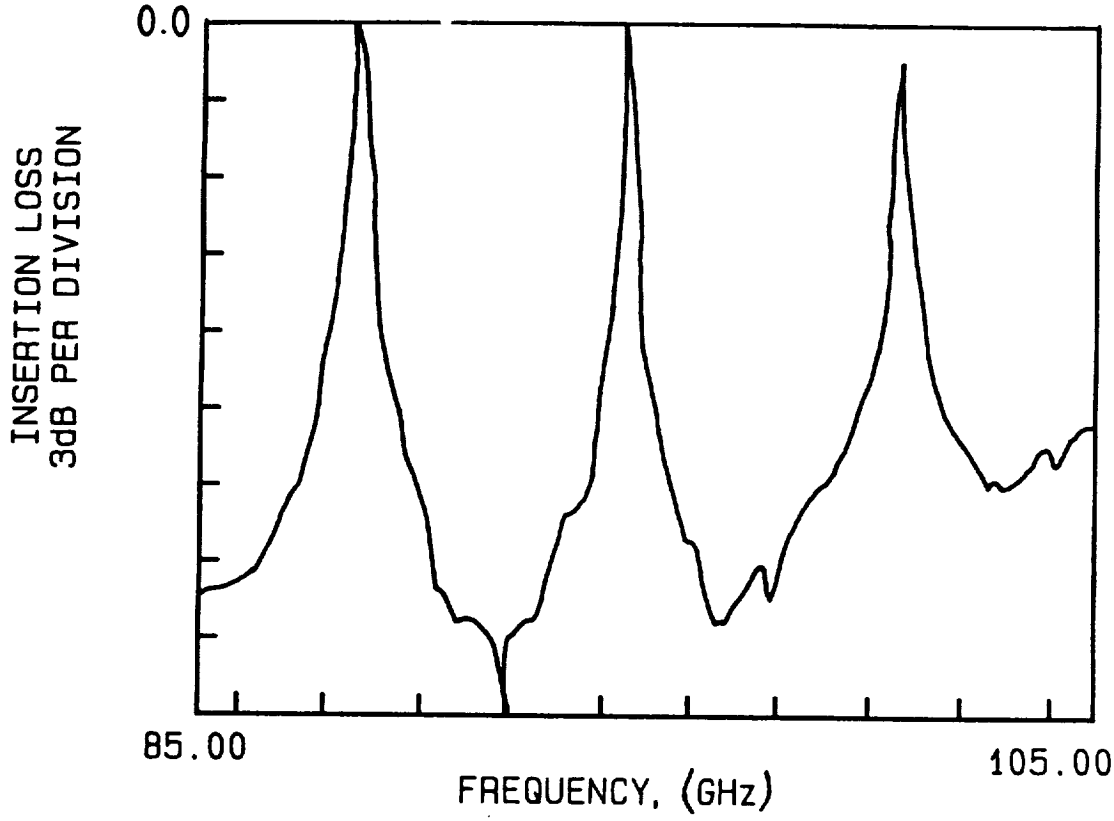

FIGURE 2.1-9

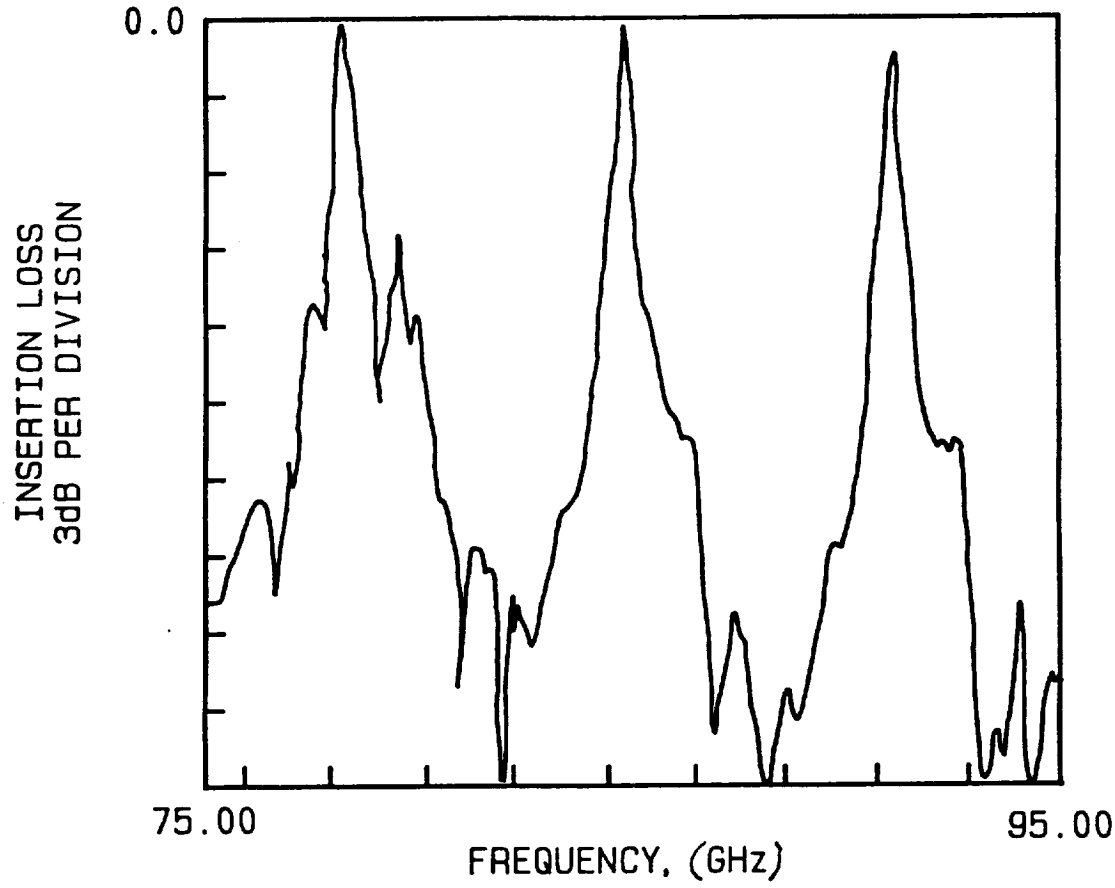

5. C.R. Predmore, N.R. Erickson, G.R. Huguenin, and P.F. Goldsmith, "A Continuous Comparison Radiometer at 97 GHz," IEEE Trans. Microwave Theory Tech., MTT-33, 44-51, 1985.

6. E.P. Valkenburg and V.E. Derr, "A High-Q Fabry-Perot Interferometer for Water Vapor Absorption Measurement in the 100 Gc/s to 300 Gc/s Frequency Range," Proc. IEEE, 54, 493-498, 1966.

7. P.F. Goldsmith and H. Schlossberg, "A Quasi-Optical Single Sideband Filter Employing a Semiconfocal Resonator," IEEE Trans. Microwave Theory Tech., MTT-28, 1136-1138, 1980.

8. H.M. Pickett and A.E.T. Chion, "Folded Fabry-Perot Quasi-Optical Ring Resonator Diplexer: Theory and Experiment," IEEE Trans. Microwave Theory Tech., MTT-31, 373-380, 1983.

2.2 SUBMILLIMETER FEEDHORNS

As discussed elsewhere in this report, waveguide mixers have various advantages for use at longer submillimeter wavelengths, in terms of control of diode embedding impedance at frequencies critical for mixer operation. In order to take advantage of these, however, radiation must be efficiently coupled in from free space. The ideal free space-to-waveguide transformer or feedhorn would have the following properties:

(1) Low loss
(2) Symmetric, highly Gaussian pattern with minimum sidelobes
(3) Polarization purity
(4) Ease and reproducibility of fabrication

These qualities cannot necessarily all be satisfied by just any type of submillimeter feedhorn. At centimeter and millimeter wavelengths, scalar or hybrid mode feedhorns satisfy the first three criteria. The question of fabrication is dictated by the requirement of the quarter

wavelength deep grooves spaced by a half wavelength or less, which form the reactive surface of this type of feedhorn. Although the grooves are responsible for the desirable properties of scalar feedhorns, the fabrication difficulties represented at submillimeter wavelengths are suffuciently great that we have been forced to utilize a feedhorn having simpler construction and greater ease of fabrication.

Among the alternatives available, we find that the dual mode feedhorn, while relatively simple to fabricate, is a narrowband device. Dielectric lined feeds are broadband, but launching the proper mode presents a major problem. Consequently, we are left with the most basic feedhorns as options - the rectangular and smooth-walled conical feedhorns. These are well-analyzed theoretically, and extensive data is available for design. The conical feedhorn appears advantageous in terms of ease of fabrication. As discussed further in Section 2.2.1 it has moderately low sidelobes and fair polarization purity. The major problem is the inherent assymetry in its radiation pattern. This can be corrected with an assymetric optical system based on Gaussian beam propagation, as discussed in Section 2.2.2.

2.2.1 Conical Feedhorns

The radiation pattern of conical feedhorns can be analyzed with reasonable accuracy by using an aperture field method. We assume that the electric field distribution in the aperture is the same TE_{11} mode as launched by a rectangular-to-circular tranformer in the throat of the horn, as shown in Figure 2.2-1. The geometry for calculating the radiation pattern is given in Figure 2.2-2. In the horn aperture of radius a, r' and ϕ' are the polar coordinates while θ and ϕ describe the position of an observation point taken to be in the far field of the horn.

The TE_{11} mode field distribution is given in terms of radial and azimuthal coordinates by:

FIGURE 2.2-1 - SMOOTH WALLED CONICAL FEEDHORN

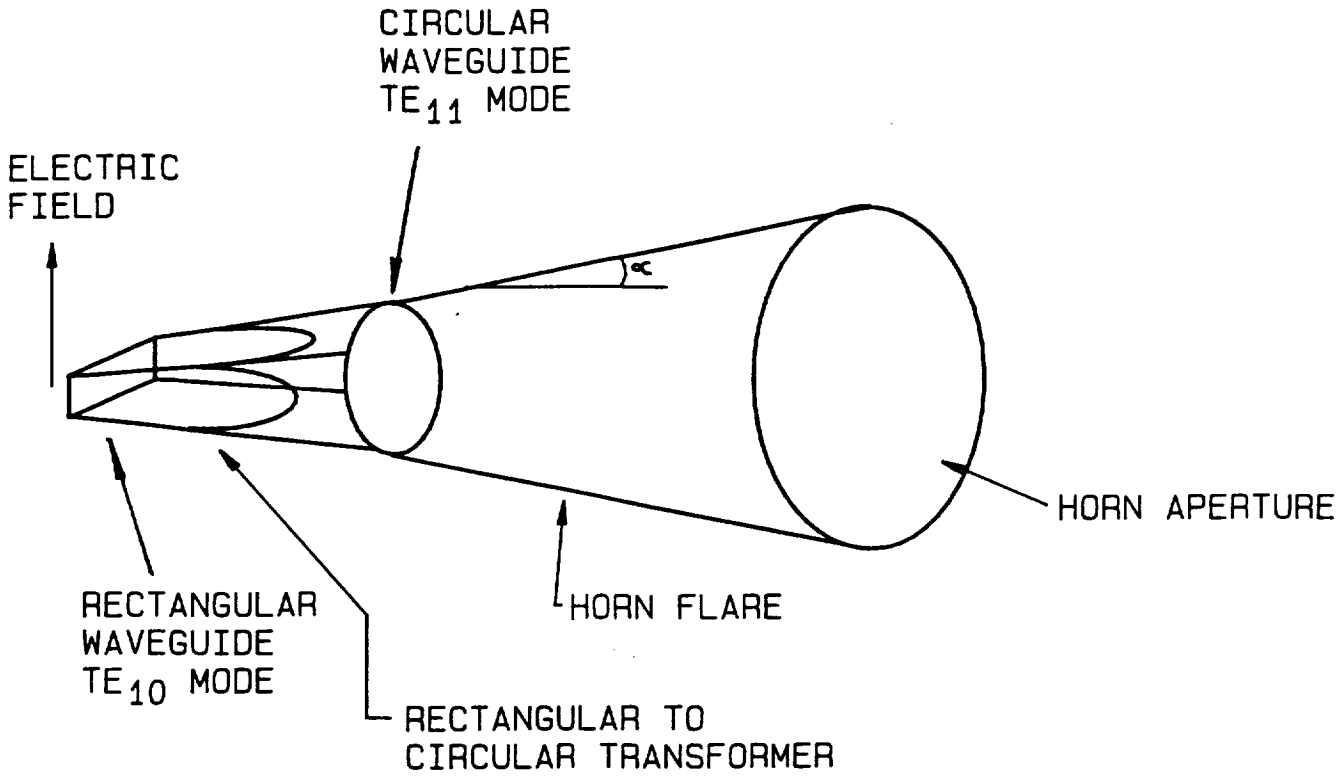

FIGURE 2.2-2 - GEOMETRY FOR CALCULATING RADIATION PATTERN OF CONICAL FEEDHORN

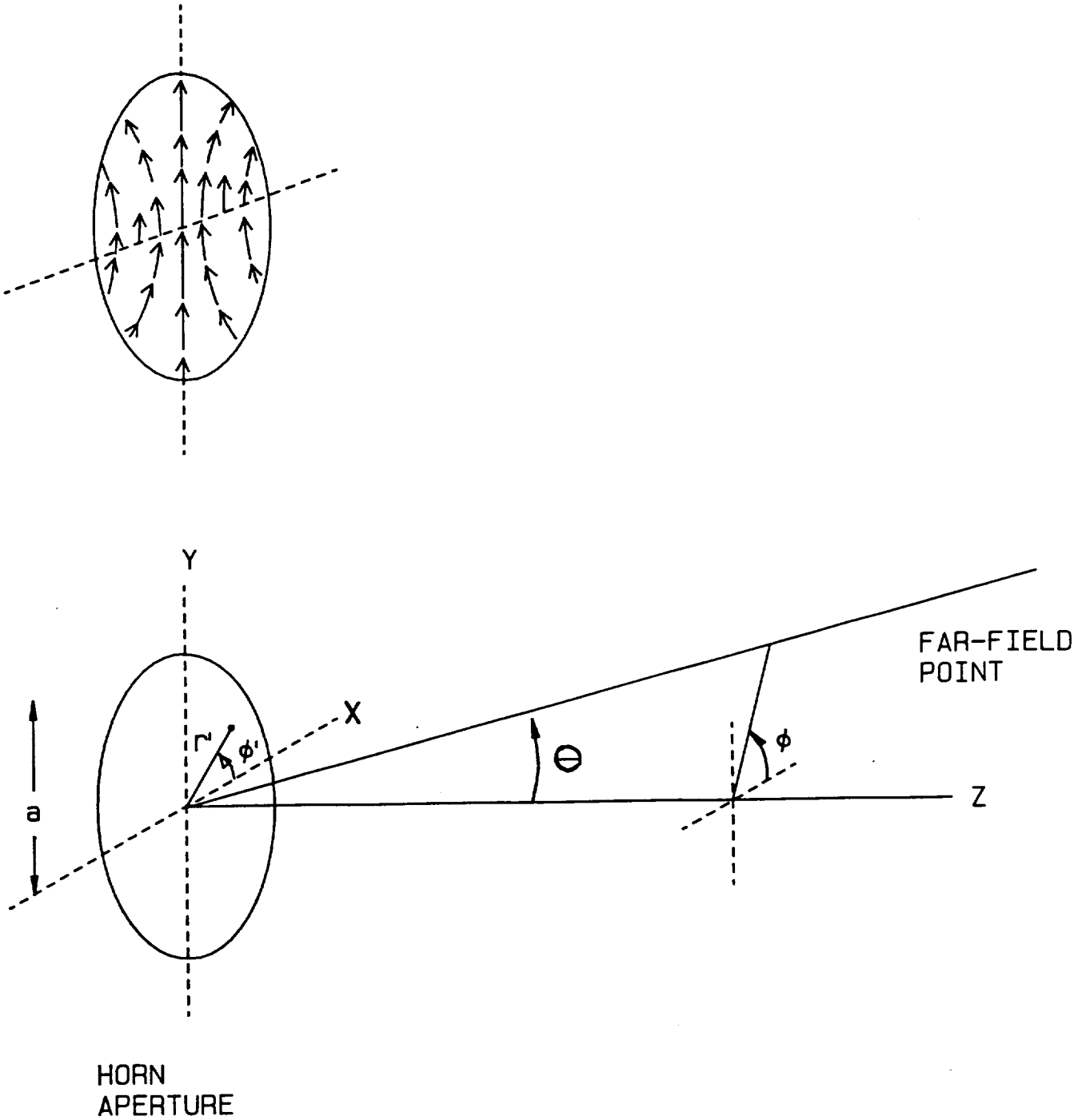

$$E_r = \frac{Aa}{1.841r'} \quad J_1\left(\frac{1.841r'}{a}\right) \quad \sin \phi'$$

$$E' = A \quad J_1'\left(\frac{1.841r'}{a}\right) \quad \cos \phi'$$

where A is a constant, J_1 and J_1' are the first order Bessel functions and derivative thereof, respectively. The first zero of J_1 is 1.841, reflecting the fact that $E_\phi' = o$ at the wall of the feedhorn which is taken to have infinite conductivity. The Cartesian components are given by

$$E_x = E_r' \cos \phi' - Eo' \sin \phi'$$
$$E_y = E_r' \sin \phi' + Eo' \cos \phi'$$

The field in the horn aperture is assumed to be given by the above, modified by a phase function obtained by assuming that the curvature of the wavefront is determined by the condition that the field lines be perpendicular to the walls in the flared section. This approximation will hold accurately only for horns of modest flare angle θ_o.

In this case the radius of curvature of the spherical wave is equal to the slant length L_s of the horn, given by

$$L_s = a/\sin \theta_o.$$

The aperture phase function is

$$\delta(r') = \frac{-\pi r'^2}{\lambda L_s} = \frac{-\pi a^2}{\lambda L_s}\left(\frac{r'}{a}\right)^2$$

We define a normalized radial aperture coordinate p given by

$$p = r'/a \qquad 0 \leq p \leq 1$$

so that the aperture phase distribution can be written

$$\delta\phi = 2\pi\Delta p^2$$

where $\Delta = a/2\lambda L_s$

is the axis-to-edge phase difference mesured in wavelengths. Thus, the aperture field components are given by

$$U_x^A(P,\phi') = A \exp(j\delta\phi)\left[\frac{J_1(1.841p)}{1.841p}\right] - J_1'(p)\cos\phi'\sin\phi'$$

$$U_y^A(P,\phi') = A \exp(j\delta\phi)\frac{J_1(1.841p)}{1.841p}\sin^2\phi' + J_1'(p)\cos\phi'$$

The far field radiation patterns are obtained using Fraunhoffer diffraction integral

$$U_{x,y}(\theta\phi) = C\int_{p=0}^{1}\int_{\phi'=o}^{\pi} pdp\sin\phi' d\phi' U_{x,y}(p,\phi')\exp[jup\cos(\phi'-\phi)]$$

where we have defined

$$u = 2\pi\ a\sin\theta/\lambda$$

as a normalized off-axis angular coordinate.

It is apparent that the conical feedhorn radiation patterns will <u>not</u> be axially symmetric. It is also clear that, due to the field distribution in the aperture, there will be a significant cross-polarized component in the radiated pattern. In Figures 2.2-3a and 2.2-3b we give the <u>calculated</u> power patterns (proportional to $|U(\theta,\phi)|^2$) for a conical feedhorn with a = 1.27 cm, L_s = 12.5 cm, for a wavelength of 0.429 cm. The phase error Δ is equal to 0.15 in this case, and the patterns are typical for small phase error horns. In Figure 2.2-4a and 2.2-4b we give the <u>measured</u> patterns for the same feedhorn. The agreement is very good. In the measured patterns the contours are spaced by 3 dB and the peak of the cross-polarization (E_x) pattern is at a level of -16 dB

FIGURE 2.2-3a

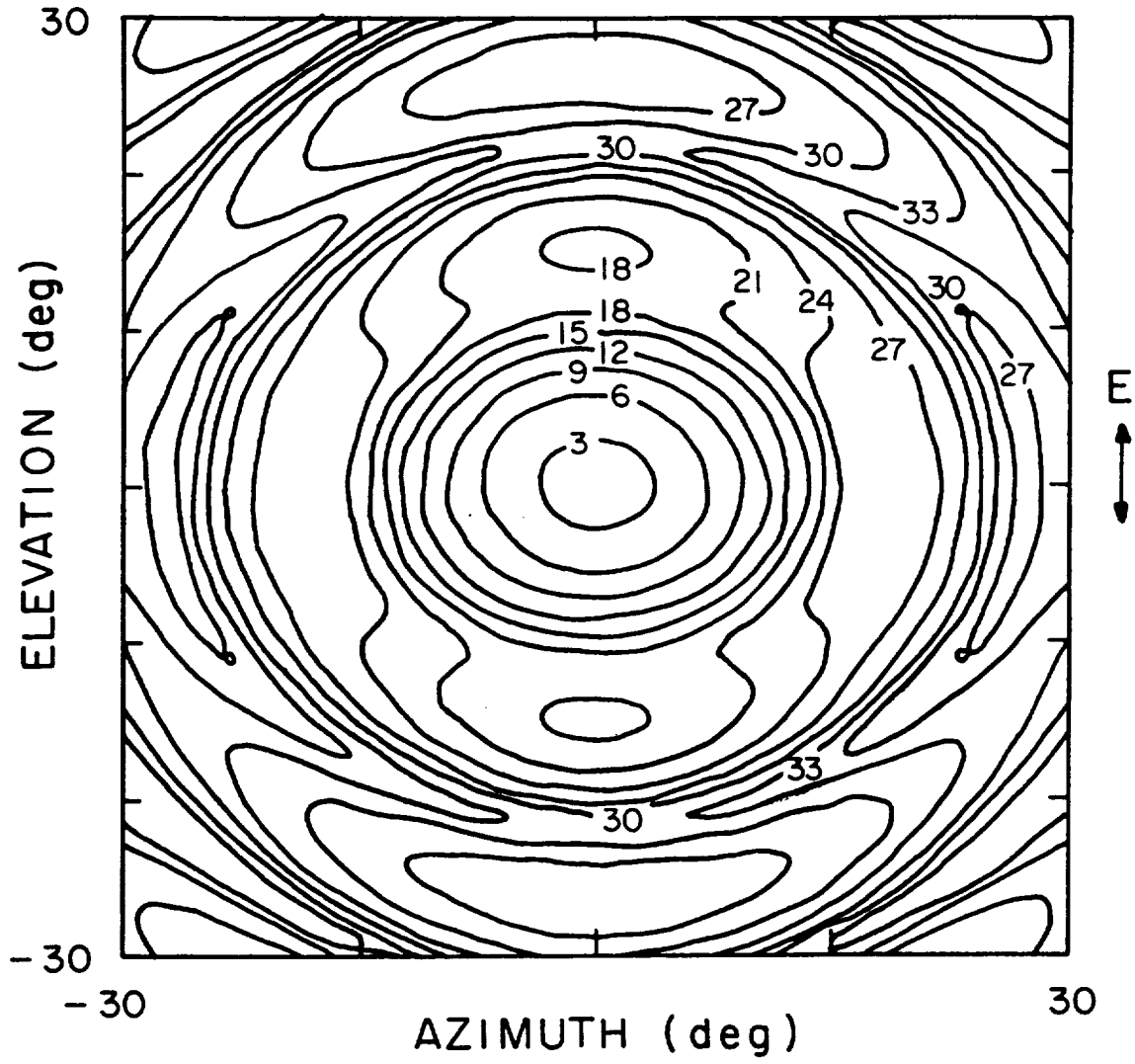

Use or disclosure of data contained on this sheet is subject to the restriction on the title page of this final report.

FIGURE 2.2-3b

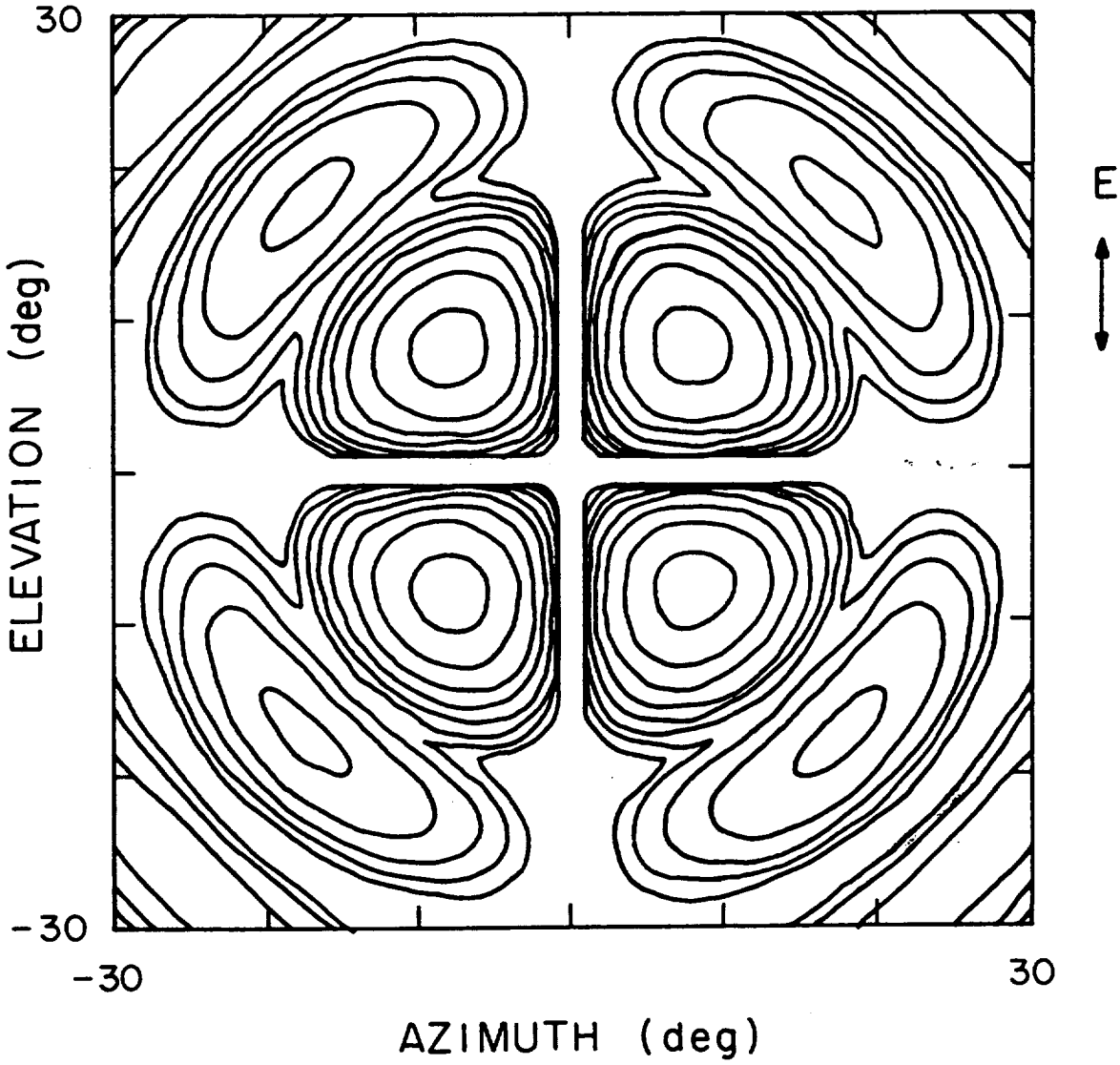

FIGURE 2.2-4a

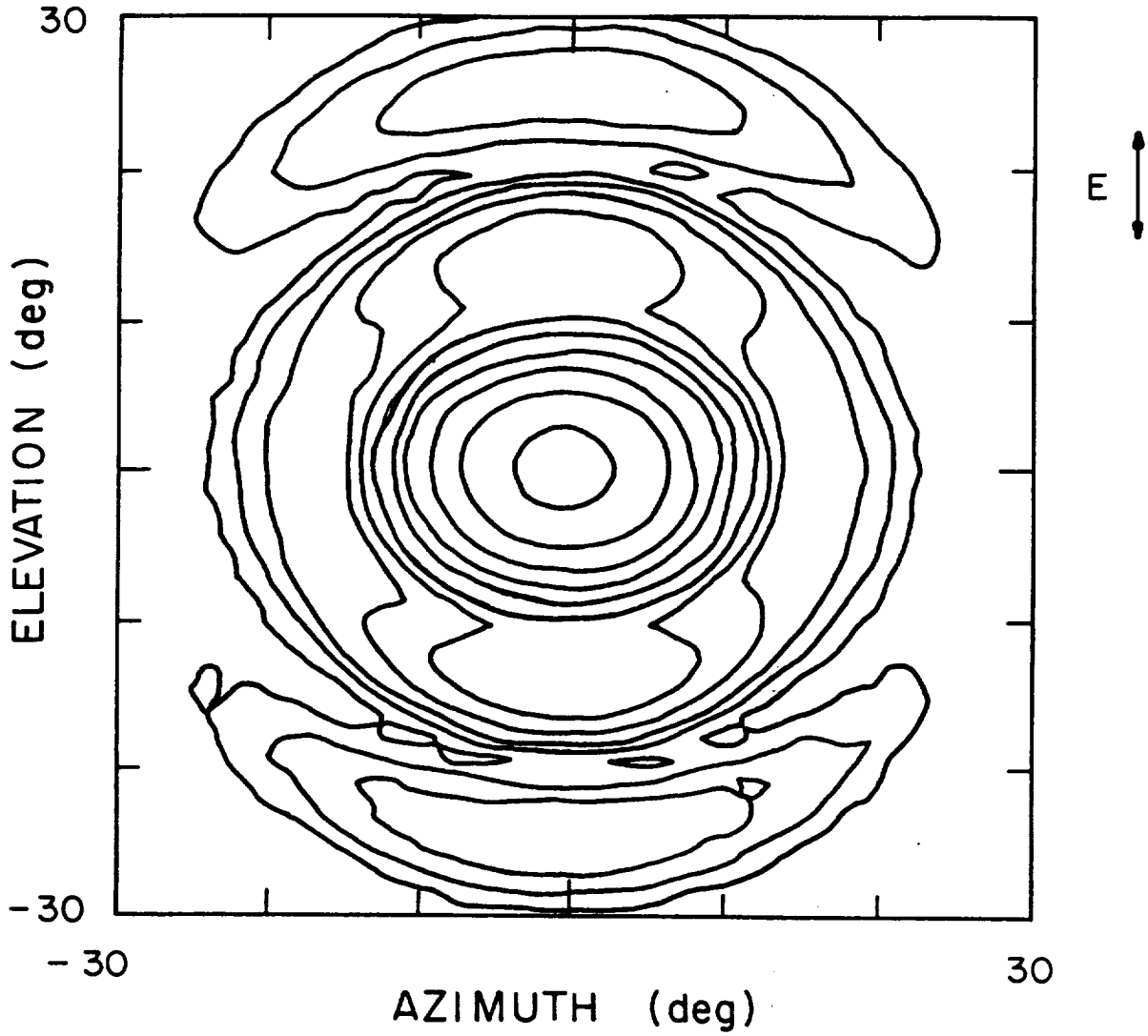

FIGURE 2.2-4b

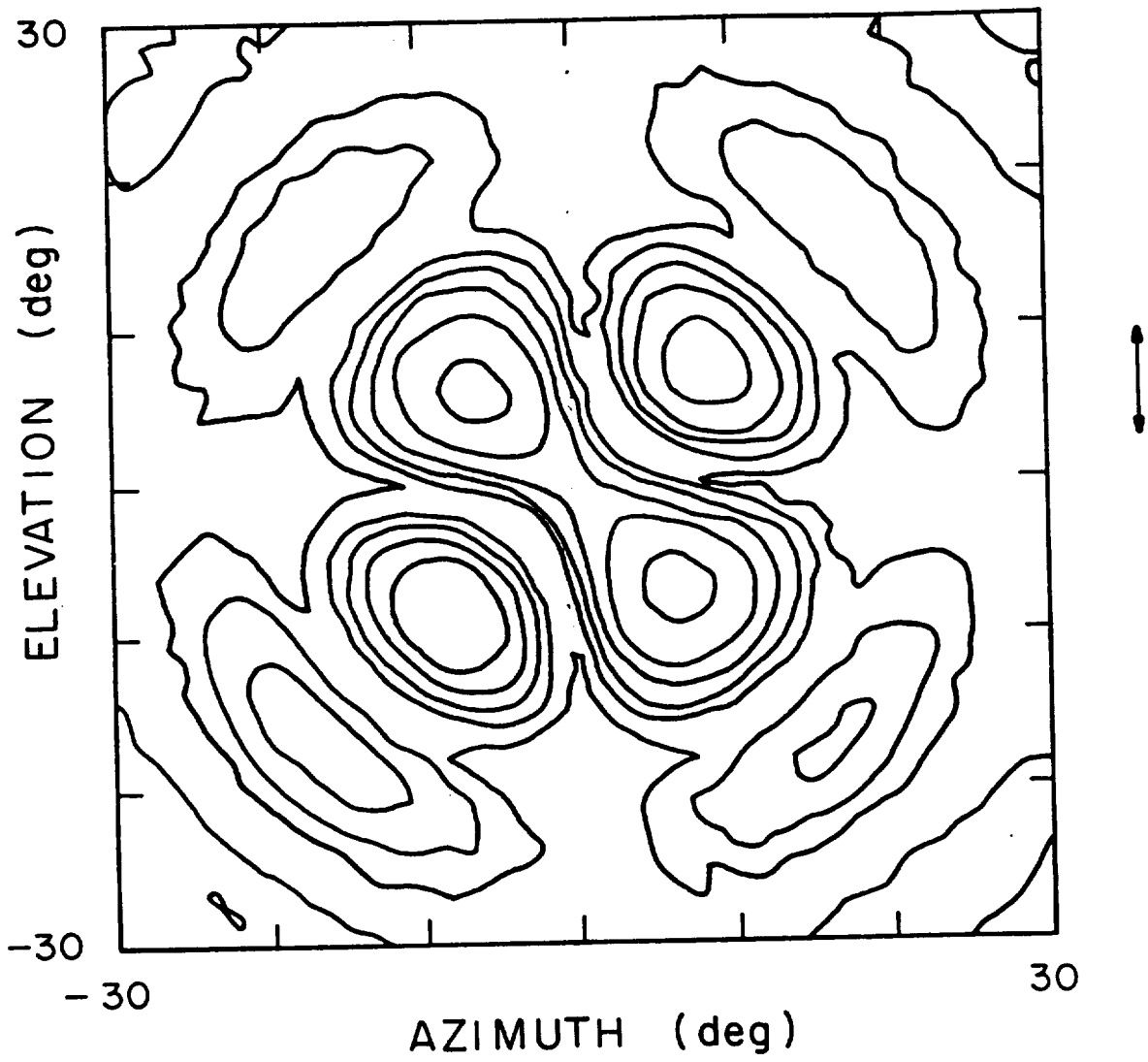

relative to the peak of the copolarization (E_y) pattern. The copolarized and cross-polarized intensities are nearly equal at the locations of the cross-polarized peaks, located at $\pm 45°$ with respect to the principal planes.

The absence of axial symmetry, as well as the E-plane sidelobes, prevent analysis in terms of a reasonably small number of Gaussian modes from being an accurate representation of the copolarized radiation pattern. If, however, we consider the beam down to -20 dB we find a relatively well-behaved pattern with a ratio of the H-plane (azimuth) width to E-plane (elevation) width of 1.25:1. Fitting a fundamental mode Gaussian indicates that for small phase error conical feedhorns ($\Delta < 0.2$) the waist radii are given by

$$W_{oH} = 0.31D$$
$$W_{oE} = 0.39D$$

where D is the diameter of the horn aperture.

2.2.2 Symmetrizing Conical Feedhorn Pattern

As discussed above, the main lobe of a conical feedhorn is asymmetric with a 1.25:1 ratio of widths, but is reasonably Gaussian in form. Since the propagation of Gaussian beams in two orthogonal coordinates perpendicular to the axis of propagation is independent, we have the possibility of correcting the pattern asymmetry using optics which treat the E-plane and H-plane differently. This can be done with a variety of elements including, most simply, cylindrical mirrors and lenses. A cylindrical mirror affects the beam parameter only of the coordinate along which the mirror is curved; the parameters of the orthogonal coordinate are not affected. Even with such a simple system it is possible to select a mirror curvature and distance to the horn which results in a symmetric beam having the beam waists for both coordinates at the same location. The analysis of this transformation has been published in the IEEE Transactions on Antennas and Propagation and is included in Appendix 2.

Two arrangements using a cylindrical mirror inclined at 45° are shown in Figure 2.2-5. In both cases, the curved coordinate is used to narrow the H-plane pattern by creating a larger effective H-plane waist. The original and corrected patterns are compared in Figure 2.2-6. The horn is the same as described in Section 2.2.1. We see that the H-plane pattern is narrowed by the desired amount. The sidelobes are largely unaffected.

While still not offering the low sidelobes and polarization purity of a scalar feedhorn, symmetrization of a conical feedhorn pattern using low loss Gaussian beam optics offers moderate efficiency, and a symmetric radiation pattern, in a system which is easy to manufacture and usable throughout the submillimeter range.

FIGURE 2.2-5

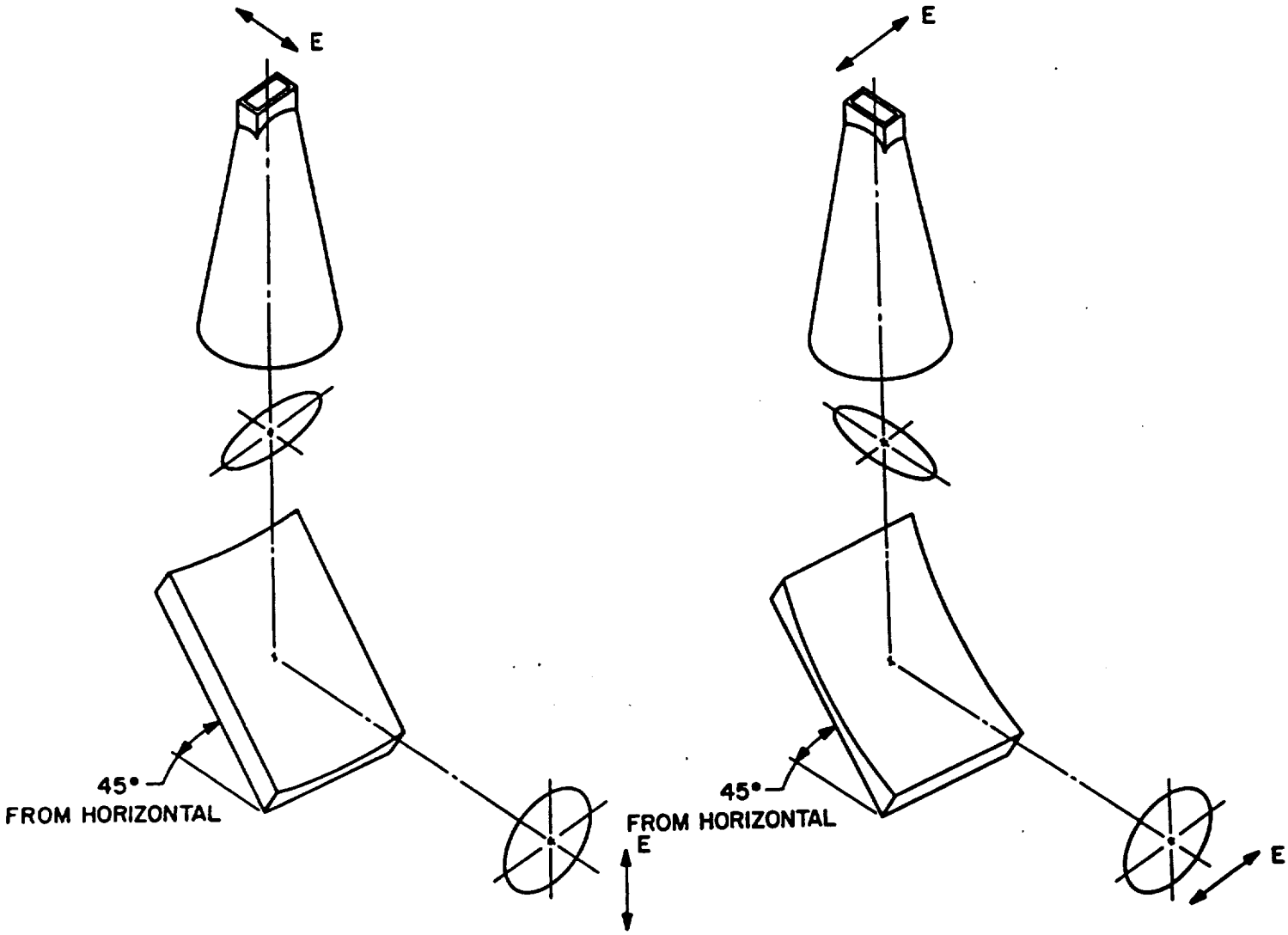

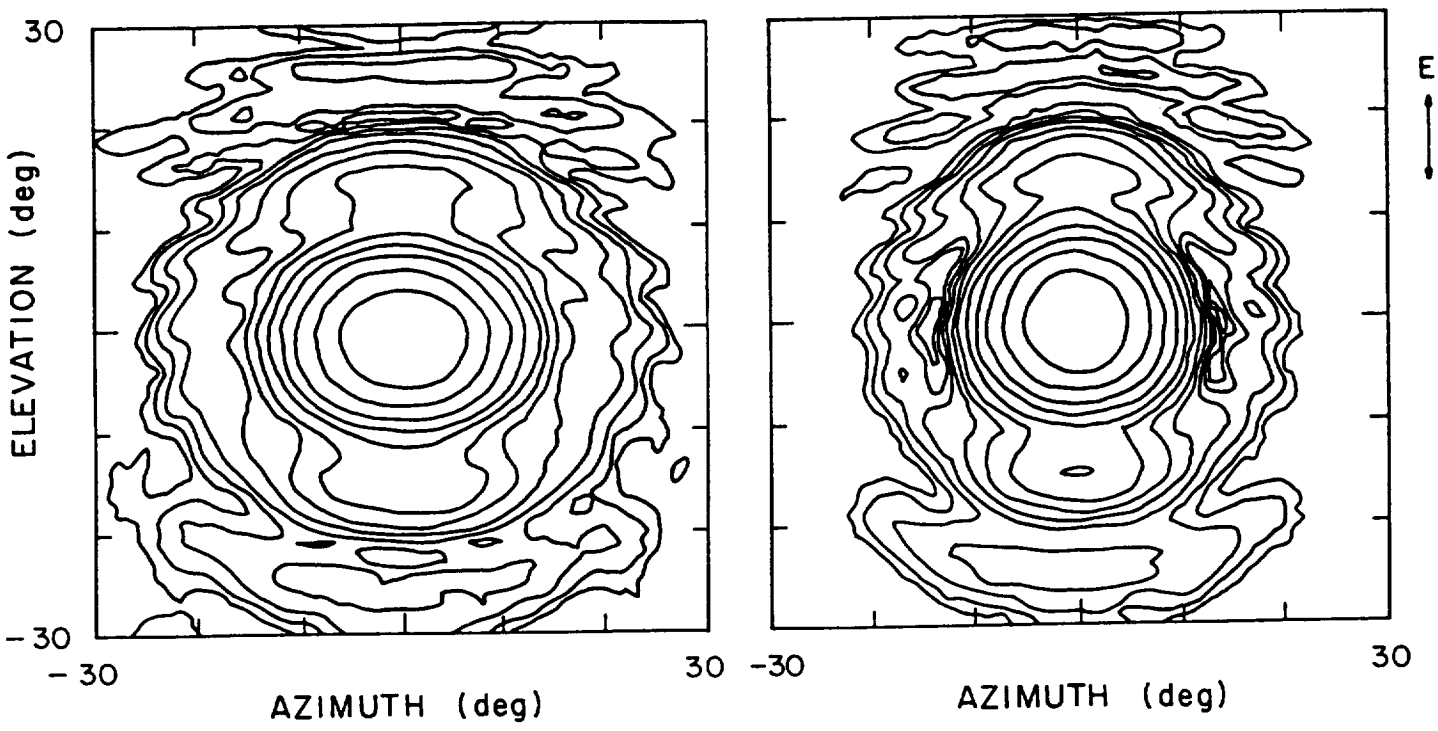

FIGURE 2.2-6

2.3 RECEIVER OPTICS

In order to simplify construction of the mixer we used a smooth-walled conical horn of the type discussed in Section 2.2 integrated into the mixer waveguide, with just a smooth taper transition from the circular horn to the reduced height rectangular waveguide. A conical horn was selected because it has inherently lower side-lobes than a rectangular horn, and is more easily machined. However the E-plane and H-plane beam patterns differ in width by 20% for such a horn requiring some optical correction. Initially we planned to do this correction with a cylindrical mirror as discussed in the previous section, but we tried this corrector and found it did not work as planned. Then we tried focussing with a simple off-axis ellipsoidal mirror, and found that this could produce equal E- and H-plane patterns. The reason for this is that the phase centers for the E- and H-plane beams are at different locations in the horn and thus it is possible to operate with one plane

in focus and the other somewhat out of focus. With the ellipsoid we happened to choose, in combination with the horn flare angle, we could produce almost identical far field patterns. The two planes still originate from different phase centers even after the mirror, but if the mean location is chosen in a system then the patterns will still be of equal width. This difference in phase center locations is the apparent reason the cylindrical corrector did not behave as planned. Phase center locations are a complex function of the flare angle of the horn. In this case the phase centers are located further inside the horn than expected, making it impossible to locate the cylindrical mirror properly.

The collimated beam has a full width of 1.5 degrees to the 3 dB points or 2.7 degrees to the 10 dB points. The optics diameter is 1.25 in. (32 mm) with a beam waist approximately at the mirror with W = 7.8 mm. This leaves a clearance of 4 W within the optics.

A sideband filter was designed for the receiver to improve calibration accuracy. This is necessary because mixers may have unequal sideband response even with a very low IF relative to the signal frequency, and because this radiometer was designed for a frequency where the atmospheric attenuation is a very sensitive function of frequency. Due to the relatively high system temperature, there is little disadvantage to terminating the unwanted sideband at ambient temperature. A Martin-Puplett interferometer was chosen because it is readily tunable, making for a more versatile system, and because its losses are very low. It is probably not the best choice for a truly fixed-tuned system, since it is more fragile and able to get out of adjustment. This sideband filter adds a loss to the signal of 10%, partially due to truncation of the sidelobes of the signal beam, and partially due to cross-polarization reflection by the grids. There is virtually no actual loss in such a filter. The sideband ratio of the mixer is approximately 45/55 at an LO of 556 GHz.

The filter can be tuned for any frequency by a single-turn knob on the outside of the receiver. This knob produces a 0.025" difference in path which is more than one wavelength at 557 GHz.

3.0 RF COMPONENTS

3.1 FREQUENCY TRIPLER

Two triplers were made for this system of somewhat different design. Both were based on studies of optimum tripler efficiency, and used the lowest possible output waveguide height for best output watch (an ~0.0045 in. high guide seemed a practical minimum height). The principle difference was in the choke structure connecting the two waveguides. One choke was based on the tripler prototype which has a fairly narrow fixed-tuned bandwidth while the other was designed to have a wider bandwidth.

In practice there did not appear to be a large difference between triplers. With 50 mW input the prototype design produced 3.0 mW. Peak efficiency for the first was 10%, while for the second 9%, but for both the peak occurs at only 20 mW input. Both show a strong saturation in output above 30 mW input; for the first the output increases from 2.6 to 3.0 mW when the input varies from 30 to 50 mW. The reason for this sharp saturation is not understood. The tripler was studied in considerable detail to investigate this problem. The diode C(V) relationship was measured with a sensitive Boonton bridge and found to be essentially that of an abrupt junction, with the expected 20 V reverse breakdown. The input VSWR was reasonably low even at 50 mW input. One odd effect was in the behavior of output power versus bias voltage. The output was quite flat over a wide range of bias voltages, an effect which could not be modeled using a multiplier analysis program for any set of embedding impedances. In fact this flat behavior is rather abnormal for triplers of this design and remains unexplained. This subject would have been pursued further, perhaps by changing the diode, except for the discovery that more LO power was not needed.

3.2 HARMONIC MIXER

The generalized theory of mixing predicts that fundamental and second harmonic mixing in an exponential diode can have comparable conversion loss in an optimized mixer,[1] although greater LO power is needed for harmonic mixing. However the noise behavior requires a more detailed treatment, which is now easily done using a computer program by Seigel.[2] This program includes all diode parameters including junction capacitance, and allows inputs of circuit impedances at 3 harmonics of the LO. Mixer bias voltage and current are also parameters (and thus indirectly the LO power). Outputs are conversion loss for conversion products up to the third harmonic, and the mixer noise temperature for fundamental mixing. For this study the mixer noise temperature for harmonic mixing may be found approximately by deriving a diode effective noise temperature from:

$$T_{Mixer} = (L_c - 2)\, T_{Diode}$$

$$T_D = \frac{T_{M1}}{(L_{c1} - 2)}$$

And using this T_D in the same formula but with L_c for harmonic mixing:

$$T_{M2} = (L_{c_2} - 2) \quad \frac{T_{M1}}{(L_{c1} - 2)}$$

where L_{c1}, L_{c2}, T_{M1}, and T_{M2} refer to the conversion loss and mixer noise for fundamental and second harmonic mixing, respectively. These formulas are from the resistive attenuator mixer noise model of Kerr[3] and are only correct as long as all loss in the mixer occurs at the same effective temperature. For a submillimeter mixer where the series resistance plays an important role in the conversion loss this is not strictly true since the diode junction noise may have a rather different effective temperature than that of the series resistance (which should be at ambient). However, use of this formula saves rewriting the noise analysis portion of the program.

Since harmonic mixers tend to require a substantial LO power which may not always be available at 278 GHz, this power was put in as a constraint in the mixer impedance optimization. In the program we also assumed that the impedances at the two sidebands and the LO were the same for each harmonic. The impedance at the second LO harmonic was chosen to equal the closest match achievable in a waveguide mixer, and the third harmonic impedance was chosen at an estimated value (its exact value is not critical). The major variable was then the impedance at the LO fundamental frequency. Once an approximate value was found, the mixer bias current was optimized and fixed. LO power was fixed at 2 mW since only this much could be expected at the diode junction. At this point the conversion loss was calculated for a range of fundamental impedances, and plotted on a Smith chart, shown in Figure 3.2-1. Points near the conversion loss minimum are desirable since the IF contribution will be minimized here, although a low mixer noise temperature is also needed. As may be seen, the conversion loss is fairly insensitive to the fundamental impedance except for a narrow region where much lower loss appears possible. This region may be partly an artifact of the computer program since very low conversion loss appears in one area (not plotted). Such a sharp resonance in impedance space is of marginal interest in any case since it is very hard to achieve such a precise circuit impedance. However, with a tunable backshort it is possible to achieve a wide range of impedances, and there is some evidence for a sharp resonance in the experimental data. This plot also shows a typical impedance circle measured for a model mixer as the backshort is tuned.

Also shown in Figure 3.2-2 is a plot of expected mixer noise and conversion loss versus LO power, at a constant bias current of 0.2 mA and for impedances of $Z_1 = 100$, $Z_2 = 80 + 120\ j$, and $Z_3 = 50 + 50\ j$.

An interesting effect discovered in this modeling is that for a range of readily obtainable embedding impedances, the effective diode noise temperature is well below ambient, typically 200 to 240 K. This leads

FIGURE 3.2.1 DOTTED LINE = IMPEDANCE CIRCLE OF MIXER MODEL
AS BACKSHORT IS TUNED
SOLID LINE = CONVERSION LOSS CONTOURS
NUMBERS = CONVERSION LOSS IN dB

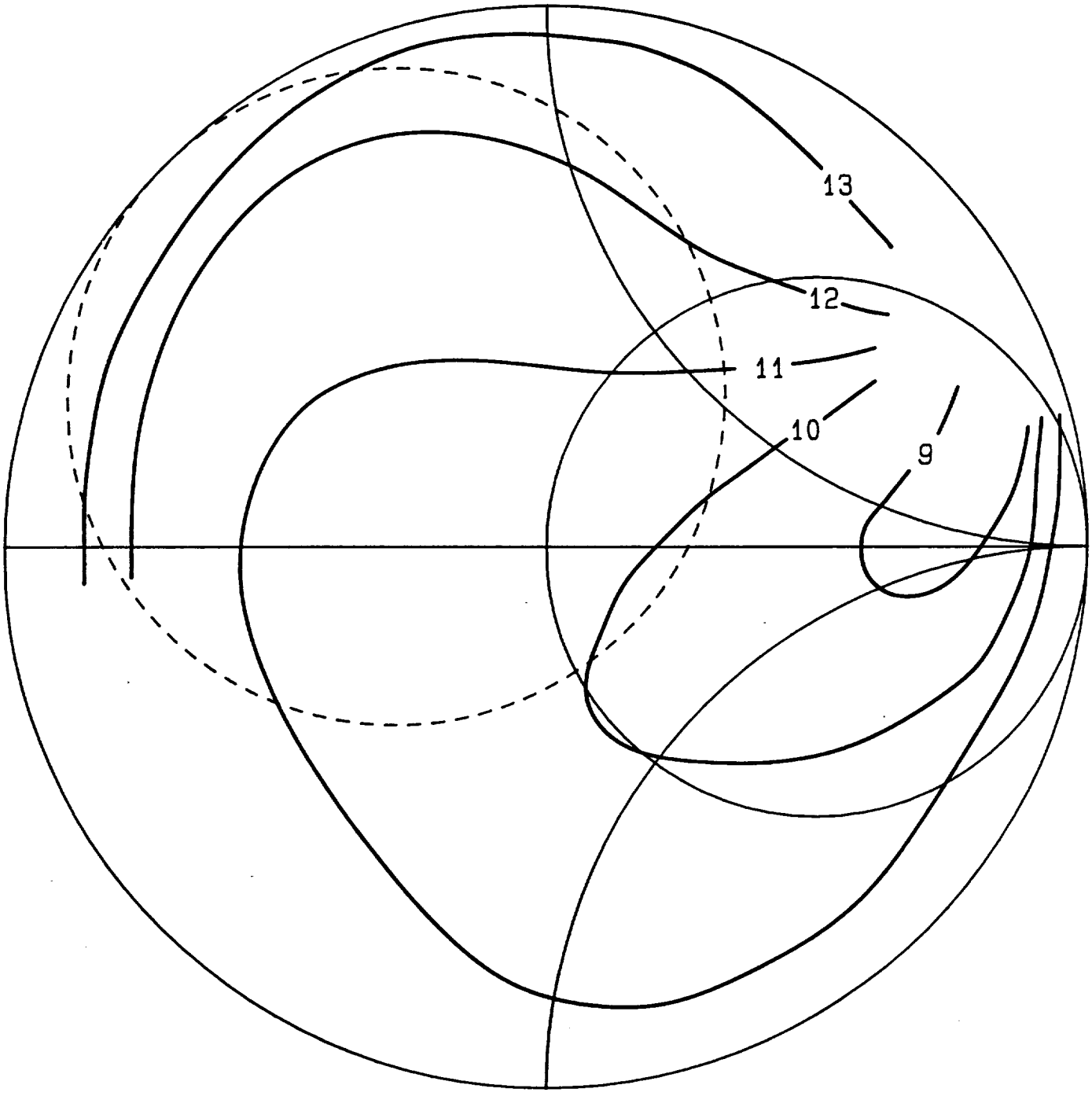

FIGURE 3.2-2

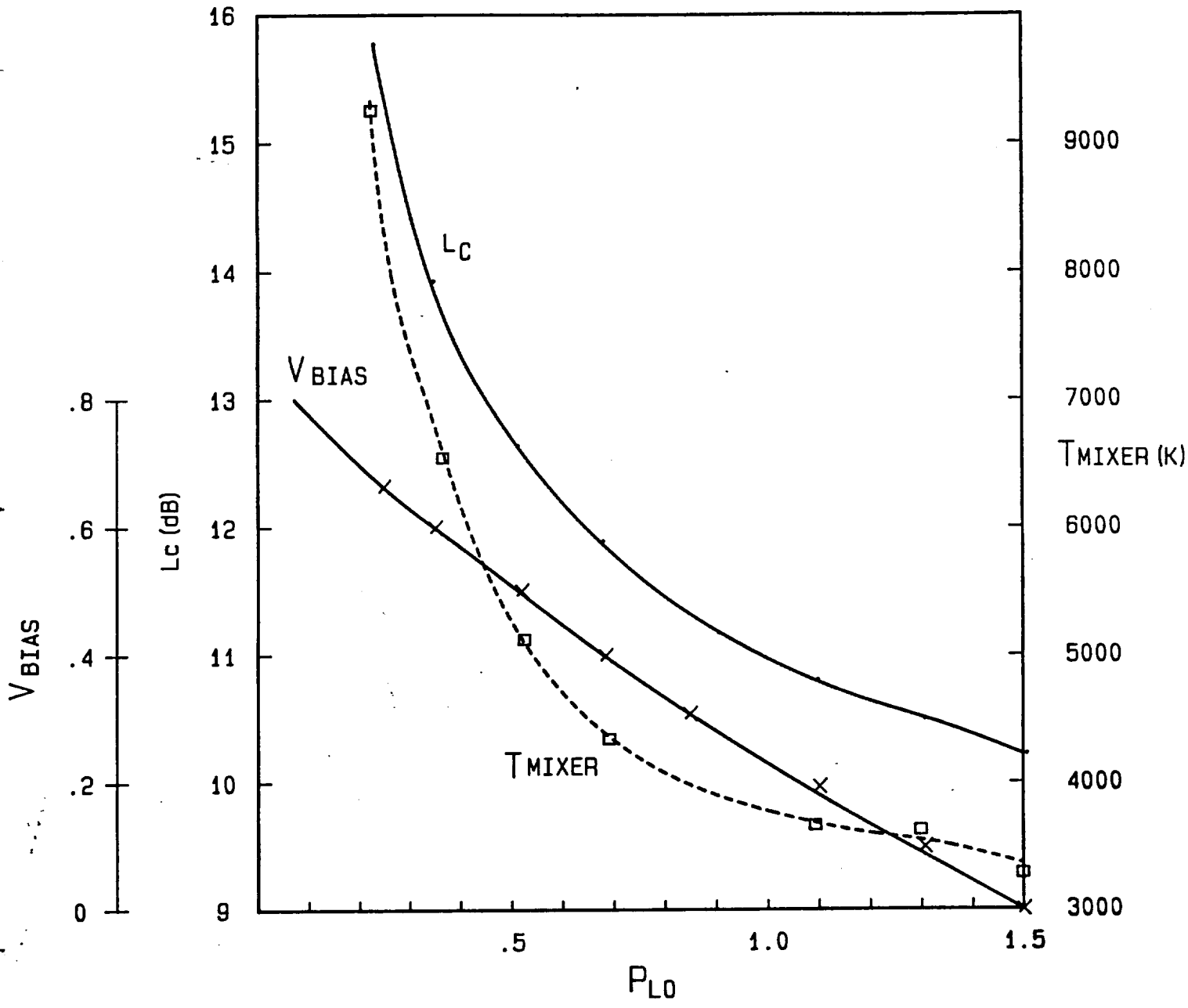

to a relatively low mixer noise temperature. In addition, the conversion loss is not substantially higher than for a fundamental mixer (only 1 to 2 dB difference), and fundamental mixers typically show somewhat higher diode noise. Thus the overall difference in noise between the two mixers is relatively small.

3.2.1 Mixer Modeling

In order to design an actual mixer having the optimized impedances it is necessary to do some modeling in order to fully understand the waveguide embedding structure. Initially the signal waveguide dimensions and whisker length were chosen to achieve a reasonable impedance at the signal frequency. The waveguide height was chosen to be as low as practical for reasonable fabrication since even the lowest height was too great for optimum matching.

The whisker impedance was then modeled at the LO frequency. This behavior is somewhat complex, and does not appear as a simple inductance due to the presence of evanescent waveguide modes.

Using Touchstone, a computer-aided microwave design program (EESOF, CA), a three section coaxial filter was designed to present a short circuit at the top wall of the waveguide for the signal frequency, but a nearly optimum LO impedance when the effect of the contact whisker and LO waveguide were taken into account. The LO backshort was assumed to be at the open circuit position in this design to maximize the fixed tuned bandwidth and minimize losses. In addition this allows the most flexibility in tuning if an error is made in design or fabrication. In designing this filter, coaxial impedances were constrained to be between 20Ω and 60Ω to avoid excessively difficult construction. The LO waveguide impedance was allowed to vary down to 150Ω, and in fact ended up at near this minimum. This filter was then incorporated into the model and its effect verified.

After two iterations a filter was designed which met the objectives fairly closely. The circles of impedance as the LO backshort is tuned

pass near the optimum impedance, with fairly mimimal frequency sensitivity. In addition, the open circuit backshort position falls reasonably close to the optimum so that backshort tuning should not be too critical.

The final part of the model was a three section filter in the IF port to prevent leakage of LO power, and to present a short circuit termination at this port so that the LO impedance at the diode would be better defined.

The construction of the model and mixer is shown in Figure 3.2-3. Both filters use variations in the diameters of both the inner and outer conductors to achieve the largest impedance ratio. In addition, only the first section of each filter is designed to be cut off to higher modes at the highest operating frequency. This allows the following sections to be larger for greater strength and ease of fabrication. Note that the first sector of the center conductor of the filter consists entirely of the diode chip, which is cut into a roughly circular shape.

3.2.2 Experimental Results

The receiver was tested initially with two GaAs Gunn oscillators of different construction. Tune-up of the mixer proved to be tricky because of excessive noise, apparently from the LO source, which can be partially rejected only by a combination of tunings of the output tripler backshort and the harmonic mixer LO backshort. With a signal-to-noise ratio meter this tune-up is fairly quick, but would not be possible otherwise.

Since InP oscillators were available, we tried one and found that the LO noise was much less, so much so that tune-up was very smooth and seemed a lot less critical. As a practical matter this made system operation much smoother, although the ultimate system performance was only about 10% lower in noise. Due to the much easier tune-up and the lower power consumption, InP Gunns were used in all further tests.

FIGURE 3.2-3

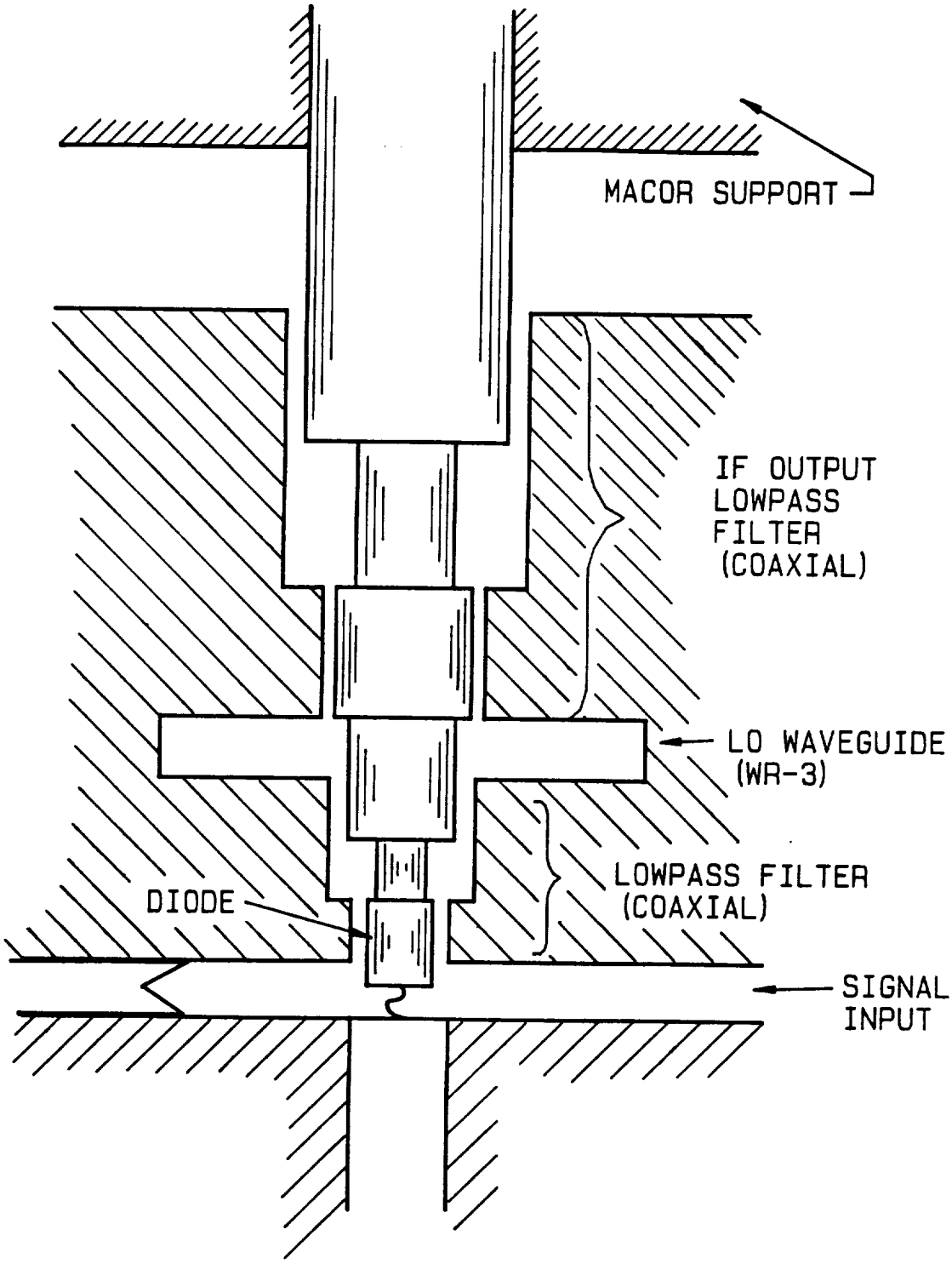

Only one mixer diode and contact whisker were used in these tests, thus these results may only be regarded as a sample of one. A variety of InP oscillators were used with two triplers to explore the tuning range of the harmonic mixer. These results are summarized in Figure 3.2-4. Typical bias current was 0.20 mA at all points with bias voltage varying from 0.5 to 0.65 V. LO power was unknown point by point but was probably 2 mW minimum at the tripler output. The tripler and mixer were connected by a 1.5 inch length of WR-3 waveguide with an insertion loss of 1.5 to 2 dB. While these units could have been connected together directly with more LO reaching the mixer, better results were obtained with the 1.5 inch piece of waveguide. The reason for this is that the guide plus the mismatches at both ends form a cavity which favors the coupling of LO power to the mixer while suppressing the conversion of input power by fundamental mixing. This resonance also acts to filter the noise from the LO source. However, this type of filter is not very tunable and may not have the correct resonant frequency for an arbitrary LO. Evidence for such an effect is seen as the mixer is tuned. Certain frequencies work significantly better than those only about 1 GHz away. On the average, the tuning is quite flat and shows no systematic variation over the range sampled.

Subsequently, a lower loss waveguide was specially made to connect the two devices, consisting of a WR-3 to WR-4 taper and then back to WR-3 in a single electroformed waveguide. This taper had a loss of only 0.7 dB, but gave no better performance than the higher loss straight guide. However, enough variables are present in this system to mask any small improvement in one area. In part this is because the mixer is not really short of LO power, as is discussed later, and a small change should not be very noticeable.

In order to investigate the agreement with theory the noise temperature of the mixer was plotted vs LO backshort position and is shown in Figure 3.2-5. This curve shows a very smooth variation with a very broad optimum as predicted by the theory. A sharp spike near the null in

FIGURE 3.2-4

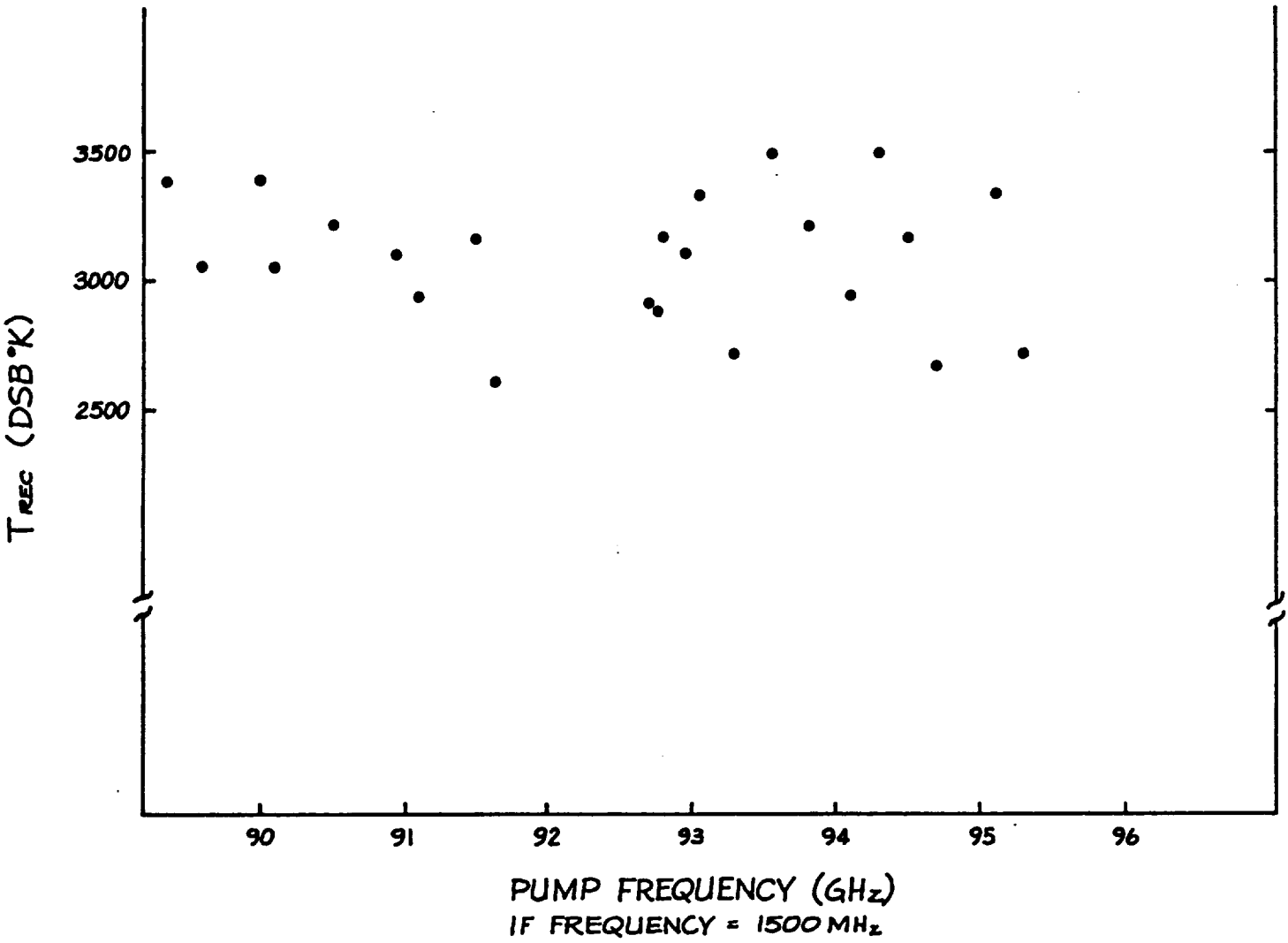

FIGURE 3.2-5

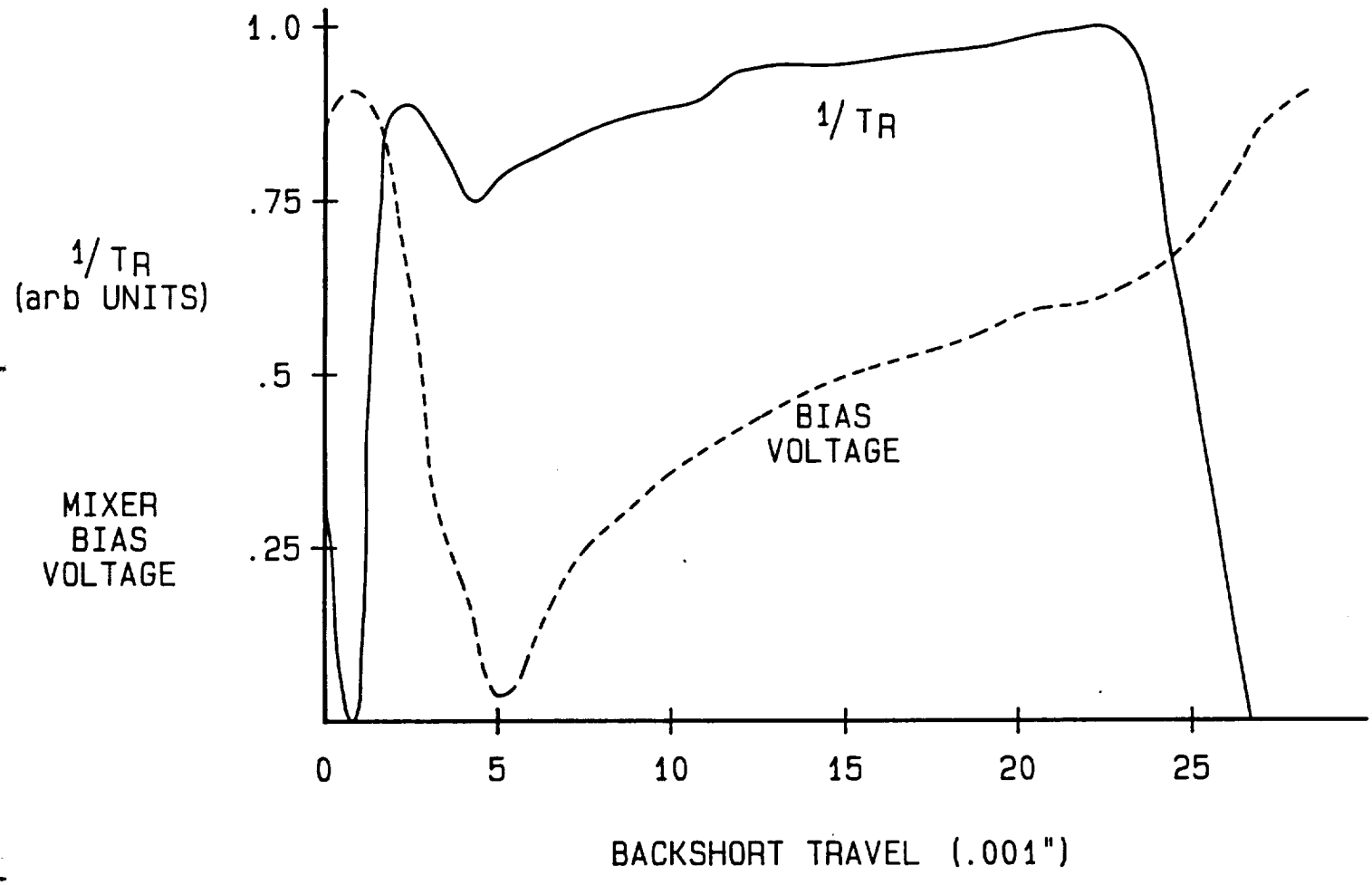

performance is not explained well, but is an observed characteristic at most frequencies. In fact, at some frequencies this is the best operating point. This corresponds to an impedance very close to the perimeter of the Smith chart, and it is rather surprising to see such an effect. The receiver total power output was constant to within 1 dB over this backshort tuning so that the noise temperature and conversion loss are fairly well correlated.

Using the model, a measurement was made of impedance vs backshort position, and this is plotted as well on the Smith chart in Figure 3.2-1. While detailed agreement is poor, in a general way the behavior is similar, given the uncertainties in translating the model to the actual unit at nearly 100 times higher frequency. The backshort motion does cause the impedance to pass near the optimum operating region predicted by theory, but the theory does not predict a double peak in the behavior. The interaction of the tripler and mixer can perturb these impedance circles significantly and may be part of the discrepancy. These curves predict that for a harmonic mixer of this construction, LO backshort tuning should be quite non-critical, and that is what is observed.

Since LO power is relatively difficult to obtain even for a harmonic mixer, we also measured the behavior of the noise temperature and conversion loss vs LO power into the tripler (and indirectly its output power). These results are summerized in Figure 3.2-6. As can be seen the conversion loss is fairly strongly saturated even with a tripler input of 35 mW, and so there is no real need for a high power pump source, particularly since the tripler's output power saturates quickly for more than 30 mW input.

IF matching for the mixer is made difficult because of the inherently high IF impedance of a harmonic mixer, and because of the length of the choke structure which prevents attaching a matching circuit as close to the diode as is desirable. To aid in matching the impedance of the macor support section was made at 50Ω , which was as high as practical,

FIGURE 3.2-6

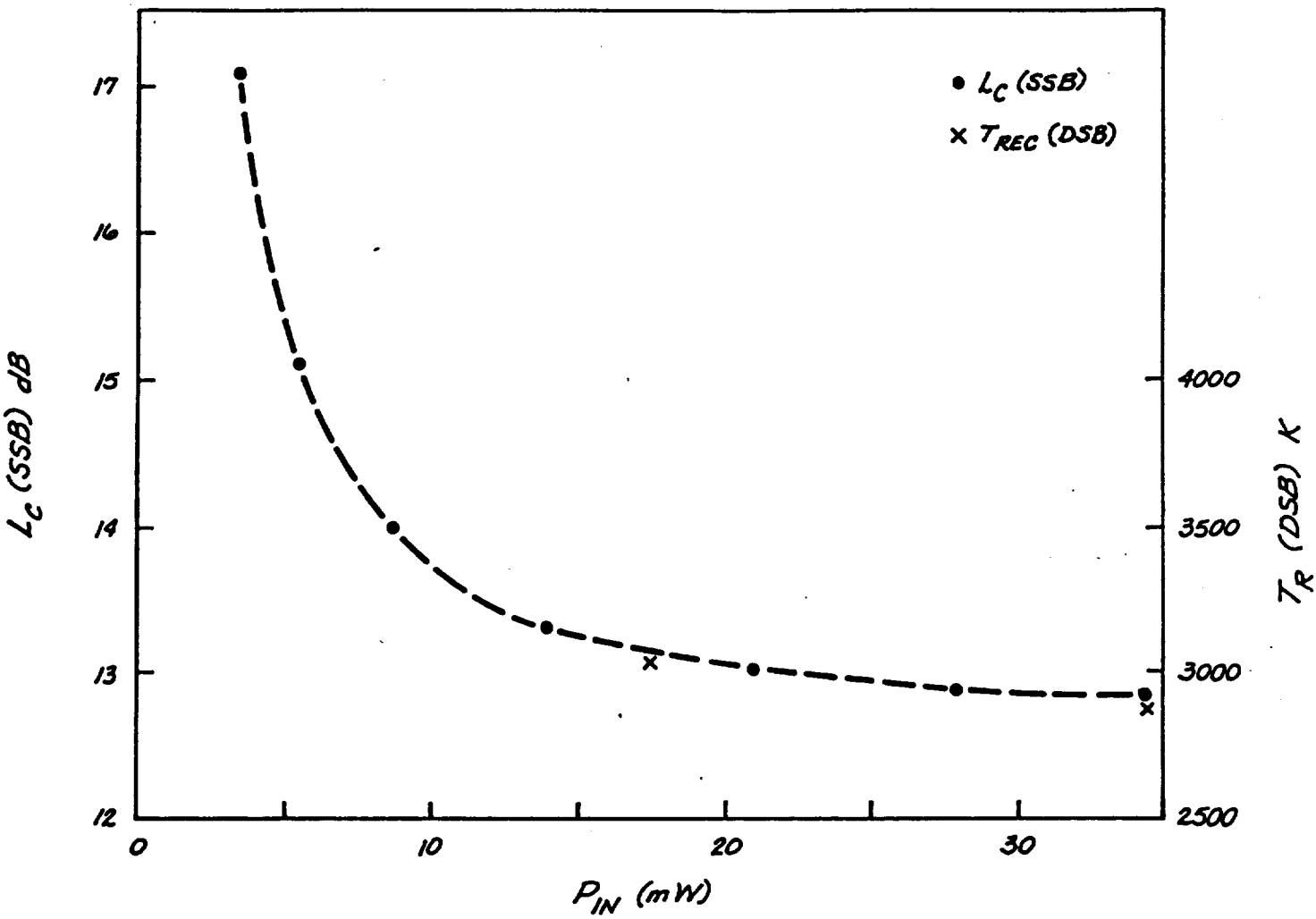

and its length kept to a minimum. In actual use the IF impedance was measured to be 350Ω, and a VSWR < 1.6:1 match was made over the range 1.2 to 1.75 GHz using a lumped inductor plus a short circuited quarter-wave stub in microstrip on ϵ=10.2 Duriod circuit board. This matching circuit incorporated a DC block and bias T to minimize external components.

Using a FET IF amplifier nominally centered at 1.5 GHz, the receiver noise was measured over the IF band using a 50 MHz BW tunable filter. The noise temperature increased less than 10% at the edges of the 1.2 to 1.7 GHz band. However the system incorporates a 450 MHz BW filter centered at 1525 MHz which provides a practical limitation on useful bandwidth (although this filter could be removed).

The minimum conversion loss measured was 13 dB, about 3 dB higher than predicted by the mixer program. This difference is possibly consistent with the input waveguide loss, but seems about 1 dB too high. The measured diode effective temperature is 240 K, exactly as predicted by the program. Thus, we find reasonable overall agreement between theory and experiment, but a number of small details which don't match.

REFERENCES

1. P.F. Goldsmith, Ph.D. Thesis, University of California, Berkeley, 1975.

2. P.H. Seigel, Ph.D. Thesis, Columbia University, 1983 (Published as NASA Tech. Paper 2287).

3. A.R. Kerr, IEEE Trans. Microwave Theory Tech., Vol. MTT-27, pp. 135-140, 1979.

3.3 GUNN DIODE OSCILLATOR DEVELOPMENT

This section deals with the development of Indium Phosphide (InP) Gunn diode oscillators as the fundamental source or driver for the multiplied source. The technical requirements and objectives for the oscillator are stated in Section 3.3.1. Following these, the technical approaches for realizing the oscillator are described in Section 3.3.2. The details of experimental work conducted during the course of this development are presented next. This includes the results from measurements of the electrical characteristics of the oscillator, and considerations for its phase locking to the reference. Conclusions for future work are summarized at the end in Section 3.3.5.

3.3.1 Objectives for the Development of InP Gunn Oscillators

The Gunn oscillator development work for this program was prompted by a number of technical considerations and system related issues. Due to the recent availability of high performance Indium Phosphide Gunn diodes, it is now possible to reliably produce a significant amount of power at the millimeter frequencies in the W-band. There are many other advantages associated with these InP devices, such as:

1. Low DC power consumption
2. High efficiency
3. High fundamental frequency of operation
4. High power output
5. Lower noise

The low DC power consumption stems from the high DC to RF conversion efficiency of the newly developed InP Gunn devices. Due to the current limiting contact, it is possible to obtain desired operating points while maintaining a reasonable junction temperature. The low DC power consumption is highly attractive from the viewpoint of space applications. Typical operating points for InP devices range from 1.2 Watts to 3.5 Watts.

The efficiencies typically observed in InP devices are superior to their Gallium Arsenide counterparts by a factor in the range of 2 to 4. In the W-band, efficiency ranges from 3% to 5% for high power operation, while in the Ka-band (26.5 to 40 GHz), efficiencies greater than 10% are readily achieved.

The InP devices are capable of operating fundamentally at frequencies beyond 100 GHz in contrast to the 70 GHz limit for Gallium Arsenide devices. Hence, it is possible to produce both fundamental and second harmonic power at W-band using InP devices of suitable type. In the present work, it was decided to study the system characteristics under fundamental and second-harmonic operation of the pump source.

The AM noise of the InP devices is reported to be lower than the corresponding GaAs device. This was investigated for the present application by comparing the system performance with both GaAs and InP Gunn oscillators driving the multiplier.

With this background, the objectives of the development are:

(1) To conduct a comparative study of system performance with GaAs and InP Gunn devices.

(2) To design and evaluate both fundamental and second-harmonic InP device oscillators for the multiplier-driver application.

(3) To examine performance characteristics and operating behavior of various types of InP devices with a view to establish their suitability for the present application.

(4) To design and optimize Gunn oscillators for phase-locked operation using a space efficient scheme.

These and other incidental issues were the primary motivation for the Gunn oscillator development.

3.3.2 Technical Requirements

The Gunn oscillators provide the fundamental drive power for the multiplier (tripler) at 92.6 GHz. In order to achieve the required RF power output from the multiplier, the following performance characteristics and specifications were originally indicated:

Center frequency:	92.6 GHz
Power output:	60 mW
Mechanical tuning:	$\pm$200 MHz
Electrical (bias) tuning:	$\pm$250 MHz
Power output variation with bias tuning:	$\pm$1.5 dB
Monotonic bias tuning characteristics	
Thermal coefficient of frequency:	$\leq$ 4 MHz/°C
Thermal coefficient of power output:	$\leq$ 0.035 dB/°C
Power through the sample port:	1 mW typical
External quality factor Q_{ext}:	$\geq$ 250

Other mechanical requirements were:

(1) A second sampled output power port for the purpose of phase locking directly.

(2) Outline and configuration to match the system mechanical layout.

In addition to the basic requirements, some system-related technical goals were also established, i.e.:

- Power consumption less than 2.5 Watts.
- Bias tuning rate of > 300 MHz/Volt.

3.3.3 Design Approaches and Development Plan

As indicated earlier, two distinctly different electrical designs are applicable to the W-band source using InP devices: fundamental source, and second-harmonic extraction.

Fundamental driver source: Several InP devices are available for fundamental use at frequencies in the neighborhood of 94 GHz. These can be classified as follows:

(1) High power devices, (VA9122S13) which typically provide 60 milliwatts of power at 94 GHz at nominally 10 Volts bias.

(2) Medium power devices, (VA9122S10) which provide 30 milliwatts of power at lower bias voltages.

These devices, however, have drastically different behavior in terms of their mechanical tuning characteristics, external Q, and bias characteristics when used in traditional oscillators. The RF performance of these will be described later. The first fundamental oscillator design utilizes a resonant disk in conjunction with a cylindrical coupling post to produce power over a design frequency range. Figure 3.3-1 shows the details of this type of oscillator. A backshort is utilized to optimize the performance. The frequency of operation is primarily determined by the dimensions of the disk, which is selected to be one half guide wavelength at the operating frequency. A dielectric rod can be introduced under the disk to tune the frequency. The basic oscillator design was studied in considerable detail since it appeared most promising as far as the required power level for the multiplier was concerned.

The second fundamental design is structurally very similar to the first one, except that the backshort location plays a dominant role in determining the output frequency. The nominal distance between the Gunn device (coupling post) and the backshort position is approximately a multiple of a half guide wavelength. The coupling post and disk dimensions control the output power and exert a second order influence on the output frequency. There are other mechanical features of the cavity that have an effect on the performance of the Gunn diode oscillator. These were examined in depth, and the results are presented in Section 3.3.4. Fundamental mode design requires the use of a Gunn

FIGURE 3.3-1 - RESONANT DISK-TYPE FUNDAMENTAL GUNN OSCILLATOR

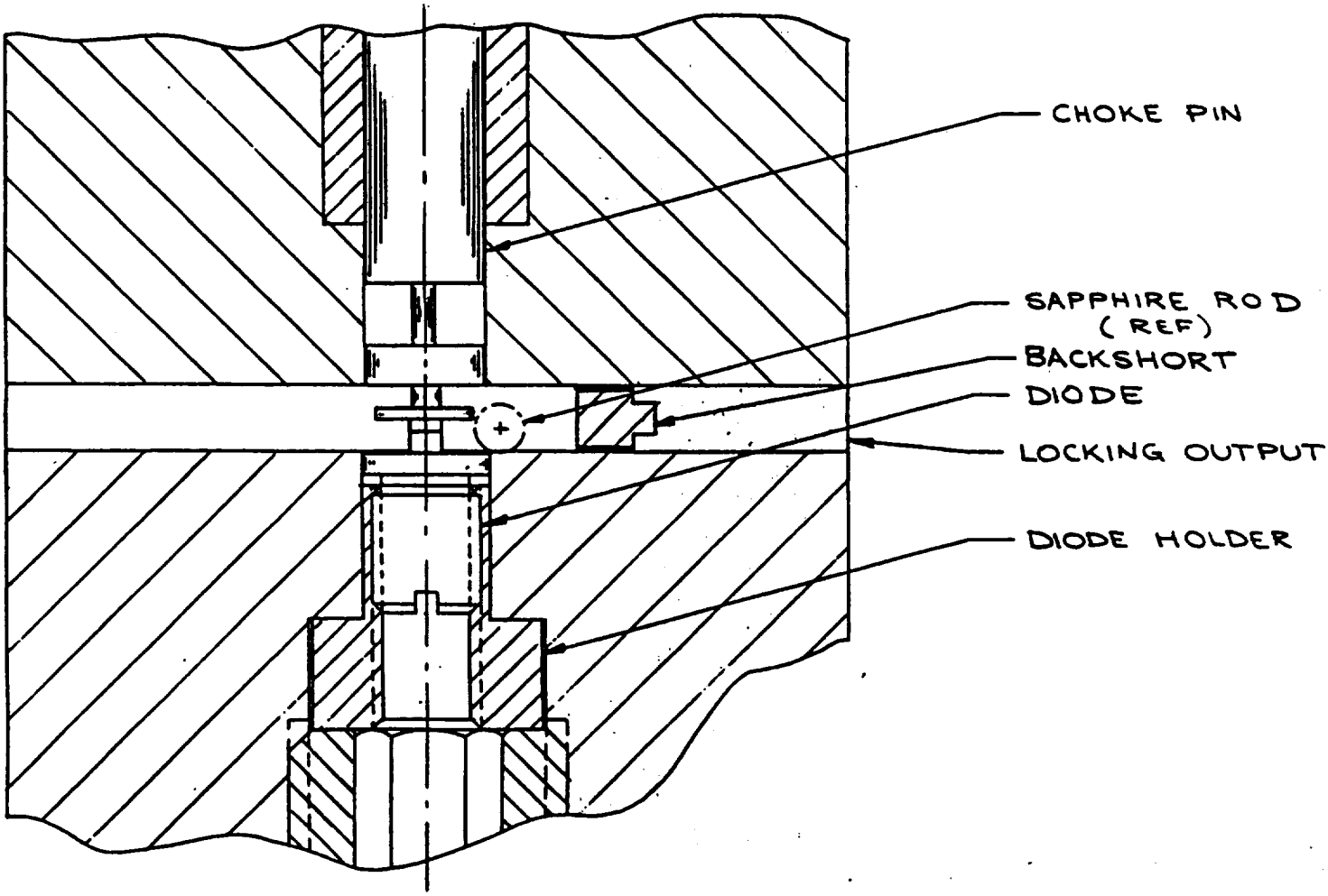

device which has an active layer dimension that can provide sufficient gain at the W-band frequency of interest.

Second Harmonic Design: This design utilizes the second-harmonic extraction of a fundamental frequency oscillation in a suitable cavity configuration. Power at the fundamental frequency is produced by means of a disk and post resonator circuit, in combination with the Gunn device itself. The fundamental frequency is below the cutoff frequency of the output waveguide and therefore cannot propagate through it. The disk itself is capable of supporting the second-harmonic frequency in the form of a radial transmission line. Thus, an efficient transfer of second-harmonic power can be achieved. The backshort location plays a relatively insignificant role in determining the resonant frequency. However, it is primarily used for optimizing the power output to the main output port. Since the fundamental frequency is established by the disk, and is uncoupled to the output port (due to the waveguide cutoff), this type of oscillator is relatively uninfluenced by the output load variation, etc. A dielectric rod under the disk can be used to vary the operating frequency, while the backshort location is used to optimize the power output. Obviously, this design utilizes devices which operate at approximately half of the desired W-band output frequency.

One more design feature needs some discussion. This pertains to the frequency sampling technique for phase locking purposes. A small amount of power is extracted from the "back port" of the Gunn oscillator by means of an iris or a leaky backshort structure. The back coupling arrangement must not significantly influence the basic operation of the oscillator. The results of this implementation will be reported in the text following this section.

The developmental work for this program was divided into the following major tasks:

(1) Device evaluation for fundamental and second harmonic operation

(2) Design, fabrication, and evaluation of at least one fundamental and one second-harmonic oscillator

(3) Study of phase-locking and "backport" sampling characteristics

(4) Delivery of final product(s)

3.3.4 Fabricational Details and Experimental Results

The Gunn oscillators for the program were constructed using a universal WR-10 cavity for both fundamental and second-harmonic operation. The mechanical configuration of the oscillator is shown in Figure 3.3-2. The design is capable of accommodating a sapphire rod "side tuner" drive, as well as a backshort drive (or an optional port with waveguide mounting flange). The diode mount was designed to permit convenient replacement of diodes, and to allow their rotation and vertical relocation. This makes it possible to study the influence of diode mounting parameters on the performance of the oscillator. The choke and resonator were universal as well, to allow interchangeability of various different types of resonators. Chokes with systematically varying parameters were fabricated. Backshorts, both contacting and non-contacting types, were constructed in addition to iris-type backwalls. Several housings were used in the investigation to allow simultaneous evaluation of performance, and to establish the repeatability of results.

Two distinctly different oscillator designs were implemented for the fundamental operation. The first utilized the medium power device (VS9122S10), the bias characteristics of which are as follows:

V_{op} = 4.8 volts,
I_{op} = 225 mA,
Test frequency = 94 GHz,
Typical power output = 35 milliwatts.

FIGURE 3.3-2 - W-BAND GUNN OSCILLATOR

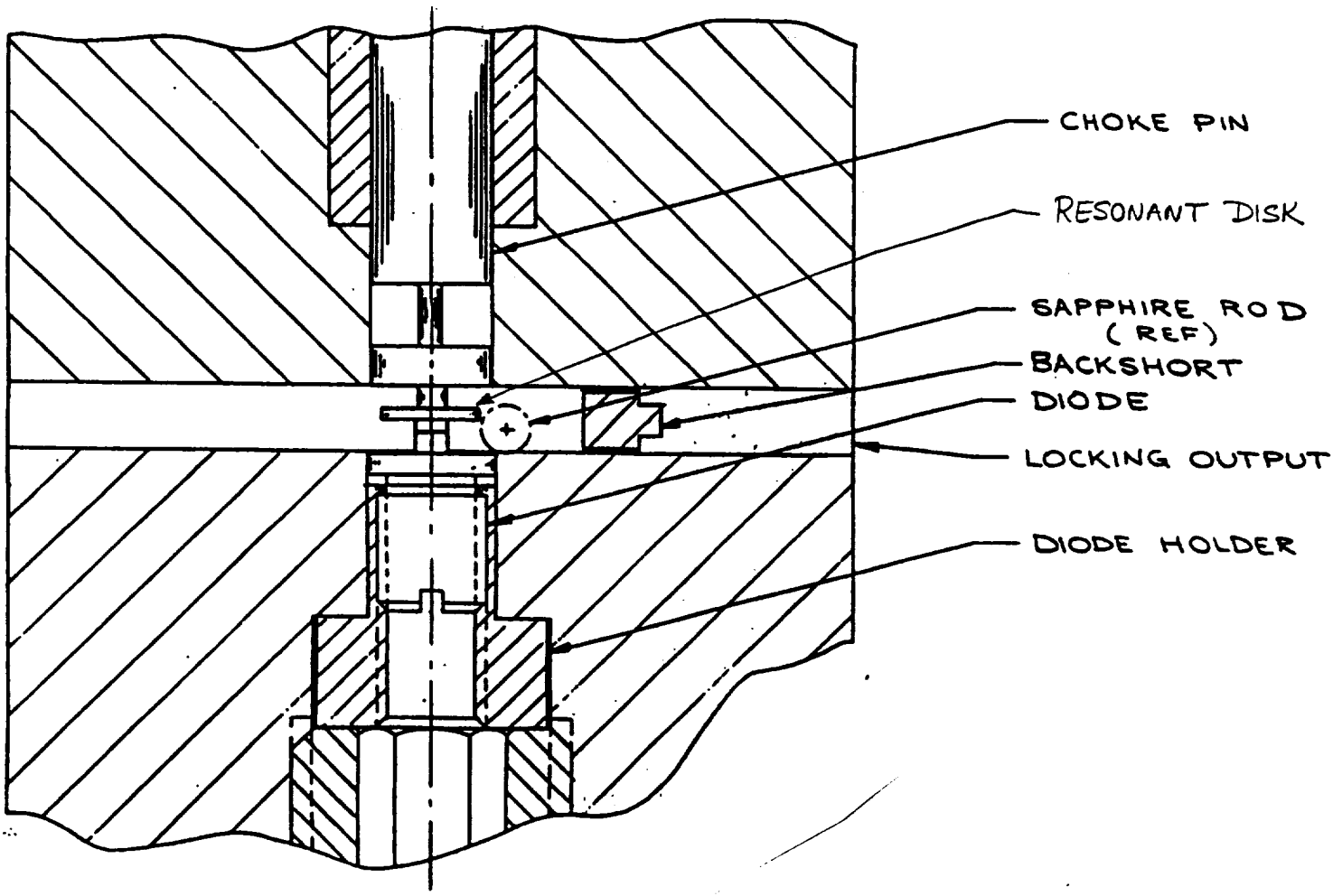

In order for this device to operate at 92 GHz, the Gunn device flange had to be raised 0.010 inches above the waveguide floor. The coupling post diameter of 0.040 inches was optimal. The device typically produced 25 to 35 milliwatts of power in the frequency range of interest. However, this oscillator suffered from several drawbacks, which are:

(1) The power level of 30 to 35 milliwatts was considered marginal for meeting the requirements of the frequency multiplier.

(2) The oscillator was predominately backshort tunable, which presented some problems in the extraction of power from the "backport". In addition, there was a strong load dependence on operating frequency and characteristics. In fact, over load and environmental ranges, the oscillator was prone to changing modes, as demonstrated by abrupt frequency and power changes. It necessitated the use of an isolator, which further reduced the output power.

(3) The bias tuning characteristics were not optimal for phase locking purposes. The bias-tuning curve was not monotonic over the entire tuning range.

In view of these observations, it was decided to discontinue any further investigation of this design or device for this program. Further work was conducted using the high power fundamental device.

The second design employed the InP device VS9122S13, the typical characteristics of which are:

V_{op} = 10 Volts,
I_{op} = 180 milliamps,
F_{nom} = 94 GHz,
P_{nom} = 65 milliwatts.

This device was investigated in considerable detail. It was tested with a number of similar diodes and optimized each time for the 92.6 GHz

nominal frequency. The summary of performance of the final unit is given below, while Table 3.3-1 is the recorded data for the unit.

Frequency range (mechanically tuned) = 91.5 to 93.5 GHz;
Minimum power at frequency of interest = 60 milliwatts;
Bias tuning range (3 dB point) = 245 MHz;
Backshort pulling (total) = $\pm$125 MHz;
Power output through the backport $\leq$ 1 milliwatt

TABLE 3.3-1

BIAS TUNABLE InP GUNN DIODE OSCILLATOR DATA

Model No. GDM-10 Serial No. 118

Job No. A-125 Date: 5/8/86

Operating Conditions

Operating bias voltage 10 Volt Threshold voltage N/A

Operating bias current 218 mA Threshold current N/A

Bias Tuning Characteristics (Diode No. 1) VSB 9122S13 S/N 226B-05		
Bias Voltage V_B (Volts)	Frequency (GHz)	Power (mW)
10.0	92.876	60
9.9	92.850	52
9.7	92.820	49
9.5	92.793	46
9.3	92.762	42
9.1	92.732	40
8.9	92.698	36
8.7	92.666	33
8.5	92.631	30
8.3	92.600	27
8.1	92.560	24
7.9	92.527	21
7.7	92.497	18
7.5	92.463	15
(Diode No. 2) VSB 9122S13 S/N 227B-106		
10.8	92.760	65
10.5	92.970	60
10.0	92.600	57

Thermal drift characteristics of the prototype unit were recorded by temperature cycling the unit. A best-fit curve was derived by processing the data numerically. This data is presented in Figure 3.3-3. An average drift coefficient of -3.3 MHz/°C was observed.

FIGURE 3.3-3 - THERMAL DRIFT DATA

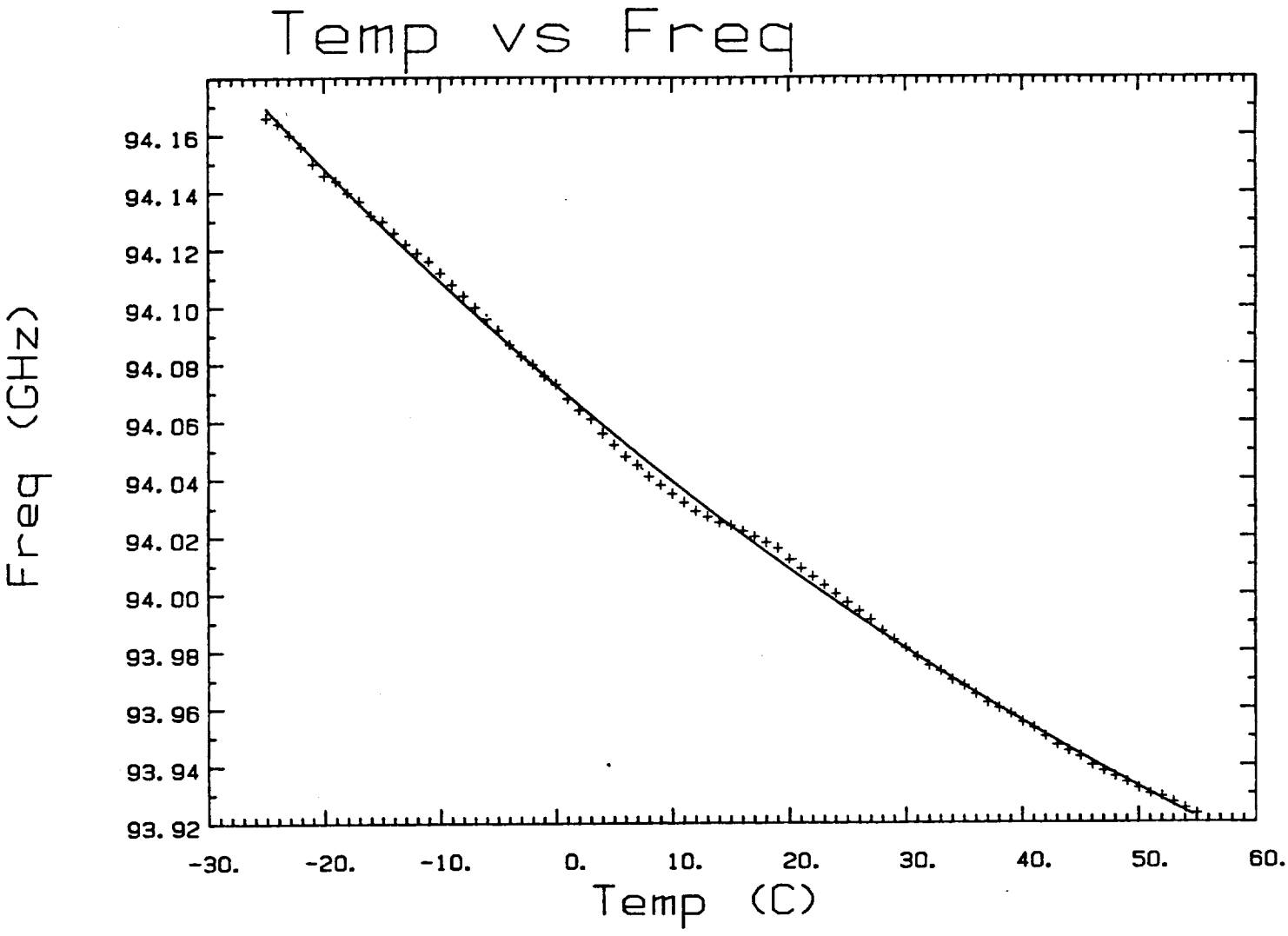

This unit was integrated with the multiplier and rigorously tested. The results of their combined performance are discussed in a later section.

Second Harmonic Design: This design used a 44 GHz InP device, Varian VSQ9119S3, the bias characteristics of which are:

V_{op} = 12 Volts,
I_{op} = 200 mA,
F_{nom} = 44 GHz,
P_{nom} = 250 mW,
Efficiency = 10%

The cavity and resonator dimensions are shown in Figure 3.3-4. This design is very similar to a corresponding GaAs oscillator for these frequencies. The summary of final data on this unit is given below:

Frequency range (mechanical tuning) = 91.4 to 94 GHz.
Power output at 92.6 GHz = 45 milliwatts.
Typical thermal coefficient of frequency = -4 MHz/°C.
Bias tuning range (3 dB point) = 350 MHz.
Backshort frequency pulling = $\pm$70 MHz.

The fundamental-to-second harmonic content ratio for this oscillator is 45/250 or -7.6 dB, which is considered excellent on the basis of a large data base.

This unit exhibited much less load pulling of its operating characteristics than was the case with the high power fundamental mode oscillators. It was tested together with the multiplier for their combined features, which will be presented in the appropriate section. The oscillator conformed rather closely with the theoretical design of the second-harmonic oscillator. Even though the power output was lower than the fundamental mode unit's by 1.5 dB, the drive level was found to be adequate, and resulted in a trouble-free operation.

A leaky backshort was introduced instead of a standard non-contacting short at the same general location. The amount of output through this

FIGURE 3.3-4 - SECOND-HARMONIC InP GUNN OSCILLATOR DETAILS
RESONANT DISK DIMENSION = 0.078"

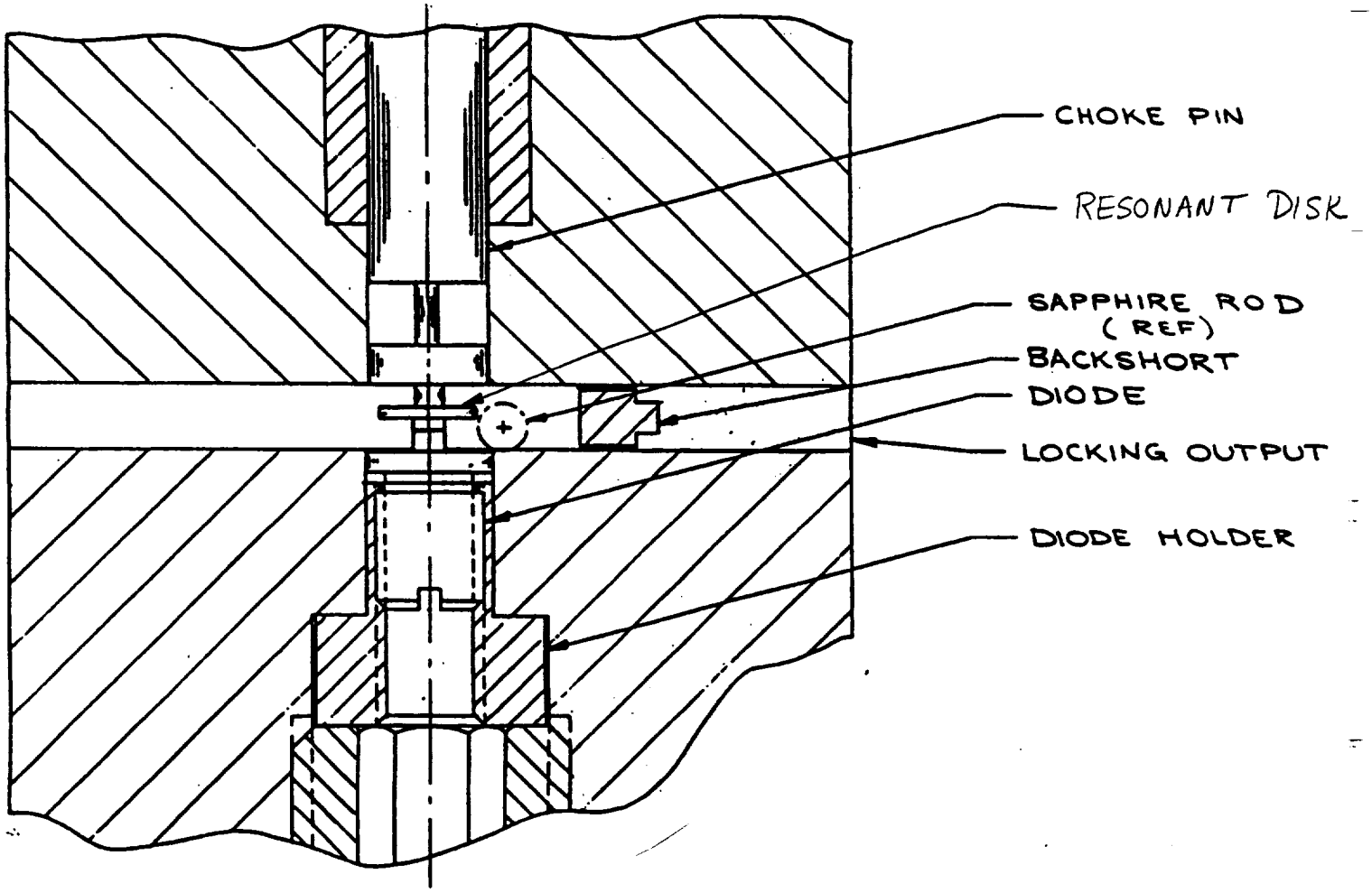

sample port is controlled by the dimensions of the short. The operating frequency and the power output through the main port is not appreciably perturbed by this arrangement. Similar results were obtained by using an appropriate iris at the location of the short.

The oscillator bias tuning characteristics were used to achieve phase locking over a small range around the nominal center frequency. The thermal drift of the oscillator was sufficiently small to allow compensation by bias tuning for realizing the phase lock. The frequency sampling port was connected to a harmonic mixer/diplexer. The details of the phase locking scheme and its performance are presented in Section 4.0.

3.3.5 Recommendations for Further Work

This investigation has established the appropriateness and distinct advantages of InP Gunn devices for high-frequency frequency multiplier driver applications. However, some additional work may be necessary to extend the results to other applications, particularly at higher frequencies. Our key recommendations are:

(a) A program to realize useful power at higher frequencies, well beyond 140 GHz. Higher power output will thus extend the capability of multpliers well beyond what was achievable using GaAs diodes.

(b) Development effort to realize wide-band mechanically and electrically tunable sources for instruments and tunable radiometer applications.

(c) Additional work in third-harmonic operation of Gunn devices.

(d) Mechanical and electrical integration of Gunn oscillators and frequency multipliers.

3.4 CIRCULATORS

3.4.1 Introduction

Research was carried out on ferrite turnstyle circulators to develop a 94 GHz isolator of moderate bandwidth. Reproducibility and economy of fabrication were key issues.

The basic turnstyle design is shown in Figure 3.4-1. The transformer matches the higher waveguide impedance to the relatively low ferrite impedance. The ferrite resonator may be either a triangular or a circular geometry. The triangular resonator has the potential for broader bandwidth[1], but is much more expensive due to the precise machining tolerances required. For this reason a cylindrical geometry was chosen, since reasonable fabrication cost was important.

The frequency of operation for the cylindrical resonator may be determined from the modes allowed to propagate in this structure. The basic modes are shown in Figure 3.4-2; a vertical mode, β, and two counterrotating modes $\beta+$ and $\beta-$.

Non-reciprocal propagation occurs in the ferrite when an axial DC magnetic field is applied as shown in Figure 3.4-3. The magnetic field causes the ferrite permeability tensor to become asymmetric:

$$\mu = \begin{vmatrix} \mu_{xx} & \mu_{xy} & 0 \\ \mu_{yx} & \mu_{yy} & 0 \\ 0 & 0 & \mu_{zz} \end{vmatrix} ,$$

with the off-diagonal elements $\mu_{yx} = -\mu_{xy}$. In the zero field case $\mu_{xy} = 0$ and $\mu_{xx} = \mu_{yy} = \mu_{zz}$.

These off-diagonal elements cause the counterrotating modes $\beta+$ and $\beta-$ to experience different propagation velocities. If the proper ferrite dimensions and DC magnetic bias are selected then the modes, launched by

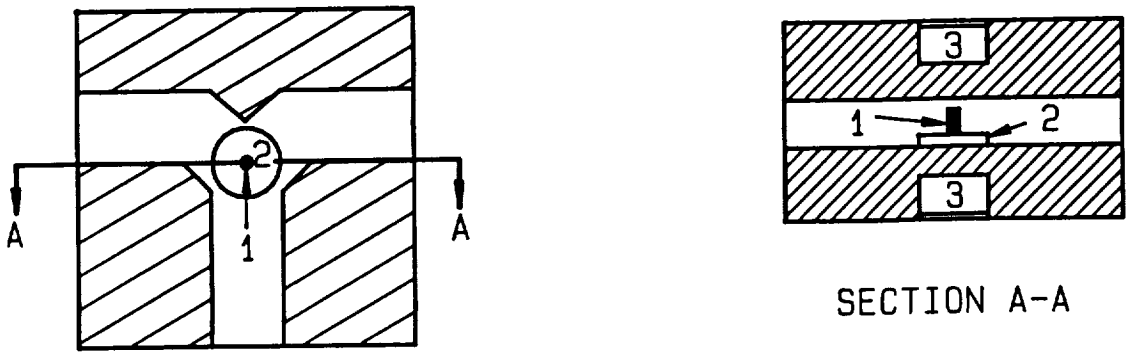

FIGURE 3.4-1 – TYPICAL TURNSTYLE JUNCTION CIRCULATOR SHOWING: 1) THE FERRITE RESONATOR; 2) THE TRANSFORMER; 3) THE MAGNETS.

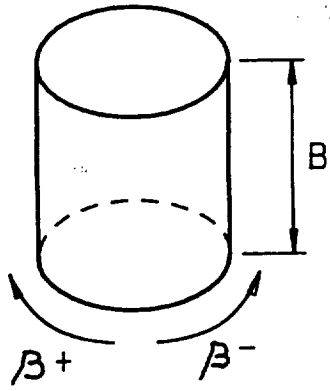

FIGURE 3.4-2 – THREE MODES OF PROPAGATION ARE SUPPORTED BY THE FERRITE RESONATOR; AN IN PHASE AXIAL MODE, B; AND TWO COUNTER-ROTATING MODES β^+ AND β^-.

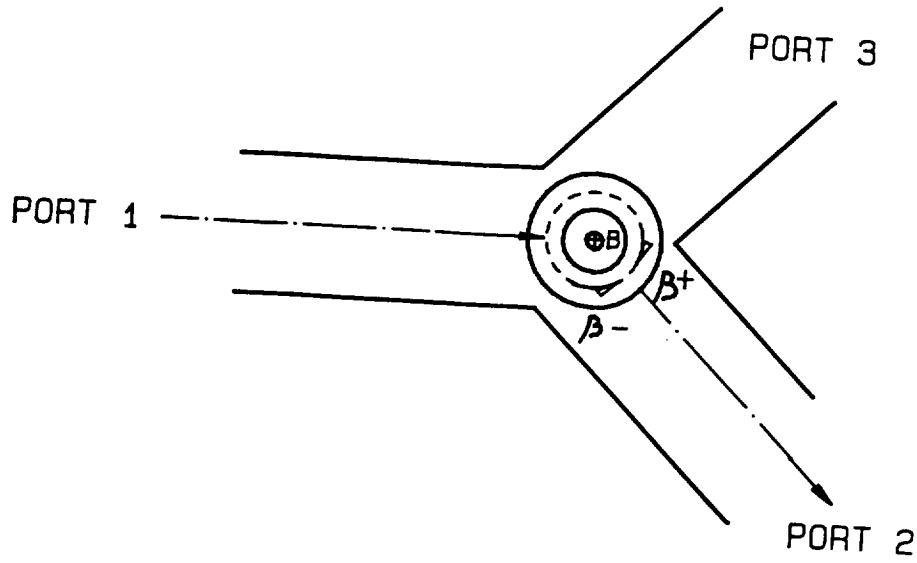

FIGURE 3.43 - TOP VIEW OF A FERRITE RESONATOR BIASED WITH AN AXIAL MAGNETIC FIELD $\vec{B}$. THE RESONATOR DIMENSIONS AND $\vec{B}$ ARE CORRECT FOR CIRCULATION FROM PORT 1 TO PORT 2, WITH PORT 3 ISOLATED FROM PORT 1.

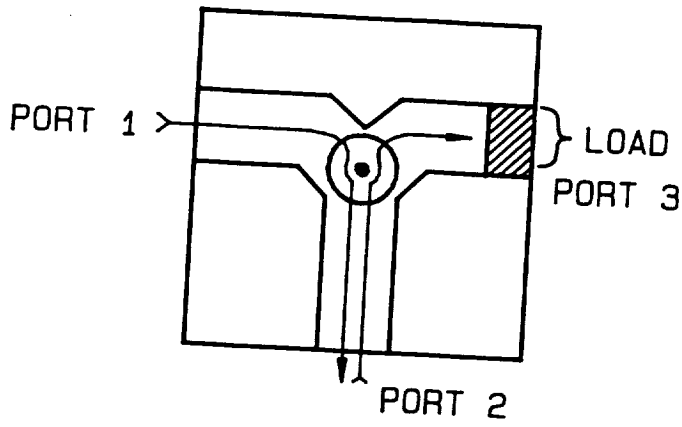

FIGURE 3.44 - THE LOAD AT PORT 3 CAUSES THE CIRCULATOR TO BECOME AN ISOLATOR. A SIGNAL APPLIED AT PORT 1 APPEARS AT PORT 2. A SIGNAL INTO PORT 2 IS ABSORBED AT PORT 3. PORT 1 IS SAID TO BE ISOLATED FROM PORT 2.

a signal incident at port 1, will add constructively at port 2, and cancel at port 3. Thus circulation is said to occur from port 1 to port 2, while port 3 is isolated from port 1. Similarly circulation takes place from ports 2 to 3, and 3 to 1.

A circulator becomes an isolator when one port is terminated in a matched load, as shown in Figure 3.4-4. Isolation takes place due to the fact that although signals may propagate from port 1 to port 2, any reflected or incident signals at port 2 are absorbed by the load at port 3. Port 1 is said to be "isolated" from port 2.

3.4.2 Research

Research was carried out in three basic areas:

(1) the optimal dimensions of a ferrite cylinder for circulation at 94 GHz when a saturating DC axial magnetic field is applied

(2) the correct transformer dimensions for a good match between the waveguide the ferrite

(3) a good load to terminate one of the circulator ports to create an isolator

A saturating DC axial magnetic field is assumed in the selection of the ferrite dimensions, since a saturated state is easy to maintain over temperature. If the ferrite was magnetized at a level below saturation the off diagonal elements μ_{xy} and μ_{yx} would change with temperature due to their dependence on the ferrite's saturation magnetization, a temperature sensitive quantity. This would lead to changes in the propagation constants of the counterrotating modes, which determine the circulation properties of the device.

To obtain an estimate of the ferrite diameter required we refer to the relation given by Denlinger[2]:

$$\frac{1}{2}\frac{\beta diff}{\beta ave} = \frac{2}{3(2n-1)},$$

where

$\beta diff$ = the phase difference between the two counterrotating modes.
βave = the average phase shift of the two counterrotating modes.
n = 1,2,3..., the mode number.

One would like to use n = 1, since this results a large $\beta diff/\beta ave$ ratio (i.e. broadest bandwidth). Unfortunately, at 94 GHz the low saturation magnetization of the ferrite (5250 Gauss) does not permit a solution for n = 1. The lowest order mode with a solution is n = 2.

For n = 2: $\frac{1}{2}\frac{\beta diff}{\beta ave} = 0.22$

Referring to Denlinger it is then found that $D_F/\lambda_o = 0.219$ for n = 2, where D_F is the ferrite diameter. From $\lambda_o = 0.126$ in. at 94 GHz we get $D_F \simeq 0.0276$ in. Estimating that fringing increases the effective diameter by 1.075[2] the actual diameter required is: $D_F/1.075 = 0.026$ in.

Denlinger gives the following phase relation that may be solved for L_F, the ferrite length, once n is known:

$$2\,\beta_o L_F \left(\frac{\beta_{ave}}{\beta_o}\right) = (2n - 1)\ \pi.$$

Using this results in $L_F \simeq 0.068$ in.

This is too long to fit in a WR-10 waveguide (0.050 in. high). For this reason it was decided to try various lengths of ferrite (of 0.026 in. diameter) that could physically fit into the height allowed - even though theory recommended a longer length.

Before proceeding with the ferrite length study, the transformer research should be discussed, since this element was required for the

ferrite tests. As discussed earlier the transformer matches the higher waveguide impedance (i.e. 475Ω) to the lower impedance ferrite (i.e. < 100Ω). Figure 3.4-5 shows the physical layout of the transformer/ferrite combination. At 94 GHz $\lambda g/4 \simeq 0.040$ in. Combining this with $D_F = 0.026$ in. gives $D_{Teff} = 0.106$ in. Once again, the effective diameter is reduced by 1.075 to account for fringing effects. This results in $D_T = D_{Teff}/1.075 = 0.099$ in. Given that the exact ferrite impedance was unknown, since the length was a variable, the transformer height was scaled from known circulators operating at 35 GHz. This resulted in $H_T \simeq 0.017$ in. Later measurements indicated that this was a good value.

Using this transformer the ferrite length study was conducted. Results are shown in Table 3.4-1.

TABLE 3.4-1

Circulator performance as a function of ferrite length, L_F.

L_F(inches)	f(GHz)	Insertion Loss (dB)	Isolation(dB)
0.031	98	1.0	30
0.032	95	1.0	30
0.033	94	1.0	30
0.034	92.8	1.0	30

*The ferrite is saturated by the external DC axial magnetic field, D_F = 0.26 in.

It is observed that for L_F = 0.033 both good insertion loss and isolation are possible at 94 GHz. The insertion loss and isolation were further improved by using small ceramic "tweeking" rods, glued into the waveguide, to optimize the relative phase shifts between the waveguide/transformer/ ferrite assembly. With these rods an insertion loss less than 0.8 dB and an isolation greater than 15 dB were obtained over a 3 GHz bandwdith. Typical results are shown in Figure 3.4-6.

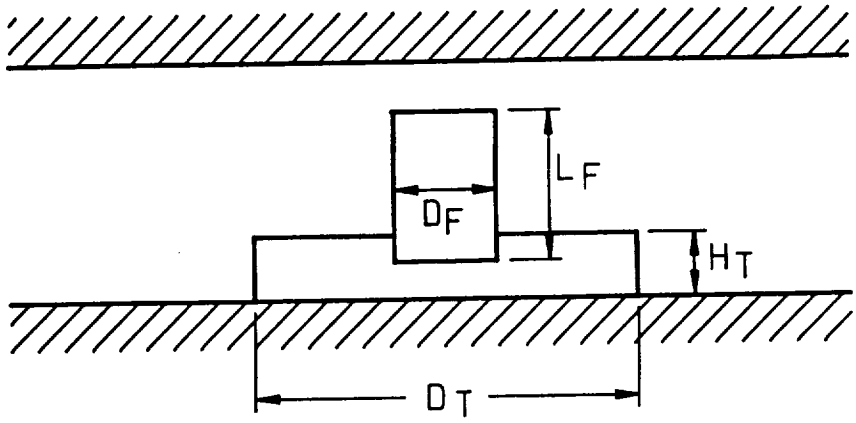

FIGURE 3.4-5 - TRANSFORMER/FERRITE COMBINATION, WHERE D_F= .026", D_T= .099", H_T= .017", AND L_F IS THE VARIABLE.

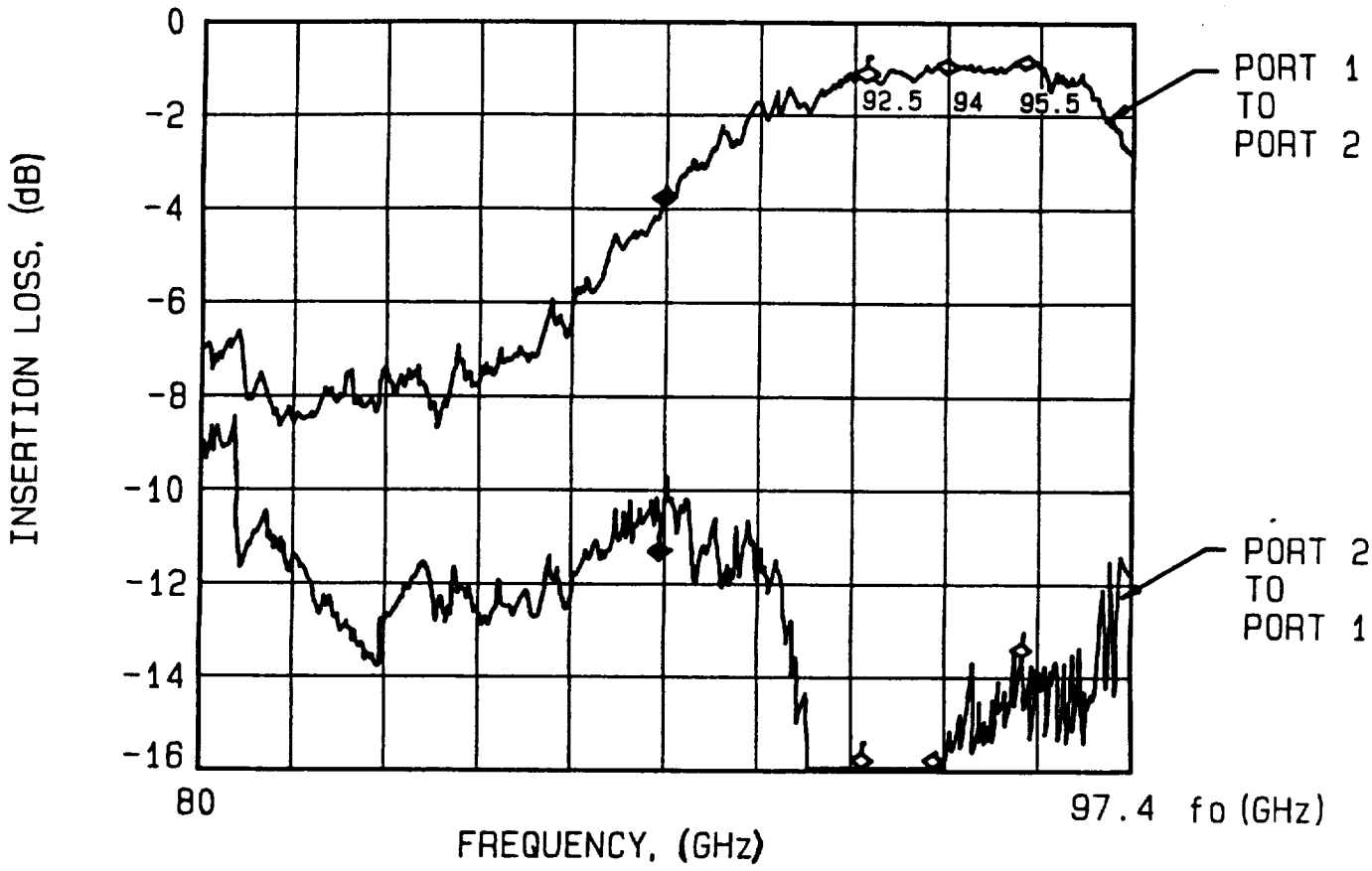

FIGURE 3.4-6

The final area of investigation was the load required to terminate one of the circulator ports to create an isolator. A wedge of Emmerson-Cummings MF-117 absorber was formed, as shown in Figure 3.4-7. The typical return loss was greater than 20 dB over 92 to 96 GHz making this a good load for the 94 GHz circulator. The results in Figure 3.4-6 were obtained using this load.

3.4.3 Conclusions

A cylindrical junction ferrite device was developed at 94 GHz. Previous theoretical work in the field provided good estimates of the transformer and ferrite dimensions, except for the ferrite length. An emperical study of circulator performance versus ferrite length produced a device that gave good performance over 3 GHz bandwidth. This suggests that there are other solutions not predicted by theory.

A well-matched load was also developed to convert the circulator into an isolator for use in a system application.

REFERENCES

1. Helszajn, James, and Nisbet; Circulators Using Planar Triangular Resonators, Vol. MTT-27, No. 2, p. 188, Feb. 1979.

2. Derlinger, Design of Partial Height Ferrite Circulators, MTT, Aug. 1974, pp. 810-813.

3.5 ENVIRONMENTAL TESTS

One of the stated goals for this project was the development of components that are space qualifiable. Due to time constraints, Millitech chose to generically test the most important components used in the system.

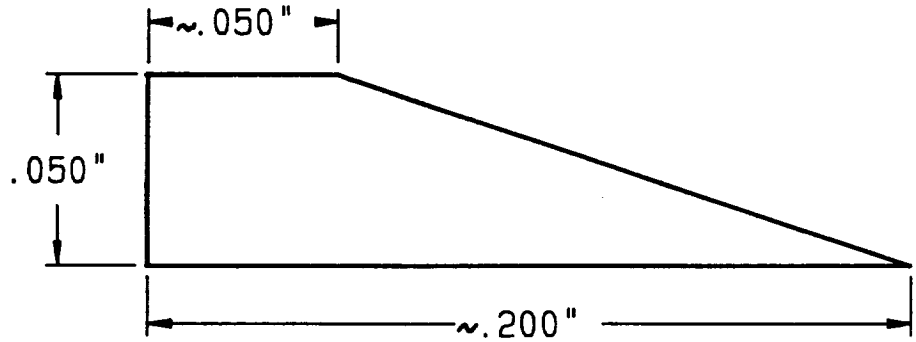

FIGURE 3.4-7 – A WEDGE FORMED FROM EMERSON CUMMING MF-117 ABSORBER MATERIAL. GREATER THAN 20 db RETURN LOSS WAS OBTAINED AT 94 GHz.

3.5.1 Whisker-Contacted Components

Four representative whisker-contacted devices (2 multipliers and 2 mixers) were taken to National Technical Systems for random vibration testing.

Vibration: If the radiometer was launched on the shuttle, the failure mode of a whisker-contacted component would most likely be due to a resonance allowing the whisker contact to be disrupted. A copy of the NTS report may be found in Appendix 3. The components subjected to the following vibration testing showed no change in the DC characteristics (a good indicator of the whisker contact condition) measured before testing.

20 Hz to 50 Hz @ 9 dB/octave
50 Hz to 300 Hz @ 0.15 g^2/Hz
300 Hz to 2 KHz @ -3 dB/octave
3 minutes for 3 axes

Temperature: Whisker-contacted components are often cooled to 20 degrees Kelvin for use in radio astronomy, and survive such temperature excursions without difficulty. All Millitech whisker-contacted components are thermally tested by soaking 8 hours at +50°C, followed by three temperature excursions from -30°C to +50°C. The chamber takes 15 minutes to change from -30°C to +50°C with the components spending an additional 15 minutes at 50°C before starting on the next 30 minute temperature cycle. The DC characteristics are recorded before the temperature cycling and then again at the completion of the test. A total change in the DC characteristics of more than 4% (the measurement error is ~2%) would be considered a failure. The device would then be recontacted and tested again. One in seven contacts will fail during temperature cycling. Contacts surviving this type of temperature testing have a history of remaining stable while in use or in storage, so no further temperature testing on the radiometer whisker-contacted components was considered necessary.

Shock/Impact: Several whisker contacted components in lab use have survived shock due to impact (i.e. being dropped from lab bench height to a linoleum covered concrete floor, ~35 inches). The ability of whisker-contacted components to survive such abuse without degradation of performance or disruption of the contact is probably due to Millitech's fabrication techniques for coolable components.

3.5.2 Low Noise Cryogenic FET Amplifiers

This particular amplifier design has been used for a number of years for cooled radiometer applications. These amplifiers are very reliable for use at 20 K. Best noise performance is at 20 K. Any increase in physical temperature will result in an increase in the amplifier noise figure. It was not known whether elevated temperatures would lead to gain instabilities (which would result in poor baselines when the system was used for spectroscopy), so the amplifier was subjected to further temperature testing. The amplifier gain was monitored from 0°C to +40°C. The results are shown in Figure 3.5-1. The gain increases as the temperature decreases, but most importantly, the amplifier shows no sign of instability as a function of temperature. It should be noted, however, that each measurement was taken only after the amplifier reached thermal equilibrium at each test point.

FIGURE 3.5-1

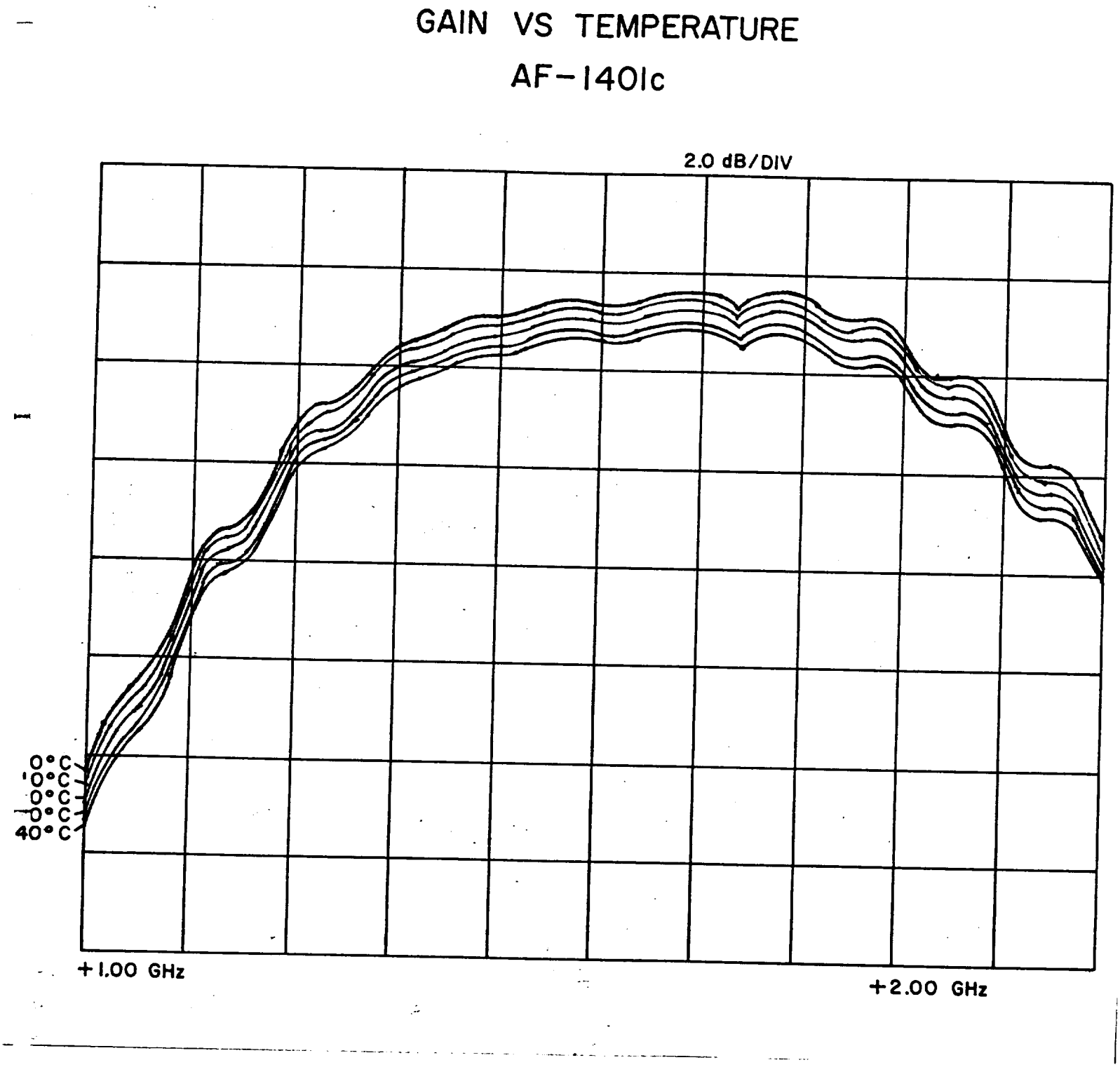

Use or disclosure of data contained on this sheet is subject to the restriction on the title page of this final report.

4.0 SYSTEM SUPPORT ELECTRONICS

The design objective of this system is to provide a compact, low power, frequency agile local oscillator for a submillimeter radiometer. Toward this end, the following list of specifications are listed:

- 92.6 GHz output center frequency
- ±200 MHz tuning range
- Minimum step size or resolution < 16 KHz
- Locking reliability
- Low power consumption
- Small physical size

These objectives were accomplished with a combination of techniques used in standard phase-locked loop systems.

Several types of phase-locked loops can be used to meet the requirements as shown in Figures 4.1-1, 4.1-2, and 4.1-3.

Although several phase locking techniques were initially evaluated and found to meet the requirements, a translation or offset second order type of loop was finally chosen because of the wide frequency tracking requirements and more easily obtainable lock indications available with this type of loop.

4.1 PHASE-LOCKED LOCAL OSCILLATOR

The type of loop chosen for this application is an analog translation loop with a digital phase detector, or that shown in Figure 4.1-3. A brief description of each loop element follows.

VCO: The VCO must be selected to have a monotonic change in its tuning curve and have a high enough tuning sensitivity to relieve the loop amplifier gain requirements. In this case, an Indium Phosphide Gunn effect oscillator is used with bias voltage tuning. This type of oscillator was also developed to provide frequency sampling through a low power back port in order to avoid the need for a coupler.

FIGURE 4.1-1 - ZERO IF TYPE LOOP

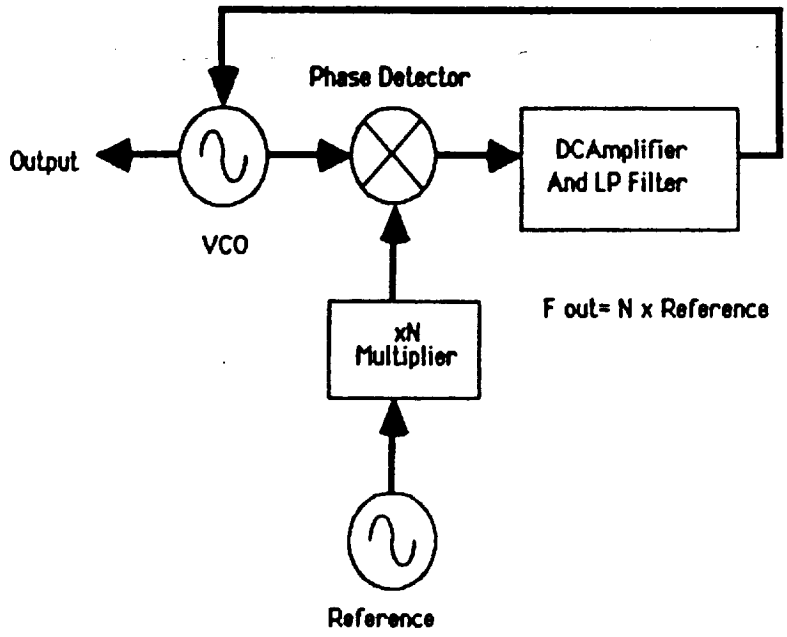

Phase Locked Local Oscillator

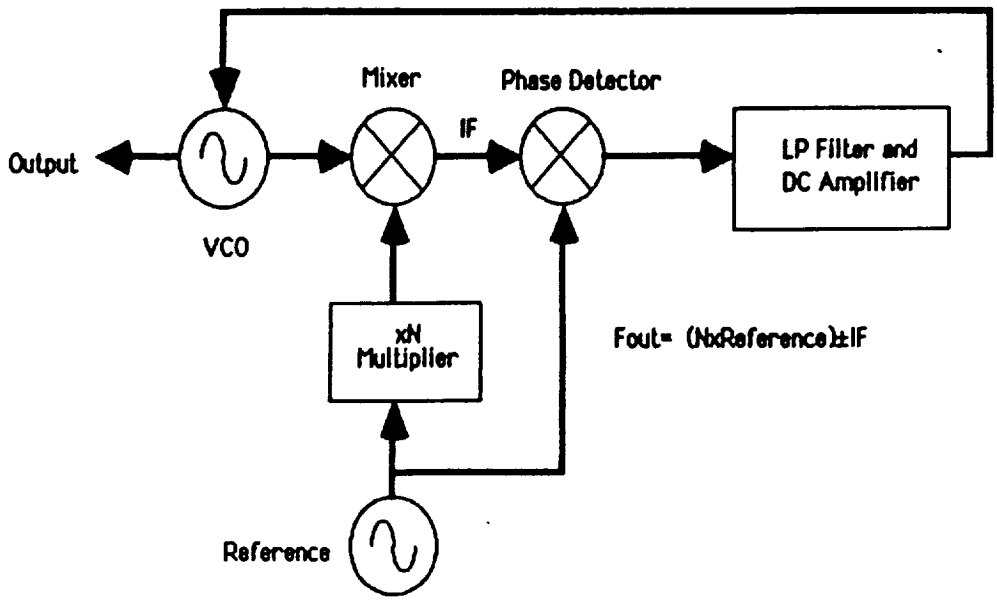

FIGURE 4.1-2 - ANALOG TRANSLATION LOOP

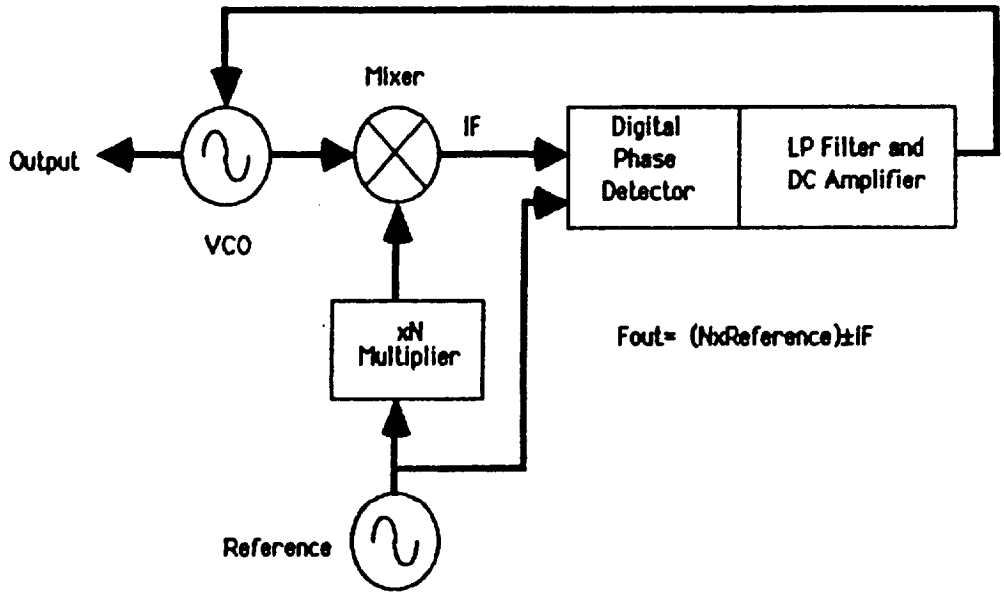

FIGURE 4.1-3 - ANALOG TRANSLATION LOOP WITH DIGITAL PHASE DETECTOR

Mixer: The mixer must have a flat enough response so that large signal amplitude variations don't occur. In this case, a harmonic mixer was chosen so that the multiplication of the reference signal would be simplified.

Multiplier: The multiplier used in this case is actually another phase-locked loop that has a wide enough RF tracking capability to follow the reference excursions and enough RF power to drive the harmonic mixer. Since this is another phase-locked loop with a relatively high power fundamental mode oscillator (100 mW), one other criteria is to avoid interference with the IF chain of the receiver. This was accomplished by choosing the internal high power oscillator's frequency to be just slightly higher than the signal chain's first IF amplifier response. This keeps any spurious response from the multiplier out of the IF pass-band filter. In addition, since most of the high power oscillator response is above the IF amplifier's sensitivity, it tends not to saturate the IF amplifier with out-of-band signals.

Phase Detector: The type of phase detector used is important to the locking characteristics of this type of loop for several reasons. An analog type of phase detector or balanced mixer can only detect phase from $+\pi/2$ to $-\pi/2$ radians difference between the two input signals before its transfer function repeats. This results in the phase detector having the ability to lock at any point where the IF frequency is equal to the reference frequency. In the case of Figure 4.1-3, the upper and lower sidebands generated by the coherent downconversion create two possible lock points for this type of phase detector. The two possible lock points create an inconsistency which usually requires extra circuitry to distinguish and correct for. The digital phase detector is chosen for its ability to detect a full $\pm 2\pi$ radians of phase information between the two inputs and therefore the ability to also distinguish frequency. This allows the phase detector to also become a frequency detector and aid in the locking characteristics of the loop.

Low-Pass Filter and DC Amplifier: These items turn out to be simple op-amp circuits that can provide a wide enough bandwidth to give the loop good frequency response. A DC amplifier turns these changes into bias current variations so that the oscillator tracks the reference.

Several ancillary circuits such as a lock detector and locking aids are also included in this block.

Reference: In this case, a synthesizer provides the reference for the phase-locked multiplier, and the synthesizer's reference (10 MHz), is also the system reference, thereby providing coherency.

4.1.1 Loop Filter Calculations

Loop calculations consist of setting an optimum loop bandwidth to both match the response of the VCO tuning sensitivity and provide a stable control system.

K_V = VCO gain in radians/Volt
$K\phi$ = Phase detector gain in Volts/radian
N = Multiplication ratio = F_{out} divided by F_{ref}
τ_1 = Filter time constant 1 in seconds
τ_2 = Filter time constant 2 in seconds
R_1 = Filter input resistor in Ohms
R_2 = Filter feedback resistor in Ohms
C = Filter capacitor in Farads
ω_n = Natural loop frequency in radians/second
ζ = Damping constant

$$\tau_1 = R_1C \qquad \tau_2 = R_2C$$

$$\omega_n = \sqrt{\frac{K_\phi K_V}{N\tau_1}} \qquad \zeta = \frac{\tau_2}{2}\ \omega_n$$

The requirements of this filter are that it have about 20 kHz bandwidth and a damping factor somewhere around 0.5 and 1, but these figures have

to be determined empirically because of VCO non-linearities, etc. as the loop is tested. The loop damping constant is affected by the delay factor introduced by the divide by 2 counter, and usually is higher than expected to provide ample phase margin and a stable loop.

Given $K\phi$ = 1.59 Volts/radian
K_V = (2π) 130 MHz/Volt
N = 9260

In this loop filter, the final optimum filter values of R_1, R_2, and C were found to be:

$R_1 = R_2 = 5.11\ k\Omega$ C = 1000 pF

Therefore, $\omega_n/2\pi \approx 26$ kHz as is reflected in the spectra of the loop IF.

The damping constant or ζ for these values is ≈ 0.4.

Additional filtering is provided by another passive lowpass filter, directly after the active one. This filter bandwidth is set to be narrower than the previous active filter to steepen the roll-off of the overall response. It also allows for a somewhat independent adjustment of the damping constant.

For the passive case:

$$\omega_n = \sqrt{\frac{k_\phi k_V}{N(\tau_1+\tau_2)}} \qquad \zeta = \frac{\omega_n}{2}\left[\tau_2 + \frac{N}{k_\phi k_V}\right]$$

The values for this filter are again found empirically and result in the following numbers:

$R_1 = 845\Omega$ $R_2 = 2.7\Omega$ C = 2.2μF

These result in the following ω_n and ζ:

$\omega_n/2\pi$ = 1.383 kHz ζ = 0.0568

4.1.2 Loop Operation

Referring to the detailed block diagram of the loop (Figure 4.1-4), the VCO of this phase-lock system is the bias tuned Gunn diode oscillator. This oscillator has dual ports: one high power port to drive the multiplier and a lower power port for frequency sampling. The frequency sampling port is connected through an isolator to the phase-lock loop harmonic mixer. Since this is an offset type of loop, an IF frequency is generated by a predetermined difference of VCO and multiplied up reference frequency. This loop uses 20 MHz as the IF frequency which is derived in the harmonic mixer. This mixer is designed to subharmonically downconvert the 92.6 GHz Gunn output to 20 MHz when driven by a 9.258 GHz source of sufficient power. The 9.258 GHz source is actually phase-locked to the 10 MHz reference of the synthesizer and acts as a simple x92 multiplier in this application. In order to multiply the 9.258 GHz up to the 92.58 GHz necessary to generate a 20 MHz IF, the 10^{th} harmonic is used.

The 20 MHz IF signal is at a relatively low power level (-37 dBm) and first must be amplified to a level (-13 dBm) by the IF strip amplifiers where it can be converted to a square wave (limited) and divided by two. The resultant 10 MHz is then compared to the reference 10 MHz and an appropriate phase error is generated that is then filtered by the abovementioned low-pass filters. The low-pass filters provide a DC voltage proportional both to phase error (when in phase lock) and frequency error (when out of phase lock). The DC voltage generated then is used to control a high power FET transistor which controls bias voltage for the Gunn oscillator.

Lock sensing and indication is provided for by an auxillary digital phase detector. This phase detector can only track the phase difference of the two signals over $\pm\pi/2$ range but gives a positive indication of phase lock because of its digital nature. One disadvantage to this type of detector is that in order to be at midrange, it must have a $\pi/2$ offset between the two input signals. The main phase detector has the

FIGURE 4.1-4 - DETAILED LOOP BLOCK DIAGRAM

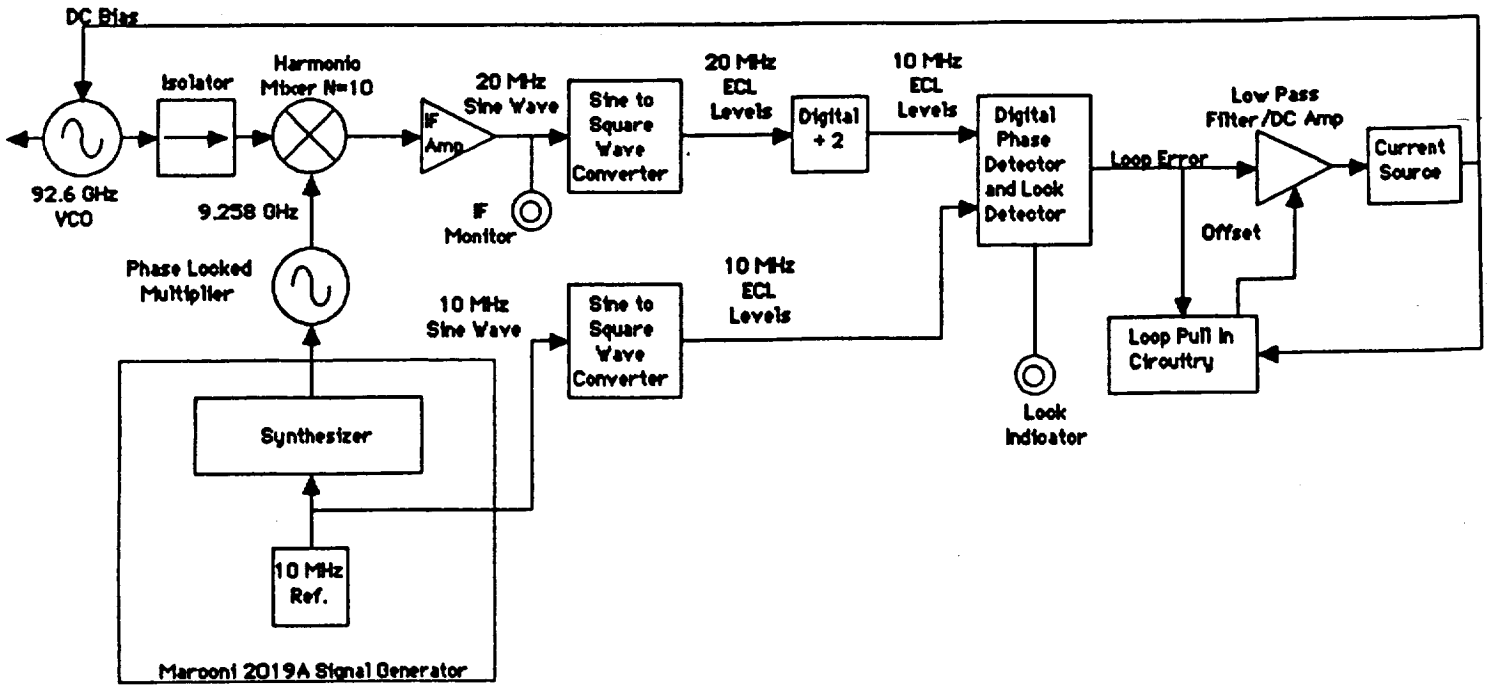

Use or disclosure of data contained on this sheet is subject to the restriction on the title page of this final report.

ability to track phase error over twice that range and at midrange requires zero phase difference. This difference required some compromise in order to show the correct state of the loop. Since the main phase detector can tolerate more phase error than the auxiliary detector, a 90° phase offset was introduced into the loop and the loop gain was increased until with maximum frequency offset, less than $\pm\pi/2$ radians of error was produced. This allows both phase detectors to operate as desired and produce the correct indication of loop state. In an out-of-lock state, however, the main phase detector still provides frequency information in order to steer the loop towards lock-up. For an in-depth description of how both of these phase detectors operate, see Reference 1.

In addition to the lock detection circuitry, two additional circuits help to steer the loop towards lock. Since the IF frequency is at 20 MHz, the opposite sideband is located only 40 MHz away and could cause the loop to hang up in an out-of-lock condition if the main phase detector detects that it is above 20 MHz on the wrong sideband. This state is avoided by detecting it and providing an offset voltage to steer the loop to the correct sideband. The other circuit ensures that the Gunn oscillator is on and providing an IF signal somewhere within the band-pass of the IF strip. If this circuit detects that the Gunn oscillator is not in the proper predetermined operating range, it steers the loop offset back towards lock. As long as these conditions are met the main phase detector provides all steering information to the loop.

4.1.3 Loop Specifications

Gunn oscillator center frequency	92.6 GHz
Tuning range	$\pm$250 MHz
Maximum hold in range (Limited to Gunn electrical tuning)	$\pm$325 MHz

Minimum step size or resolution;	9.2 kHz
DC power consumption	8.85 to 9.45 Watts
Size	Lock box 13 by 7.5 by 7.5 cm Multiplier 10 by 4 by 3.5 cm VCO, harmonic mixer combination ≈6 by 6 by 4 cm

REFERENCES

1. Best, Roland E. Phase-Locked Loops-Theory, Design and Applications, McGraw Hill Co., New York

2. Gardner, Floyd M. Phaselock Techniques, John Wiley and Sons, New York.

3. Motorola, MECL Device Data, Motorola Part #DL122R1.

4. Motorola CMOS/NMOS Special Function Data, Motorola Part #DL130.

4.2 CHOPPER

To tune up a radiometer for maximum performance (lowest noise), you must be able to switch between two temperature loads. A large ΔT is preferred for ease of measurement, so usually a room temp load (~295K) and a load in liquid nitrogen is chosen (77 K). One may, by comparing first one load then the other, come up with a value for the system temperature (T_{sys}). It can be quite tedious to hold each load in the beam, then calculate T_{sys} to see if any improvement has been made by tuning up, so a chopper was built (to be used with a signal-to-noise meter [see Section 4.3]) to facilitate this process. This particular chopper was designed to have a blade size not much bigger than the beam for compactness. The blade size is 4.25 in. in diameter with clearance of 1 5/8 in. The motor speed is 400 RPM.

4.3 SIGNAL-TO-NOISE RATIO METER

The Millitech Signal/Noise ratio meter (block diagram, Figure 4.3-1) is an instrument capable of giving the user information about the noise performance of a sensitive microwave or millimeter wave receiver. The instrument's intended purpose is to allow dynamic tuneup and optimization of a receiver by providing real time display of the receivers Y factor on the front panel.

4.3.1 General Description of Operation

The instrument consists of a very sensitive front end amplifier, a synchronous demodulator, gain adjustment stage and an analog divider. It will perform Y factor calculations based on an input voltage which is proportional to the power output of a receiver when the input of the receiver is being switched between a relatively hot source (ambient temperature) and a relatively cold source (liquid nitrogen). The input switching is performed by a chopper wheel (beam interrupter) rotating at

FIGURE 4.3-1 - SIGNAL/NOISE RATIO METER BLOCK DIAGRAM

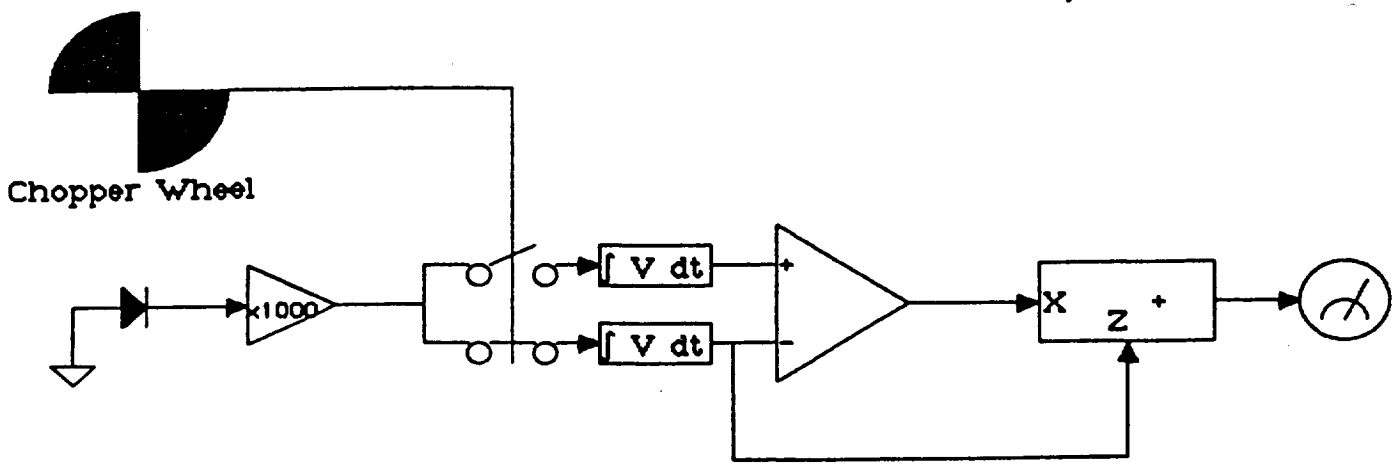

SIGNAL/NOISE RATIO METER

a fixed speed between the RF input of the receiver under test and the cold source. Attached to the chopper wheel is a microwave absorber at room temperature (hot source). The chopper wheel must provide a bistate TTL output indicating which input source (i.e., hot/cold) the receiver "sees". This output is connected to the signal/noise ratio meter and informs the meter which source the receiver is presently viewing.

The detected signal is amplified and synchronously demodulated using the chopper sync signal. The respective signals are then integrated and differenced. An analog divider performs the following calculation:

$$\alpha\ (V_{hot}-V_{cold}) \div V_{cold} = \alpha\ (P_n on - P_n off) \div P_n off = \alpha\ [Y-1]$$

where α = gain constant.

The output of this calculation is then displayed on the front panel meter when in the SWITCHED/TOTAL mode. The gain constant α, is dependent on the front panel RANGE that is selected. Since the front panel meter is calibrated from zero to 100 microamps, we can treat this as a scale from 0.00 to 1.00. Y then becomes:

$$Y = 1 + [\text{meter reading in } \mu\text{amps} \times 10^6 \div \text{range}]$$

An optional phase shifter can be installed so that blanking of the chopper edges can be accomplished. This circuit provides as much blanking of leading and following edges of the input signal as the user desires.

4.4 BIAS SUPPLY

4.4.1 BMX - Mixer Bias Box

The mixer bias supply (BMX) incorporated into the 550 GHz radiometer is a modified version of the standard Millitech BMX. The BMX is designed to provide a constant DC current source to bias the 550 GHz harmonic mixer. It also provides analog meter (0 to 1 V) indication of mixer bias voltage. A buffered voltage monitor point (BNC port) is also provided to measure mixer bias voltage with greater accuracy.

The BMX circuit consists of a low power op-amp with a positive feedback network. An externally adjustable potentiometer enables the user to vary the bias current (80μA to 500μA) in order to optimize mixer performance. The output is limited by back-to-back zener diodes to prevent overvoltage damage to the mixer. A short/operate switch is provided to prevent static discharge into the mixer.

For further information refer to Millitech drawing number B-800122, Mixer Bias Supply Schematic in Appendix 4.

5.0 CONCLUSIONS

The high sensitivity, compactness, and low power consumption of the solid-state submillimeter radiometer, designed and fabricated by Millitech under Phase II of the NASA SBIR program, represents a major breakthrough in the development of practical submillimeter systems. As a result of its outstanding performance, a variety of research and industrial applications are suggested, although cost is still a significant issue. Some of these uses are discussed below.

A major potential use is radioastronomical observations of spectral lines in the submillimeter region. At certain frequencies ("windows") in the submillimeter spectrum, ground-based observations are possible, but not at the 557 GHz frequency of the present system due to atmospheric signal absorption. As such, possible users are research institutions including the National Radio Astronomy Observatory. The study of trace molecules in the Earth's atmosphere is also possible with this instrument, an application which may be of interest to organizations such as NCAR and NASA as well as other groups studying time variability and place-to-place variation in the concentration of particular gasses.

Industrial use of the submillimeter wavelength region has not been highly developed; one reason is the lack of turnkey, easy to use systems. The present radiometer changes this situation appreciably. We anticipate a variety of applications in production process control of such materials as plastic films. Submillimeter systems are presently used for quality control in the production of high voltage cable insulator material. There are undoubtedly many other future industrial applications to be opened up when the cost of such systems is reduced by further development of low cost, high frequency devices.

6.0 APPENDICES

millitech

MilliTech Corporation / Amherst Fields Research Park / Amherst, MA 01002 U.S.A (413) 256-8591 / Telex 466480

APPENDIX 1
SPACE-QUALIFIED SUBMILLIMETER RADIOMETER

PHASE I

31 May 1984

SUMMARY

This report is concerned with certain key elements in the development of a space-qualified submillimeter radiometer. This study is not intended to be all-encompassing but rather deals with aspects which are poorly developed at present. In this study we assume that the mixer itself will be a Schottky diode.

An optimized mixer can be expected to require 1 mW or more of local oscillator power at 290 K. Since probably the greatest difficulty to the realization of a receiver is in providing this much power at a frequency of 550 GHz, we have analyzed the problem of varactor frequency multipliers operating as doublers or triplers. Optimum embedding impedances are found using a computer program which solves the problem for a wide range of power levels. Impedances at harmonics above that of the output are non-critical as long as rather narrow resonances are avoided. A model of a millimeter wave tripler was constructed and embedding impedances were measured. At the first and second harmonics, the model's impedances are nearly optimum, but the third harmonic is nonoptimum. A means of achieving a better match is proposed. An actual tripler at 100 GHz built according to this model operated at only 40% of the expected efficiency, while a doubler in a similar circuit operated at > 60% of theoretical.

Most of this work is directed at 100 GHz output devices, but is readily generalized to higher frequencies, and a 600 GHz output doubler is discussed in some detail, both theoretically and experimentally. An output power of .3 mW seems presently achievable at 600 GHz through a multiplier chain. Improved varactor diodes or a more powerful pump source will be needed to produce the additional power that a mixer will need. As an alternative, the option of a second harmonic mixer appears attractive because an actual mixer shows excellent performance at 560 GHz with a pump power which appears to be achievable with available sources.

Optical elements are essential for many functions in the submillimeter. This report discusses the effect of misalignments in optical paths, and shows where tolerances are most critical. A particularly convenient form of Fabry-Perot interferometer is studied, in which the multiple reflections

occur at normal incidence and thus avoid walk-off losses. A more sophisticated filter is described with a flat passband and good stopband which would make an excellent sideband filter for a mixer. For a mixer or multiplier application a simple high efficiency feed horn is needed, and we describe a corrector lens for a simple conical horn to create equal E and H plane patterns.

All aspects of this work should be useful in the realization of a space-qualified radiometer for 550 GHz. The most feasible approach at present would be a 70 GHz Gunn oscillator followed by two doublers in cascade pumping a second harmonic mixer. The lens-corrected conical feed horn and optical filter elements described here would be needed on the input of this mixer. However, the frequency multipliers are much more generally useful as test sources or local oscillators for receivers throughout the millimeter and submillimeter range. At present no practical alternatives are available above 100 GHz. The optical techniques proposed are also generally applicable to any receivers operating above 100 GHz and should result in more compact and lower loss filter elements.

"NOTICE - SBIR DATA - PHASE I"

This SBIR data is furnished under NASA Contract No. NAS7-926.

It is furnished in confidence with the understanding that it will not, without permission of the Contractor, be used for other than Governmental purposes nor disclosed outside the Government except for evaluation for Phase II selection purposes and under an understanding of confidentiality with the evaluator; provided however, in the event a Phase II contract is awarded as a follow-on to this Phase I contract, the Government may obtain additional rights to use and disclose this data. This Notice shall be affixed to any reproduction of this data, in whole or in part.

MILLIMETER AND SUBMILLIMETER FREQUENCY MULTIPLIERS

Frequency multipliers are useful for a variety of test source and local oscillator applications. At frequencies above ∿100 GHz they are the only compact and practical means to generate the LO needed for a Schottky diode mixer. This work deals with multipliers using Schottky varactor (variable capacitance) diodes with characteristics similar to diodes actually available. These diodes can generate harmonics with high efficiency and with little added noise. A series of optimized multipliers in cascade can, in principle, allow the generation of ∿1 mW of power up to at least 600 GHz, although present devices fall well short of this ideal. The goal of this work is to provide a means to design optimized multipliers by understanding the needed circuit impedances and the means to realize them in an actual circuit.

INTRODUCTION

Penfield and Rafuse (Varactor Applications, MIT Press, Cambridge, 1962) have described in some detail the application of varactor diodes to frequency multipliers, and this analysis serves as a useful guide. It predicts efficiency, optimum drive level, and resistive components of the input and output impedances. However, it assumes optimum drive level, perfect impedance matches at all active harmonics, and short circuits at all others. It does not predict the optimum reactive components of input and output impedances nor does it deal with the more generally encountered cases of:

1) "Overdriven" multipliers (power input greater than optimum).

2) Mismatched loads and their effect on efficiency and input impedance.

3) Mismatched second harmonic idler in the case of the tripler, and the range of optimal values.

4) Arbitrary loads on higher harmonics.

The Millitech analysis uses a computer program (P. H. Seigel, Topics in the Optimization of Millimeter Wave-Mixers, Ph.D. Thesis, Columbia University, 1983) to solve the complete non-linear problem of a variable capacitance diode in the reverse direction, in addition to the forward bias condition of variable capacitance and resistance. The analysis can include up to six harmonics and any set of complex impedances on all harmonics. Inputs are pump power, bias voltage, diode properties, and all impedances. Outputs are optimum input impedance, output power, bias current (if any), absorbed power, and the range of voltages encountered in the diode waveform. This is not an optimization program and will not predict optima in load or idler impedances; they must be solved for by successive estimates. In principle, an optimization routine could be included; but the program is fairly slow to run, and this would raise the costs prohibitively. In general, an educated appraisal plus a few subsequent iterations will get very close to the optimum. However, all results reported are based only upon such estimations and may differ slightly from true optimum conditions.

CHOICE OF DIODE

For purposes of this analysis, the diode chosen is an idealization of an available type from the University of Virginia which has been used in a number of doublers and triplers at $\sim$100 GHz with good results. This diode has a DC series resistance of 8 Ω, $C_J(0)$ = 35 fF and V_B = 22 V. Typically, the true series resistance is actually larger than the measured DC value due to heating effects; therefore 10 Ω was chosen for this analysis. We will assume an abrupt junction C(V) characteristic following theory up to V_B. Through this analysis, we will find the useful range of application of this diode and predict what modifications might be needed for better performance in certain applications.

DOUBLER ANALYSIS

For the first part of this analysis, a 100 GHz output doubler was studied. The input power was varied, and the output power and input and output impedances were computed. Initially, all higher harmonic terminations were set to 0; but subsequently a resonance was discovered in the third harmonic termination, leading to a large reduction in efficiency. Therefore, in later runs, the third harmonic load was set well away from this resonance.

Figure 1 shows the variation in optimum conditions as the power is varied. Note the peak in efficiency near 40 mW input. At lower power, the efficiency drops due to insufficient voltage modulation of the junction capacitance. At optimum, this modulation swings between forward conduction and reverse breakdown. Either reverse breakdown or forward conduction must occur at higher power. Because breakdown may be destructive to the diode, the bias voltage was lowered to maintain a peak voltage at the breakdown limit, while substantial forward conduction occurred as a by-product. This forward conduction dissipates power in the external bias supply and leads to a sharp reduction in efficiency. If the externally dissipated power is subtracted from the input, the conversion of the remaining power occurs at nearly constant efficiency.

HIGHER HARMONIC TERMINATIONS

An interesting effect was observed in the effect of the third harmonic termination upon the efficiency. If this termination is set to an inductive reactance of one-third the input reactance, a great reduction in efficiency occurs. This resonance is plotted in Figure 2 for 40 mW and 80 mW input. Note that for low power a short circuit load is only slightly worse than the best reactive load; while for 80 mW, large inductive loads seem preferred. Including a resistance in series with the load had no effect well outside this resonance. Therefore it is likely that this curve encompasses the most interesting region in the range of third harmonic impedances, and all others are nearly optimum.

MISMATCHED OUTPUT

In most real circuits covering a reasonable bandwidth, it is difficult to maintain well-matched conditions due to the inductance needed for the load. While the real component of the load may remain near optimum, the reactive part will certainly vary. Table 1 shows the effect of a few reactive mismatches, compared to a well-matched load.

TABLE 1

F_{in} = 50 GHz P_{in} = 40 mW

R_S	C_J	Bias V	Bias I	$Z_1(\Omega)$	$Z_2(\Omega)$	$Z_3(\Omega)$	EFFZ
10Ω	35fF	9.0 V	0 mA	40 + 245 i	50 + 125 i	0 + 200 i	59.0
10	35	8.5	.66	30 + 210 i	50 + 50 i	0 + 200 i	39.0
10	35	8.5	.46	30 + 220 i	80 + 50 i	0 + 200 i	45.3
10	35	7.0	.53	26 + 245 i	80 + 190 i	0 + 200 i	45.0

From these results, we see that quite a range of reactive output loads may be acceptable; and if the real part of the load is increased from the most optimum value of 50 Ω to 80 Ω , the impact of a reactive mismatch is lessened. Note that a mismatched output also changes the input impedance so that, in general, the input resistance should be set lower than the most optimum value to allow for such mismatches.

Unfortunately, the number of variables involved does not permit this same analysis at other power levels. However, it is likely to be qualitatively similar.

OPTIMUM CHOICE OF DIODE

The diode properties chosen lead to excellent efficiency at an intermediate input power. For low power (< 20 mW input) the capacitance is too large; and a smaller device should be chosen. A lower reverse breakdown would allow somewhat higher efficiency at low power through the lower R_S possible. The efficiency/power curve scales in power as C_J for a constant $R_S C_J$ product so the optimum parameters may be readily chosen. The Penfield and Rafuse analysis is a good guide to the behavior versus frequency and will not be discussed here.

For the overdriven case, a larger area diode having a similar $R_S C_J$ product but higher capacitance is desirable. A higher V_B is, of course, also desirable.

Table 2 shows the effect of increased capacitance with fixed V_B. Increasing the capacitance at fixed R_S has little benefit and lowers the input impedance substantially, making input matching more difficult. However, by maintaining a constant RC product, the efficiency increases greatly and more than compensates for the lowered impedance level.

TABLE 2

F_{in} = 50 GHz P_{in} = 120 mW

R_S	C_J	Bias V	Bias I	$Z_1(\Omega)$	$Z_2(\Omega)$	$Z_3(\Omega)$	EFF%
10Ω	35 fF	6.3 V	7.0 mA	80 + 180 i	60 + 90 i	0 + 200 i	34.6
10	70	7.1	1.1	25 + 100 i	30 + 50 i	0 + 100 i	34.9
5	70	7.2	2.2	25 + 100 i	30 + 50 i	0 + 100 i	50.9

SUBMILLIMETER DOUBLER

As an extension of these techniques, a submillimeter doubler was studied using similar diode parameters to a device actually constructed. The pump

frequency in this case is 300 GHz, with R_S = 10 Ω, C_J = 3 fF. Because these diodes show little C(V) variation at reverse bias and a rather low breakdown voltage, the reverse voltage was limited to ∿2.5V. This doubler shows a theoretical efficiency of 19% at 5 mW input and would make an ideal LO source when pumped by a doubler or tripler. The highest pump power to be expected at this frequency is ∿10 mW, leading to a somewhat lower efficiency, 17%, since the diode is already overdriven at 5 mW input. The input and output impedances seem high enough to be easily matched. The model actually constructed worked very well, showing ∿7% efficiency at 15 mW input but significantly reduced efficiency at lower input power, contrary to these predictions. However, this behavior is probably due to a reactive impedance mismatch which becomes more severe at reduced power, as the optimum reactance increases.

This device could be studied in more detail; but for the calculations to be meaningful, the actual C(V) behavior and reverse breakdown voltage are needed. These are not known in detail, although they certainly are measureable. Results of a few calculations are shown in Table 3.

TABLE 3

f_{in} = 300 GHz C_J = 3 fF R_S = 10 Ω V_B = 2.5 V

P_{in}	Bias V	Bias I	$Z_1(\Omega)$	$Z_2(\Omega)$	$Z_3(\Omega)$	EFF(%)
5 mW	0.1 V	2.6 mA	70 + 125 i	100 + 66 i	150 i	19.4
10	-0.1	6.0	70 + 80 i	100 + 50 i	150 i	16.6
15	-0.2	8.8	70 + 50 i	100 + 30 i	150 i	15.3

TRIPLER ANALYSIS

Penfield and Rafuse showed that a frequency tripler using abrupt junction varactors cannot work without "idler" currents at the second harmonic. Thus a tripler requires a minimum of three tuned circuits; and higher harmonics must be considered as well. The larger number of free parameters makes a tripler more difficult to analyze.

SECOND HARMONIC IDLER

In this program, we first studied the importance of the idler termination at a low input power and its effect on efficiency and input impedance. This study is shown in Figure 3 where the input resistance and efficiency are indicated for varying idler impedance. We find the optimum idler is inductive and of a reactance half that of the optimum input reactance. This curve is fairly broad; therefore, this termination should not be too difficult to achieve in practice over a reasonable tunable bandwidth. The resonance is sharper in the optimum input resistance, indicating that any practical tripler should have lower than optimum input resistance to accomodate an idler mismatch. Resistance in series with the idler termination can produce a large reduction in efficiency and is discussed by Penfield and Rafuse. The cases studied here agreed fairly well with their analysis.

For all further studies, it was assumed that the idler impedance was optimized and lossless in order to limit the number of free parameters.

HIGHER HARMONICS

As in the case of the doubler, a resonance is observed in the next higher harmonic (the fourth), causing a substantial reduction in output as shown in Figure 4. This behaves much like the third harmonic in the case of the doubler but has an even larger effect; and we will assume all terminations are comparable outside the vicinity of this resonance.

Harmonics higher than the fourth were not investigated in detail. A weak resonance is seen in the fifth harmonic similar to that in the fourth, but its effect is only $\sim$10%, and it is rather narrow. Outside this, all terminations seem comparable.

TRIPLER OPERATION VERSUS INPUT POWER

Assuming optimized second and fourth harmonic terminations, a study was made of efficiency versus pump power for the same diode parameters and output frequency as for the doubler. The results are plotted in Figure 5(a).

Note that the optimum input power is less than for the doubler. This is largely due to the lower input frequency which produces larger voltage swings for fixed capacitance. The saturation behavior is very similar, and it is noteworthy that the peak efficiency is only ~10% lower than that for the doubler.

Figure 5(b) shows the optimum input and output impedances over the same range of input powers. The second and third harmonic reactances are not shown, but are one-half and one-third the input reactance, respectively.

OPTIMUM CHOICE OF DIODE

The diode properties chosen lead to excellent low power performance. However, if very low power inputs were involved, the reverse breakdown could be reduced (which would reduce R_S) or the capacitance could be reduced for a fixed V_B. For high power operation, more capacitance or V_B is needed. To demonstrate the effect of capacitance, an alternate diode having the same R_S and V_B but twice the capacitance was considered. Note that this diode has half the cutoff frequency. For the fairly overdriven case of 80 mW input, this diode has higher efficiency than the low capacitance version by 16%. If the series resistance is halved to maintain the same cutoff frequency, the efficiency increases by 48%. The results are shown in Table 4. A secondary consideration is the effect on input impedance. As the capacitance increases, Z_1 decreases and eventually becomes too low for convenient matching. However, for 70 fF diodes, this is still conveniently high. Another consideration is increased sensitivity to idler losses, because a fixed idler resistance will cause more loss for a lower R_S diode. Two cases were compared here with an idler resistance of 5Ω, and the higher capacitance diode remained superior.

A higher breakdown voltage would be better, but this is limited by semiconductor properties and is more difficult to increase than simply making a larger area diode.

TABLE 4

V_B = 22 V F_{in} = 33 GHz P_{in} = 80 mW

R_S	C_J	Bias V	Bias I	$Z_1(\Omega)$	$Z_2(\Omega)$	$Z_3(\Omega)$	$Z_4(\Omega)$	EFF(%)
10 Ω	35fF	5.5 V	7.0mA	200 + 280 i	140 i	70 + 85 i	200 i	23.9
10	70	6.7	2.1	60 + 164 i	80 i	35 + 50 i	200 i	27.7
5	70	6.4	3.9	70 + 152 i	70 i	35 + 40 i	200 i	35.3
5	70	6.3	3.6	70 + 152 i	5 + 70i	35 + 40 i	200 i	31.0
10	35	6.9	5.6	200 + 280 i	5 + 140i	70 + 85 i	200 i	21.1

BIAS CONDITIONS

Throughout this analysis, the peak reverse voltage was maintained at $\lesssim$22 V to avoid operation in the reverse breakdown region. Exceeding breakdown may lead to immediate diode failure or reduced lifetime. However, in a real device, there is no way to monitor the actual diode voltage, but there is a way to estimate the actual voltage through a combination of bias voltage and current. Figure 6 shows a plot of calculated data points obtained at a limiting voltage of $\sim$22 V for doublers and triplers. While these points have a lot of scatter, a trend is clear; and a conservative choice would be to bias below any points. However, this approach leads to lowered efficiency since these points are all at optimum bias. Experience indicates that much higher bias voltage is possible in actual operation. In an actual series of triplers built for 90 - 110 GHz using a diode believed very similar to the model diode, bias conditions in operation have fallen on a line shown at the top of Figure 6. This load line appears to be safe since no failures have occurred as a result of this operation. However, this does not mean that reverse breakdown is not exceeded, only that for this diode it is nondestructive. Note also that points for the tripler lie below most doubler points, due probably to the lower pump frequency for triplers.

TRIPLER MODELING

In an effort to better understand the embedding structure of practical multipliers, and to compare theory with practice, a large size scale model

of a successful 100 GHz tripler design was built. A cross-section of this tripler is shown in Figure 7. This model was made in a way which allowed a coaxial line to reach the effective diode terminal plane in the tripler by passing down the inside of the coaxial choke. In this way, the diode embedding impedances could be measured and compared to the computer predictions. No actual tripler operation of this model was attempted.

The actual tripler has an input in reduced height K_a waveguide, which couples to a coaxial line. The coaxial line has a bias filter on one side of the waveguide and a low pass filter on the other side to allow pump power to reach the diode, which is mounted in the output waveguide. This filter has a stop band which includes the second and third harmonics. To provide the proper inductance at the input a coaxial resonator is included in series with the contact whisker, which is $\lambda/6$ long at the input. This line appears as an inductance at the pump but is $\lambda/2$ long at the output and thus has no effect there. The output waveguide is reduced height, with the width chosen to prevent propagation of the second harmonic over the full band. Both waveguides are provided with tuning backshorts.

The available signal generator covered 2 - 8.5 GHz, and to cover three harmonics, fixed the scale factor at 13.5. Both input and output waveguides were equipped with contacting backshorts and their other ends terminated in absorbing foam. The DC bias choke was eliminated in the model for simplicity and replaced by a short to the waveguide wall, since this choke is known to approximate a short.

Embedding impedances were measured with an HP network analyzer over the range of backshort tuning, and circles were fitted to the data on Smith Chart plots.

Impedances were measured in the three harmonic bands corresponding to 90 - 110 GHz output. These are 2.2 - 2.7 GHz (first harmonic), 4.4 - 5.4 GHz (second harmonic) and 6.6 - 8.1 GHz (third harmonic). Peak efficiency occurs at ∿97 GHz (scaled harmonic frequencies of 2.4/4.8/7.2 GHz). The input impedance varies somewhat over the band due to the coaxial resonator, but the mean value is close to optimum. The data show an imput impedance of 50 + 330 iΩ is achievable at 2.4 GHz, which is very close to the low

power optimum. At the second harmonic the impedance varies considerably, but is inductive over nearly the full band of interest, reaching the optimum inductance near mid-band. At the upper end of the band the inductance becomes too large, but may be reduced by bringing the backshort close to the diode plane. The result is that only a single maximum is found in the output backshort tuning at frequencies much above that where the efficiency peaks. This behavior has been observed in the actual triplers. An idler impedance of 90 i Ω to 140 i Ω is possible at 4.8 GHz depending on the output backshort setting. The higher value is close to the optimum of 170 i Ω and is attainable by avoiding the closest tuning peak. The output impedance is very weakly dependent on the frequency since the coaxial resonator is on resonance. This impedance is found to be quite non-optimum. An output impedance range of 10 + 110 i Ω to 50 + 160 i Ω is attainable depending on backshort tuning. This does not permit a simultaneous match to the real and imaginary components of the optimum load of 40 + 120 i Ω and reduces the output coupling to ~80% of optimum. An analysis of the data shows that a nearly optimum impedance could be achieved with comparable whisker inductance but half the waveguide impedance (waveguide reduced to 1/4 height). While this is easily done at 100 GHz, it becomes progressively more difficult at higher frequencies; so another approach is needed in submillimeter applications. This alternative may be less whisker inductance, but of course this affects the input and idler impedances and requires a complete re-analysis.

If these results are compared to the theoretical efficiency predictions, we find that 40% efficiency is expected, while the measured value is 16% at best. The discrepancy seems rather large, but it is important to recognize that circuit losses are not considered, and there is also the possibility that the real circuit impedances do not exactly equal those predicted. In order to test the predictions it is necessary to estimate circuit losses and while this is rather uncertain, they are likely to exceed 2 dB. The efficiency will also be lowered if the varactor shows a capacitance variation which is less than the abrupt junction behavior. It is fairly clear that real multipliers can be expected to show considerably lower efficiency than idealized predictions.

It is perhaps a better test of the model to compare the predicted frequency response to what is observed, and here the agreement is better. The input match variation does not produce a substantial effect over the 90 - 110 GHz band, but the idler impedance varies sufficiently to produce a factor of 2 reduction in efficiency at the edges of the band, and this is just what is observed. The output impedance variation is too slight to have any significant effect.

COMPARISON OF PRACTICAL DOUBLERS AND TRIPLERS

While no similar scale model of a doubler has been made, an actual doubler at 100 GHz has operated with an efficiency of 25 - 30% at an input power of 80 mW, using a design very similar to the tripler previously described. This compares to the 42% efficiency predicted for this power input. Thus the doubler operates closer to the predicted efficiency, and in the absence of embedding impedance data we can not say whether even better performance is possible.

Since input and output circuit losses should be similar for both devices the greater discrepancy in the case of the tripler is likely to be due to idler circuit loss. This result does not mean that a doubler is preferred for every application, since it requires a higher pump frequency where less power is available.

While no higher frequency doublers have been built, triplers have been consructed using this design up to 300 GHz. One unit at 285 GHz produced $\sim$ 2 mW output with 20 mW input. This result was obtained with a diode having $R_s = 10\ \Omega$, $C_j\ (0) = 20$ fF and $V_B = 20$ V. This device has a predicted efficiency of 28% at 20 mW input, which becomes 23% if we correct for the expected output mismatch.

The ratio of actual to predicted output of 0.45 shows that whatever the mechanism of loss may be, it does not increase significantly with frequency. Probably the limiting frequency for triplers is determined by the complexity of the required circuit, and not actual circuit losses.

A meaningful comparison between triplers and doublers is best made by comparing outputs producible at a given frequency, with available sources. To

use the example of 285 GHz, with a Gunn oscillator pump source, a doubler approach would require 2 units in cascade. The pump would then be at 71 GHz where Gunn oscillators produce ∿50 mW. If the first doubler operates at 30% efficiency, and the second at 20%, the net output is 3 mW. This is somewhat better than the tripler, but perhaps not enough so to make up the extra complexity. The exact comparison in this case depends on the details which need experimental confirmation. It also depends on the power versus frequency curve for Gunn devices, so that at much higher frequencies the cascaded doublers are preferred while at lower frequencies the triplers and doublers are about the same.

Three mW at 285 GHz should be sufficient to be doubled again to 0.3 mW at 570 GHz, if we assume that a real doubler at this frequency will operate at half of the theoretical efficiency. This is probably not quite sufficient to optimally operate a cooled mixer at this frequency. However, with better varactor diodes, efficiencies at all frequencies may be increased by a factor of ∿1.2, raising the output to 0.5 mW, which is almost certain to be enough.

A tripler is probably not practical for this frequency because of the greater circuit complexity. The very small size would almost certainly prevent the realization of a proper idler termination and result in very low efficiency.

HARMONIC MIXER

As an alternative to a fundamental mixer, and the attendant problems of obtaining sufficient LO power, a harmonic mixer presents certain simplifications.

A direct comparison has been made with the same mixer operated in both fundamental mode and harmonic mode at 557 GHz. This is possible because a harmonic mixer may be used as a fundamental mixer by LO pumping through the signal port and simply ignoring the usual pump waveguide.

This mixer operated with a receiver noise temperature of 5500 K SSB at room temperature in fundamental mode, and at 8000 K SSB in a second harmonic

mode. In both cases, a 40 K IF amplifier at 1.4 GHz was used. In harmonic mode, the pump power was only ∿3 mW which was provided in this case by a tripler of the type discussed in this report, with an 80 mW klystron pump. The rather small difference in performance in the two modes plus the much greater simplicity of the harmonic mode makes it a very attractive alternative for applications where reliability is important. The much smaller size may allow a cancellation of the system noise disadvantage through a second receiver in the opposite polarization, which provides redundancy should one channel fail.

This particular option bears further study to determine the limitations of harmonic operation. It may in fact be possible to achieve even better performance with an optimized mixer.

FIGURE CAPTIONS

Fig.1(a) Efficiency and output power versus input power for a doubler pumped at 50 GHz. Diode parameters: $C_J(0) = 35$ fF, $R_S = 10\ \Omega$, $V_B = 22$ V. (b) Input resistance and reactance for the same doubler, and output resistance. Output reactance is one-half the input reactance.

Fig.2 Efficiency versus third harmonic reactance for a doubler at 40 and 80 mW input. Input frequency 50 GHz, $C_j(0) = 35$ fF, $R_S = 10\ \Omega$, $V_B = 22$ V, $R_3 = 0$.

Fig.3 Efficiency and input resistance for a tripler versus second harmonic reactance. Input power 10 mW, $C_J(0) = 35$ fF, $R_S = 10\ \Omega$, $V_B = 22$ V, $R_2 = 0$.

Fig.4 Efficiency versus fourth harmonic reactance for a tripler at 20 mW input. Input frequency 33 GHz, $C_J(0) = 35$ fF, $R_S = 10\ \Omega$, $V_B = 22$ V, $R_4 = 0$.

Fig.5(a) Efficiency and output power for a tripler pumped at 33 GHz. Diode parameters $C_J(0) = 35$ fF, $R_S = 10\ \Omega$, $V_B = 22$ V.
(b) Input resistance and reactance and output resistance for the same tripler. Second harmonic reactance is one-half X_1, output reactance is one-third X_1.

Fig.6 Bias voltage and current for multipliers operated at the breakdown limit. Circles are for doublers, triangles are for triplers. Solid line is the operating line for an actual tripler.

Fig.7 Cross-section of a millimeter wave tripler as modeled in this study.

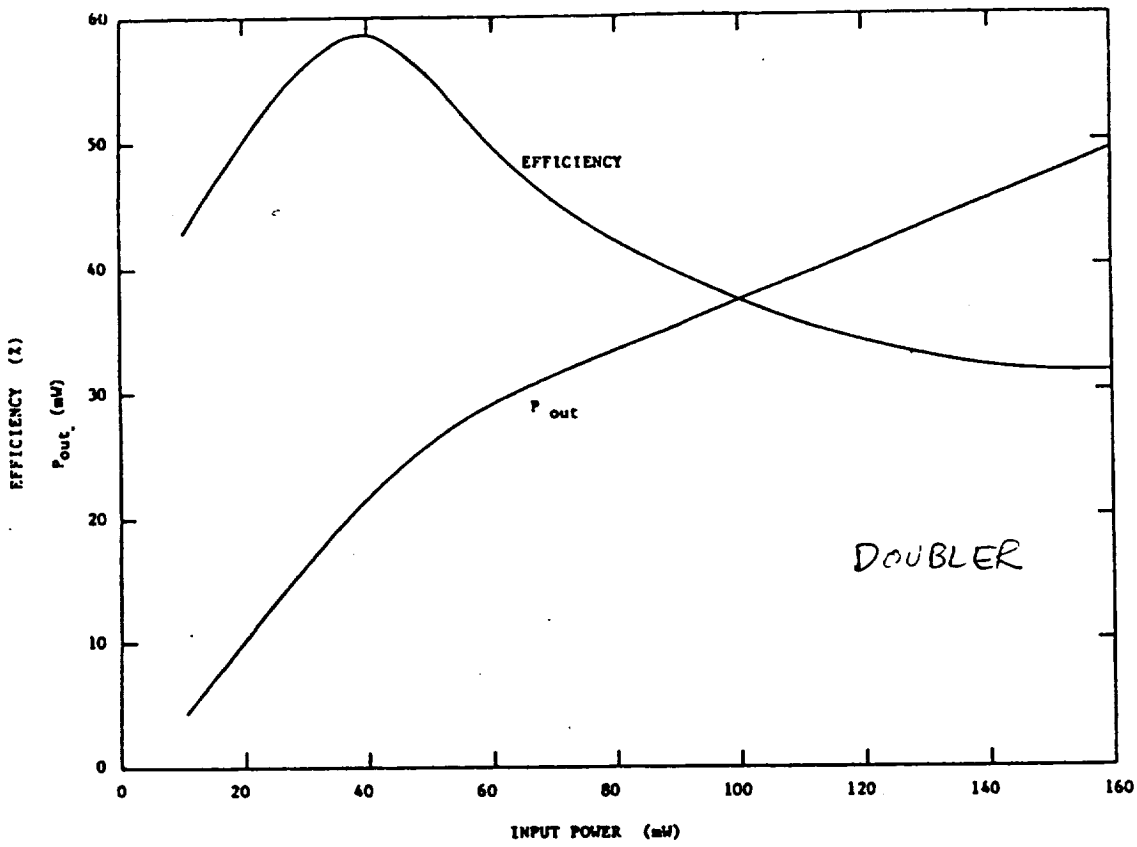
EFFICIENCY (%)
P_{out} (mW)
EFFICIENCY
P_{out}
DOUBLER
INPUT POWER (mW)

Fig. 1 (a)

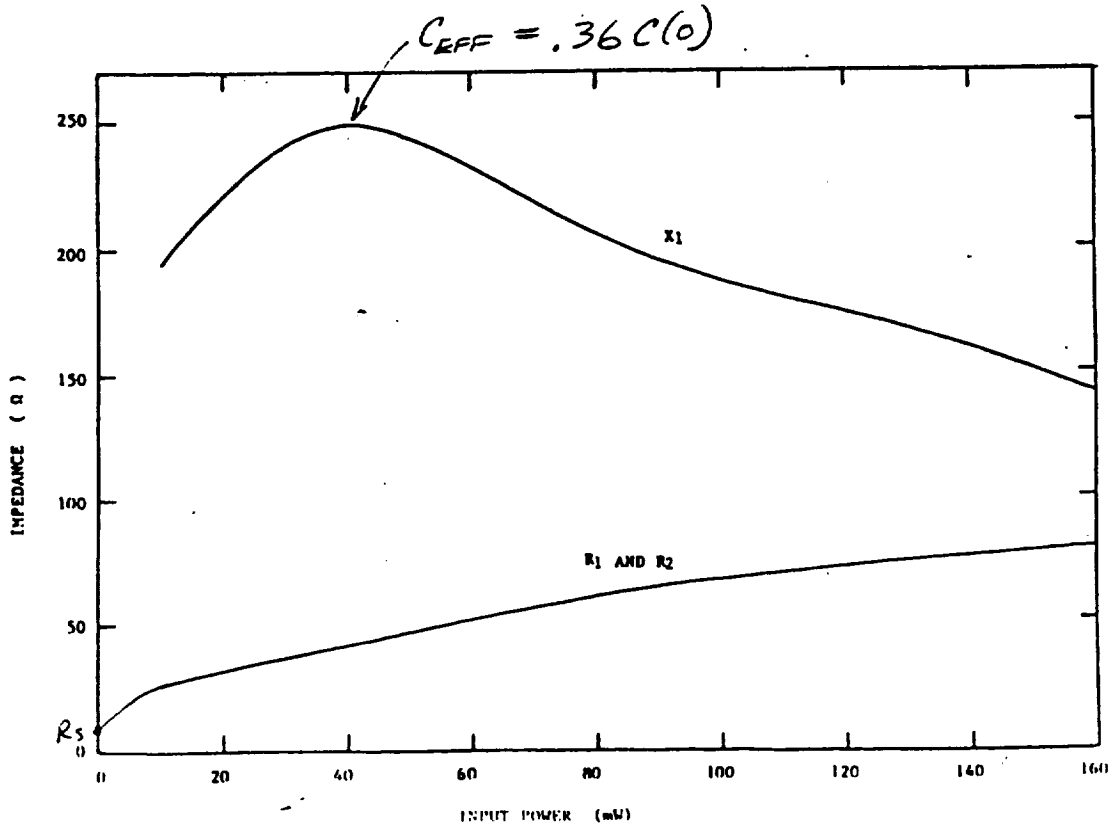
$C_{EFF} = .36\,C(0)$
IMPEDANCE (Ω)
X1
R_1 AND R_2
R_S
INPUT POWER (mW)

Fig. 1 (b)

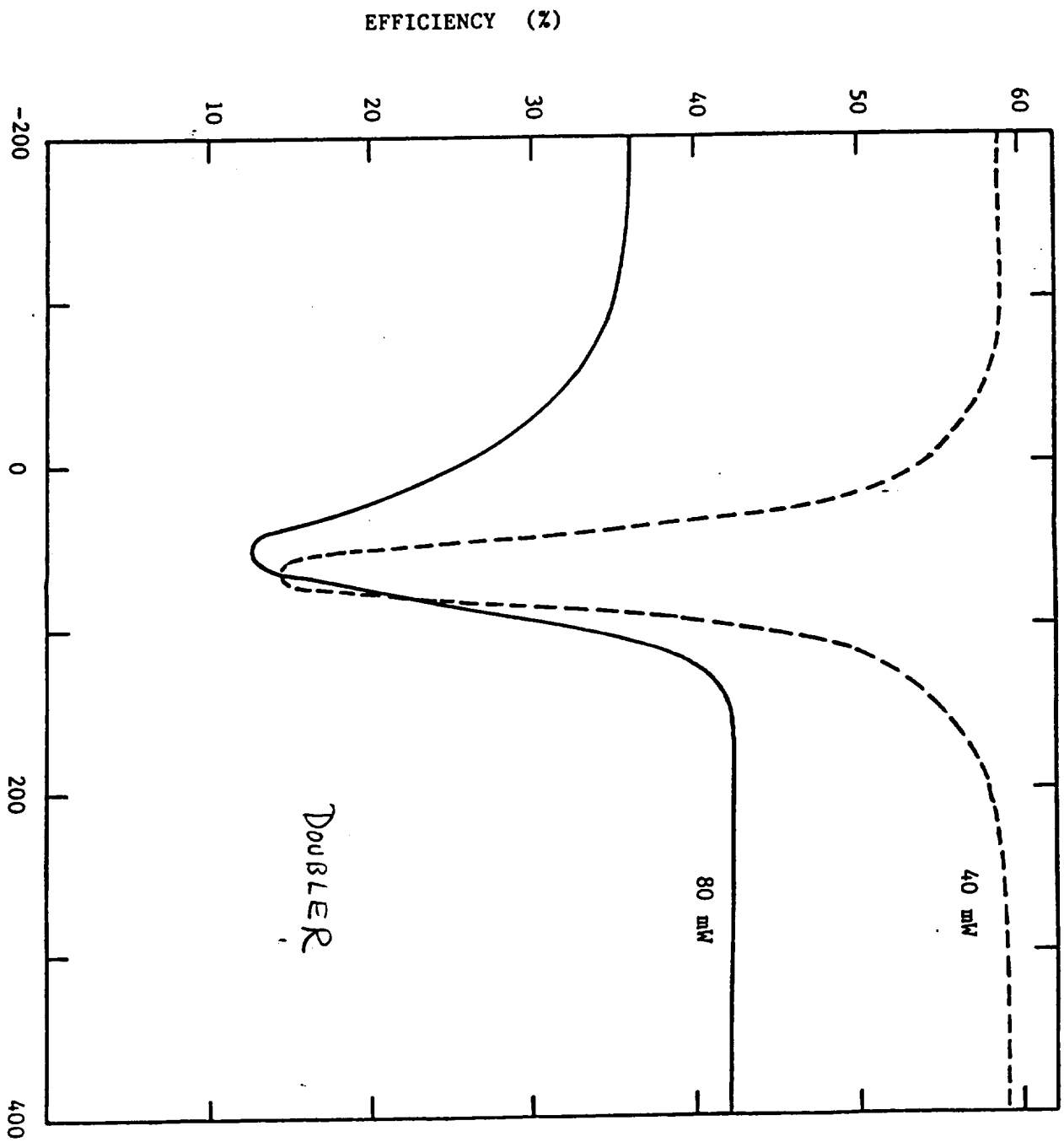
EFFICIENCY (%)
10
20
30
40
50
60
-200
0
200
400
X_3 (Ω)
R_3 = 0
DOUBLER
80 mW
40 mW

Fig. 2

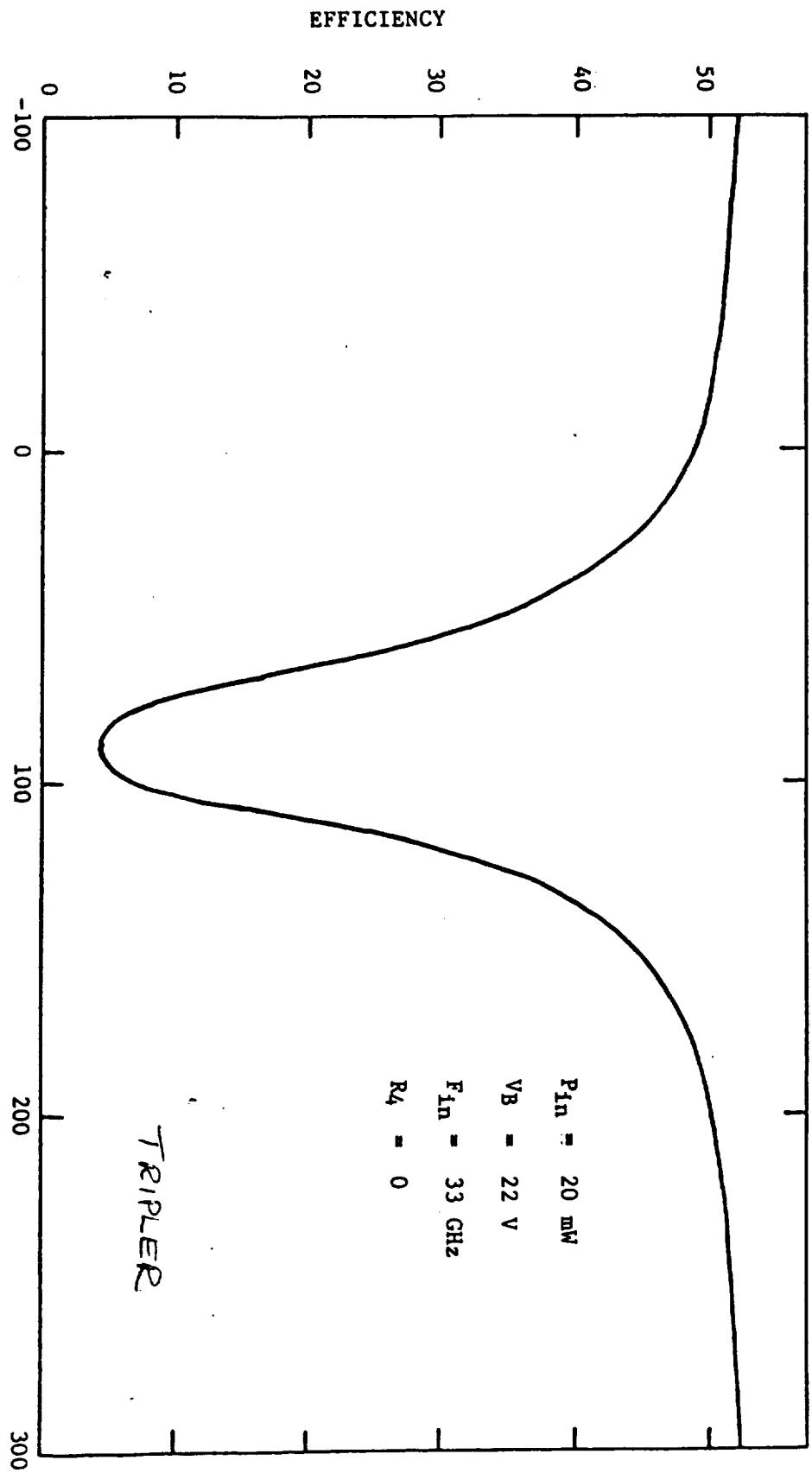
EFFICIENCY
0
10
20
30
40
50
-100
0
100
200
300
X_4 (Ω)
P_{in} = 20 mW
V_B = 22 V
F_{in} = 33 GHz
R_4 = 0
TRIPLER

Fig. 4

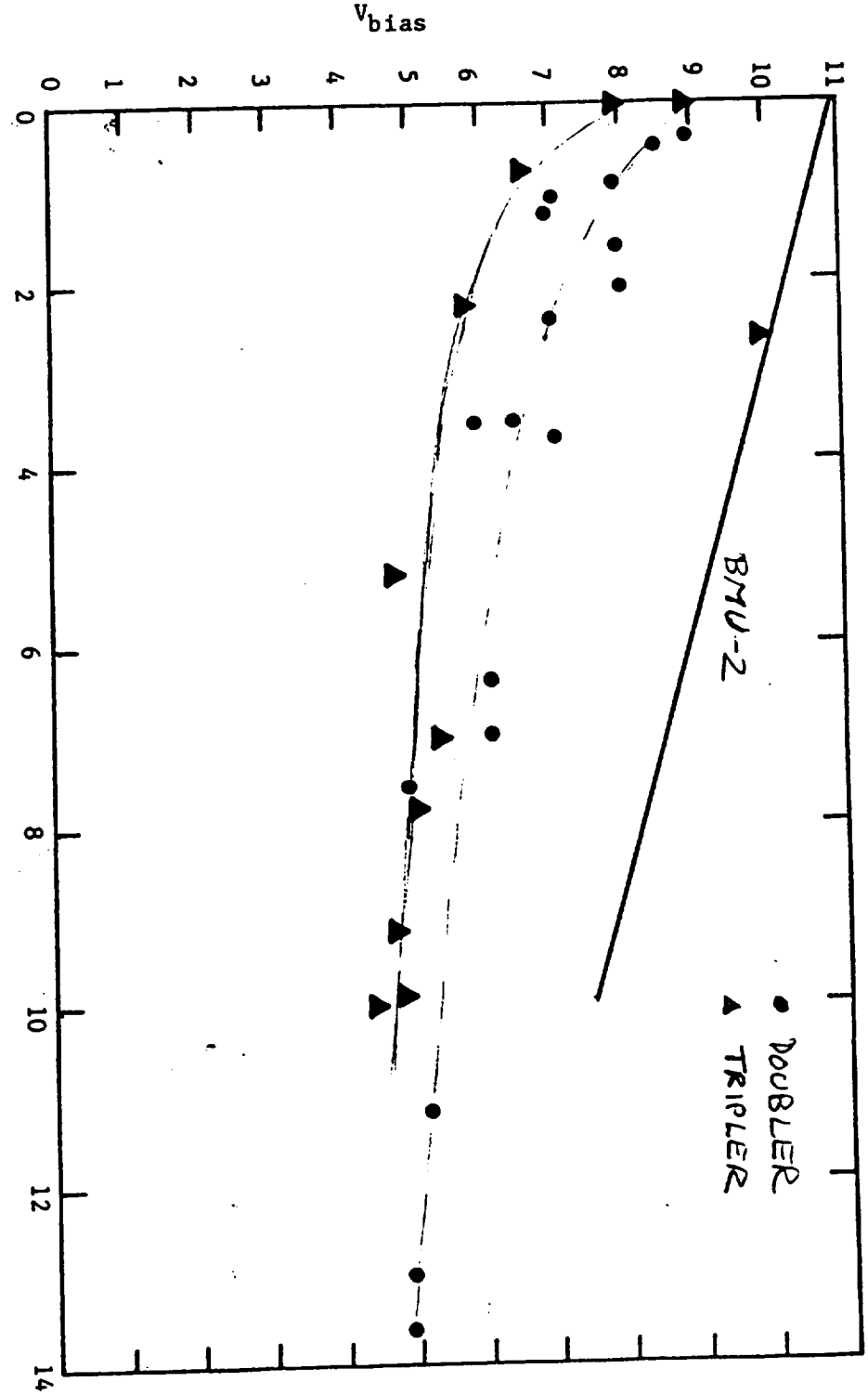
V_{bias}
0
1
2
3
4
5
6
7
8
9
10
11
0
2
4
6
8
10
12
14
BMV-2
DOUBLER
TRIPLER
I bias (mA)

Fig. 6

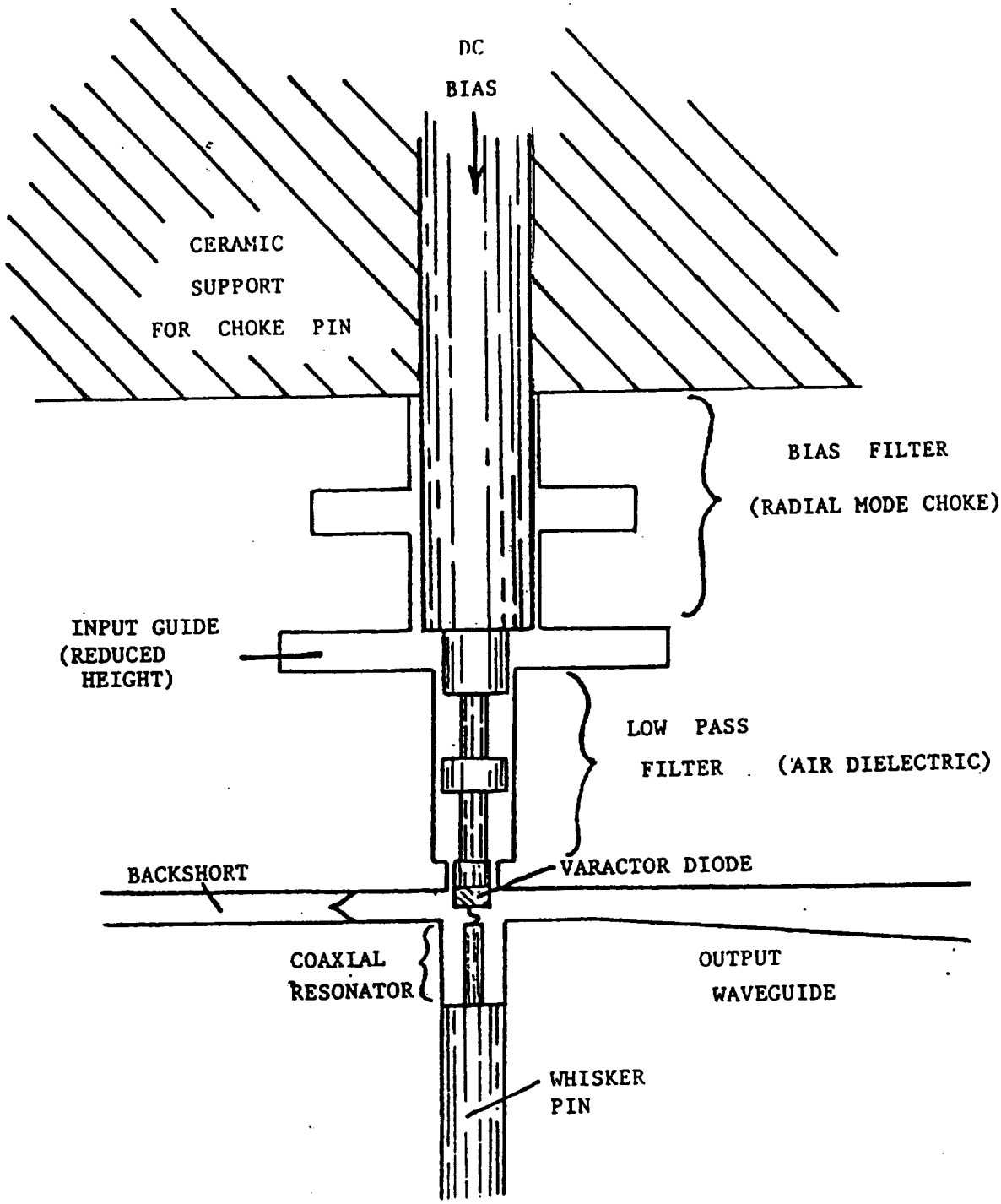
DC
BIAS
CERAMIC
SUPPORT
FOR CHOKE PIN
BIAS FILTER
(RADIAL MODE CHOKE)
INPUT GUIDE
(REDUCED
HEIGHT)
LOW PASS
FILTER (AIR DIELECTRIC)
BACKSHORT
VARACTOR DIODE
COAXIAL
RESONATOR
OUTPUT
WAVEGUIDE
WHISKER
PIN

Fig. 7

EFFECTS OF MISALIGNMENT IN GAUSSIAN OPTICS SYSTEMS

INTRODUCTION

An important question for any quasioptical system is its sensitivity to misalignments, whether these be introduced by thermal or mechanical means. While a comprehensive analysis of this problem involves rigorous diffraction theory, first order Gaussian beam theory can give us an indication of the tolerances that are required. We can identify four types of misalignments that may occur:

a. Angular offsets (tilts)
b. Lateral offsets
c. Axial displacements
d. Tilts of focusing elements

Types a through c are shown schematically in Figure 8. While this is not a complete catalog, it would appear to be a good starting point.

The first three misalignments can be analyzed in terms of the mismatch between two Gaussian beams. The two beams are assumed to be perfectly matched in the absence of any misalignment so that there is 100% power coupling between them. The beams are characterized by a beam waist radius w_o and wavelength λ. The electric field distribution at the beam waist perpendicular to the axis of propagation is given by

$$\frac{E(r)}{E(o)} = \exp - [(r/w_o)^2] \qquad (1)$$

See Goldsmith (Infrared and Millimeter Waves Vol. 6, 1982) for further discussion of Gaussian beams. Misaligned Gaussian beams have been analyzed by Kogelnik (Polytechnic Institute Brooklyn Symposium on Quasi-Optics, 1964). We will consider the fraction of power lost due to each of the effects analyzed to be small.

ANGULAR OFFSETS (OR TILTS)

The fraction of power coupled from the misaligned incident beam to the original exit beam is

$$K_{tilt} = 1 - [(\frac{2\pi w}{\lambda})\theta_T]^2 \ . \tag{2}$$

In this formula, w is the beam radius where the overlap occurs (assumed to be the same for both beams). The beam radius is related to the beam waist radius by

$$w = w_o \ [1 + \left(\frac{\lambda z}{\pi w_o 2}\right)^2]^{1/2} \tag{3}$$

where z is the distance from the waist along the axis of propagation.

(i) Tilts at beam waist

We can understand in a straightforward way the case of tilts occuring at the beam waist. We use the definition of the far-field beam growth angle $\theta w_o = \lambda / \pi w_o$, to write (4)

$$K_{tilt} = 1 - \left(\frac{2\theta_T}{\theta w_o}\right)^2 \ . \tag{5}$$

K_{tilt} approaches unity only if the angular misalignment is small compared to the characteristic growth angle of the beam.

(ii) Tilts far from the beam waist

Far from the beam waist, $w \rightarrow \frac{\lambda z}{\pi w_o}$, so that

$$K_{tilt} = 1 - \left(\frac{2z\theta_T}{w_o}\right)^2 \tag{5a}$$

A tilt due to a misplacement or motion of optical element by distance d produces $\theta_T \sim d/z$ so that

$$K_{tilt} \simeq 1 - \left(\frac{2d}{w_o}\right)^2 \qquad (5b)$$

As an example, consider a system at a wavelength of $\lambda = 0.1$ cm having a waist radius $w_o = 0.5$ cm, with a tilt occuring at the waist. This could be produced, for example, by incorrect alignment of focusing optics. We find $\theta w_o = 0.064$ radians, or 3.7°. For a tilt of 0.5°, $K_{tilt} = 0.93$, already a significant loss. In assembly and alignment of Gaussian optics systems, there is generally provision for adjustment of angles to minimize system loss. This is a reflection of the high sensitivity to angular misalignments of well collimated beams. Once alignment is completed, the system must be evaluated in terms of possible changes of angles due to thermal or mechanical effects.

LATERAL OFFSETS

For lateral offsets

$$K_{lat} = 1 - \left(\frac{x_o}{w_o}\right)^2 \qquad (6)$$

where x_o is the lateral offset (see Fig. 8) and w_o is the beam waist radius. This expression is independent of where in the beam the offset occurs. We see that the sensitivity to this form of offset is reduced for larger diameter beams; just the opposite from the case of angular offsets. For the same beam parameters as before, we find that $K_{lat} = 1 - 4x_o^2$, and for a lateral offset of .1 cm, $K_{lat} = 0.96$. This relatively high number indicates that in practice, lateral offsets are less of a problem than angular ones. Note, however, that rotation of a lens or mirror to minimize angular misalignment can produce a lateral offset.

AXIAL DISPLACEMENTS

Axial displacements can be considered as a separation along the axis of propagation between waists of the entering and exiting beams, which normally are coincident. The fraction of power coupled is given by

$$K_{ax} = \frac{1}{1 + \left(\frac{\lambda \Delta z}{2\pi w_o^2}\right)^2} \qquad (7)$$

where Δz is the distance between the waists. This is more easily understood when expressed in terms of the confocal distance

$$z_c = \frac{\pi w_o^2}{\lambda} \tag{8}$$

which is the distance from the waist in which the beam radius w increases by a factor of $\sqrt{2}$ relative to w_o. We can then write

$$K_{ax} = \frac{1}{1 + \left(\frac{1}{2}\frac{\Delta z}{z_c}\right)^2} . \tag{9}$$

For a system with $\lambda = 0.1$ cm and $w_o = 0.5$ cm, $z_c = 7.9$ cm so that $K_{ax} \simeq 0.1 - 4 \times 10^{-3} \Delta z^2$. This factor is still 0.995 for $\Delta z = 1$ cm and is evidently not a significant problem in plausible Gaussian optics systems.

LENS TILTS

A related problem is the tilt of a lens with respect to the beam. We can first consider whether the focal position of an off-axis beam is off axis by an angle equal to that of the incident radiation, i.e. in Figure 9, whether $\theta_F = \theta_B$. This is expressed in antenna parlance in terms of the beam deviation factor given by

$$BDF = \frac{\theta_B}{\theta_F} . \tag{10}$$

Lo (IRE Trans. Ant. Prop., AP-18, 1960) calculates that

$$BDF = \frac{1 + k\left(\frac{D}{4f}\right)^2}{1 + \left(\frac{D}{4f}\right)^2} \tag{11}$$

where k is a factor between 0.3 and 0.6. For a lens with D = ≈2 cm and f = 2 cm, BDF = 1 + .0625k/1.0625 ≈ 0.97. The effect of BDF not being

equal to unity is indicated in the lower portion of Figure 9. We see that since BDF = 1 would produce no motion of the focal spot (waist), the change in angle of the beam heading towards the feedhorn is $\Delta\theta = \theta_B (BDF^{-1} - 1)$, where θ_B is now the angle by which the lens is tilted. If a 2 cm diameter lens moves by a distance of .01 cm at one edge, $\theta_B = .01$ so that $\Delta\theta = .0003$ (.018°). This can be analyzed in terms of effect due to angular offset and lateral offset when coupling to the equivalent waist of the feedhorn or other beam waist. In practical situations the coupling loss due to this effect will be very small.

CONICAL FEEDHORNS FOR SUBMILLIMETER FEEDS

INTRODUCTION

Conical feedhorns have been well developed for use at microwave frequencies. Calculations and measurements by King (Proc. IRE, 38, 249, 1950) and Schorr and Beck (J. Appl. Phys., 21, 795, 1950) indicated that the radiation patterns for moderate flare-angle conical horns are characterized by low sidelobe levels over reasonable bandwidths. Conical feedhorns appear particularly attractive for the submillimeter wavelength region because of the relative ease with which they can be fabricated. Although less perfectly behaved than scalar feedhorns, the lack of a mode launching section or grooves to support the propagation of hybid modes are decided advantages when $\lambda/4$ is on the order of 1/100 inch. Below, we will consider the operation of conical feedhorns in terms of Gaussian beam propagation and quasioptical systems.

GAUSSIAN BEAM ANALYSIS

A conical feedhorn is characterized by its flare angle, θ_o, defined as half the opening angle of the cone, and its aperture diameter, usually measured in wavelengths. Values of θ_o for which patterns have been measured and calculated are in the range 5° to 45° and aperture diameters between 1.3 and 4 λ .

The radiation patterns of conical feedhorns are quite highly Gaussian, especially in the magnetic (H) plane. In a Gaussian analysis, we assume that the electric field distribution transverse to the axis in the plane containing the phase center is given by the Gaussian distribution of equation (1). If there were no truncation of the beam, the far field pattern would be a Gaussian with 1/e half angle $\theta_{w_o} = \lambda/\pi w_o$ (equation (4)). We can use the measured values of FWHM beamwidths given by King

$$\theta_{FWHM}\ (E\ plane) = 1.2\ \frac{\lambda}{d_m} \tag{12}$$

$$\theta_{FWHM}\ (H\ plane) = 1.05\ \frac{\lambda}{d_m}$$

where d_m is the aperture diameter, and assuming a Gaussian distribution, the equivalent $\theta w_o = 0.849\ \theta_{FWHM}$ so

$$\theta w_o(E) = 1.02\ \frac{\lambda}{d_m} \tag{13}$$

$$\theta_{w_o}(H) = 0.89\ \frac{\lambda}{d_m}\ . \tag{14}$$

We can then determine the equivalent waist radius w_o from $w_o = \lambda/\pi w_o$ as

$$w_o(E) = 0.31\ d_m$$

$$\text{and } w_o(H) = 0.36\ d_m\ .$$

These values are quite close to those found for scalar feedhorns, but the asymmetry is a significant problem.

One approach to correcting this (as suggested by King) is to deform the horn aperture into an elliptical shape with about 1.15:1 ratio of major to minor axes. This approach is probably feasible for small feedhorns in the submillimeter range, but the reproducibility is questionable. A preferable solution would be to compensate for the beam pattern asymmetry in the quasioptical system with which such a feedhorn is to be used.

Compensating for the unequal beam waist values to produce a symmetric beam is possible by adding an asymmetric focusing element to the quasioptical

system as indicated in Figure 10. In this case, we wish to produce a ratio $w_o(H)/w_o(E) = 1.15$. From Gaussian beam theory, it is known that if we consider two orthogonal axes, both perpendicular to the direction of propagation of the beam, the beam growth is independent and can be separately controlled. Thus, a focusing element such as a cylindrical lens can affect the beam along one axis, leaving the axis along which there is no lens curvature unaffected. Focusing mirrors can also be designed which have different effective focal lengths for the two axes. For clarity, we will use the example of cylindrical lenses in the following discussion.

We assume that the phase centers of the feedhorn for the electric and magnetic planes are the same distance behind the horn aperture. This simplifies the analysis slightly but, as will be seen, does not limit the applicability of the compensation technique. Then, as indicated in Figure 10, we are seeking to have the H-plane beam waist increased in size by a factor 1.15 compared to the E-plane beams waist; but its location should be at the same position along the axis of propagation. We define the demagnification ratio

$$M = \frac{w_o(H)}{w_o(E)} = 1.15 \tag{15}$$

and the confocal distance

$$z_c(E) = \pi w_o^2(E)/\lambda . \tag{16}$$

We can solve the Gaussian beam propagation equations and determine that the required cylinder lens focal length is

$$f_{cyl} = M\left(\frac{M^2 + 1}{M^2 - 1}\right) z_c(E) \tag{17a}$$

and that it is to be located a distance

$$d = M z_c(E) \tag{17b}$$

from the feedhorn phase center (which is the desired location of both beam waists).

As a design example, if we want a beam with 10° FWHM pattern at 500 GHz, (λ = 0.6 mm), we require that

$$\Theta w_o = 0.148 \text{ radians and}$$

$$w_o(E) = 0.13 \text{ cm.}$$

The feedhorn aperture diameter is then 0.47 cm. The E-plane confocal distance is

$$z_c(E) = 0.89 \text{ cm,}$$

the cylinder lens focal length is f_{cyl} = 7.37 cm, and it is to be located a distance

$$d = 1.02 \text{ cm}$$

from the feedhorn phase center. In the curved plane, the radius of curvature is approximately equal to the lens focal length assuming it is made of quartz. The lens size should be approximately 4 times the beam radius, w which is given by

$$w = w_o \left[1 + \left(\frac{\lambda d}{\pi w_o^2}\right)^2\right]^{1/2} .$$

In the present situation, w = 0.2 cm so D_{lens} = 0.8 cm. The maximum lens thickness is 0.011 cm. The absorption losses in such a lens will be negligible; and by suitable anti-reflection coating, the overall loss should be very low.

This approach thus appears very promising as a way of obtaining submillimeter feedhorns with highly symmetric patterns in addition to having the valuable attributes of economical and straightforward fabrication.

SINGLE SIDEBAND FILTERS

Most spectral line astronomy with heterodyne systems can benefit from the use of a single sideband filter as this generally (1) improves the calibration accuracy of the system and (2) reduces confusion from unwanted lines in the image sideband.

The major exception occurs in certain applications when it is desired to observe lines simultaneously in opposite sidebands. At the present time, the most reasonable approach would appear to be the evaluation of different types of SSB filters so that the most promising alternatives can be further developed specifically for use at submillimeter wavelengths.

The type of SSB filter that is desired depends to some extent on the overall system configuration requirements. For spaceborne applications, the "sky" is the coldest termination easily achievable. If the major purpose of the SSB filter is to improve calibration accuracy, the image beam can profitably be directed into empty space, thus adding the minimum to the system temperature. The danger in this approach is pickup of an unwanted signal in the image band as could be produced by an extended emission source. If empty space is not judged suitable for terminating the image, a matched load at low temperature must be provided.

The type of SSB filter most widely used at millimeter wavelengths is the polarization-rotating Michelson, or Martin-Puplett interferometer (see Goldsmith 1982 and original references given therein). This type of device offers low loss. However, its transmission function is strictly sinusoidal so that there is a problem obtaining the large IF bandwidths necessary for submillimter spectroscopy ($\Delta f \approx 1$ GHz is a reasonable minimum) unless the IF frequency is appropriately increased. Goldsmith (1982) gives the expression

$$\Delta f = \frac{8}{\pi} \mathcal{L}^{1/2} f_{IF} \tag{18}$$

for the SSB transmission bandwidth having loss less than $\mathcal{L}$ near resonance when the filter is operated in lowest order. For $\mathcal{L} = 0.9$, we obtain $\Delta f = .24\ f_{IF}$ so that to obtain $\Delta f = 1$ GHz, $f_{IF} \approx 4$ GHz. This is certainly not impossible but may be an undesirable restriction on mixer design. Thus, other devices deserve investigation.

An alternative form of SSB filter is the multiple beam or Fabry-Perot interferometer. The choice of mirror reflectivity gives additional freedom in defining the transmission function, but the multiple passes through the device result in greater problems with beam growth due to diffraction and

lateral motion or "walkoff" if the mirrors are at non-normal incidence. This problem has been analyzed in detail by Arnaud, Saleh, and Ruscio 1974 (IEEE Trans. Microwave Theory Techniques, MTT-22, p. 486). The results for a free-space Fabry Perot interferometer (FPI) can be summarized by the fraction of power transmitted in original incident Gaussian mode, (assumed to be close to unity) given by

$$K_{to} = 1 - (G^2 + D^2)$$

$$D = \frac{2\lambda d \cos \theta_i}{\pi w_o^2 T} \qquad (19)$$

$$G = \frac{2\sqrt{2}\, d \sin \theta_i}{w_o T}$$

where D is the diffraction loss and G the walkoff loss, with d being the mirror spacing, θ_i the angle of incidence, w_o the beam waist radius, and T the power transmission of a single mirror. Note that the walkoff loss is zero at normal incidence, and that it decreases only as w_o^{-1} rather than as w_o^{-2} for the geometrical loss, and that it is independent of wavelength. For practical reasons, $\theta_i \gtrsim 10°$ is convenient, and taking T = 0.25 and

$$d = \frac{\lambda_{IF}}{8} \approx 1 \text{ cm}$$

as required to get good rejection of the image, we find

$$D = \frac{2.5\lambda}{w_o^2} \quad \text{and} \quad G = \frac{1.6}{w_o} .$$

It is readily apparent that the diffraction loss at $\lambda = 0.5$ cm can be made quite reasonable for a waist radius of a few millimeters, but that the walkoff loss is a major problem unless the beam waist radius is several centimeters. Since the beam diameter is $3 - 4\ w_o$ minimum, this is a major inconvenience, and we see that geometrical walkoff is a major obstacle. Fabry-Perot interferometers which avoid problems of walkoff have also been developed by Gustincic 1976 (Proc. Soc. Phot-Opt. Instrum. Eng. 105, p. 40) and by Watanabe and Nakajima 1978, (Electronics Letters, 14, p. 81).

These devices have significant promise for use in compact systems. The Gustincic ring resonator has recently been analyzed in detail by Pickett and Chiou 1982 (IEEE Trans. Microwave Theory Techniques, MTT - 31, p. 373). It can have very low loss, and is readily tunable, but suffers from the limitation of having the usual Fabry-Perot response.

$$|\tau|^2 = \frac{1}{1 + \frac{4R}{(1-R)^2} \sin^2 \frac{\delta\theta}{2}} \qquad (20)$$

where R = 1-T is the mirror power reflectivity and $\delta\theta$ is the round trip phase delay. What is really desired is a device with a broader bandwidth transmission response. The polarization-rotating device described by Watanabe and Nakajima would appear to have significant potential in this area. A schematic diagram is shown in Figure 11.

Operation as a single sideband filter is as follows. If we have an input signal vertically polarized, it passes through the wire grid and is converted to circular polarization by a quarter-wave plate (QWP A). If it is in the transmission bandpass of the FPI, it is transmitted, and then is converted back to linear polarization by QWP B. If it is reflected by the FPI, it is reconverted to linear polarization by QWP A; but due to the reversal of handedness of circular polarization on reflection from the FPI, it is horizontally polarized after passing through the QWP and hence is reflected by the wire grid. In practice we probably would have the mixer at the input port. Note that if we use the device to transmit the unwanted sideband, QWP B can be omitted without any sacrifice. It can be omitted as well if we want to leave the system sensitive to circular polarization. In this device, the FPI is operating at normal incidence so that only diffraction losses are present; if w_o = 0.5 cm so that the beam diameter = 2 cm, these are already negligible. The wire grid has nearly perfect performance in the 500 μm range, with the result that the major sources of loss are the quarter wave plates (QWP) and the FPI mirrors.

For a QWP made of an anisotropic material, the thickness is given by $d = \lambda/4\ n$, where Δn is the difference in the indices of refraction. For

sapphire, $\Delta n \cong 0.35$ so that $d = 0.7\ \lambda$. The transmission through a dielectric QWP is given by

$$|\tau|^2 = \exp[-\alpha d] \tag{21}$$

where $\alpha = \frac{2\pi n}{\lambda} \tan\delta$,

$\tan\delta$ being the loss tangent. We see that this reduces to

$$|\tau|^2 = \exp\left[-\frac{\pi n}{2\Delta n} \tan\delta\right] \tag{22}$$

For sapphire, $\tan\delta \sim .002$ at 900 GHz (Lowenstein, Smith, and Morgan, 1973, Appl. Opt., 12, 398) and we find that $|\tau|^2 = 0.97$. It is also promising to note that values of $\tan\delta$ for sapphire and other dielectrics decrease considerably upon cooling.

The FPI mirrors can be constructed of free-standing metal mesh. In the submillimeter region, the losses should not exceed a few percent for useful reflectivities. The possibility exists of making the FPI with more than two mirrors. In this case, the reflection and transmission functions can be tailored to have more desirable broadband characteristics. Having the FPI at normal incidence is critical for this, otherwise the walkoff losses would be prohibitive. Another method of achieving this is to use a series of dielectric slabs for the FPI. Very desirable transmission function characteristics can be achieved. As an example, Figure 12 shows the response of a 2-slab FPI with each slab having $n = 3.5$ and thickness 0.125 cm; the slabs are separated by a distance of 0.5 cm. A very flat passband approximately 4 GHz wide is obtained; this filter was designed for an IF of 5 GHz so that the minimum response occurs for $f \approx 560$ GHz, 10 GHz higher than the signal band around 550 GHz. The major drawback of the dielectric FPI is the absorptive loss. This is highly sensitive to the material used, and detailed comparative measurements must be made to determine the optimum design.

FIGURE CAPTIONS

Fig. 8: Gaussian beam with no misalignment (top) as compared to beams having three types of misalignment: angular offset, lateral offset, and axial displacement.

Fig. 9: The lens is tilted with respect to the incident radiation in both illustrations. Top: the feedhorn is aligned with the beam and the beam deviation factor (BFD) equals unity. Bottom: the position of the feedhorn is shown for the beam deviation factor equal to 1 and for BFD < 1.

Fig. 10: Technique for changing beam waist radius in one plane by addition of asymmetric focussing element.

Fig. 11: Polarization rotating device for use as a single sideband filter.

Fig. 12: Response of a two-slab FPI. Each slab has n = 3.5; thickness = 0.125 cm. The slab separation is 0.5 cm.

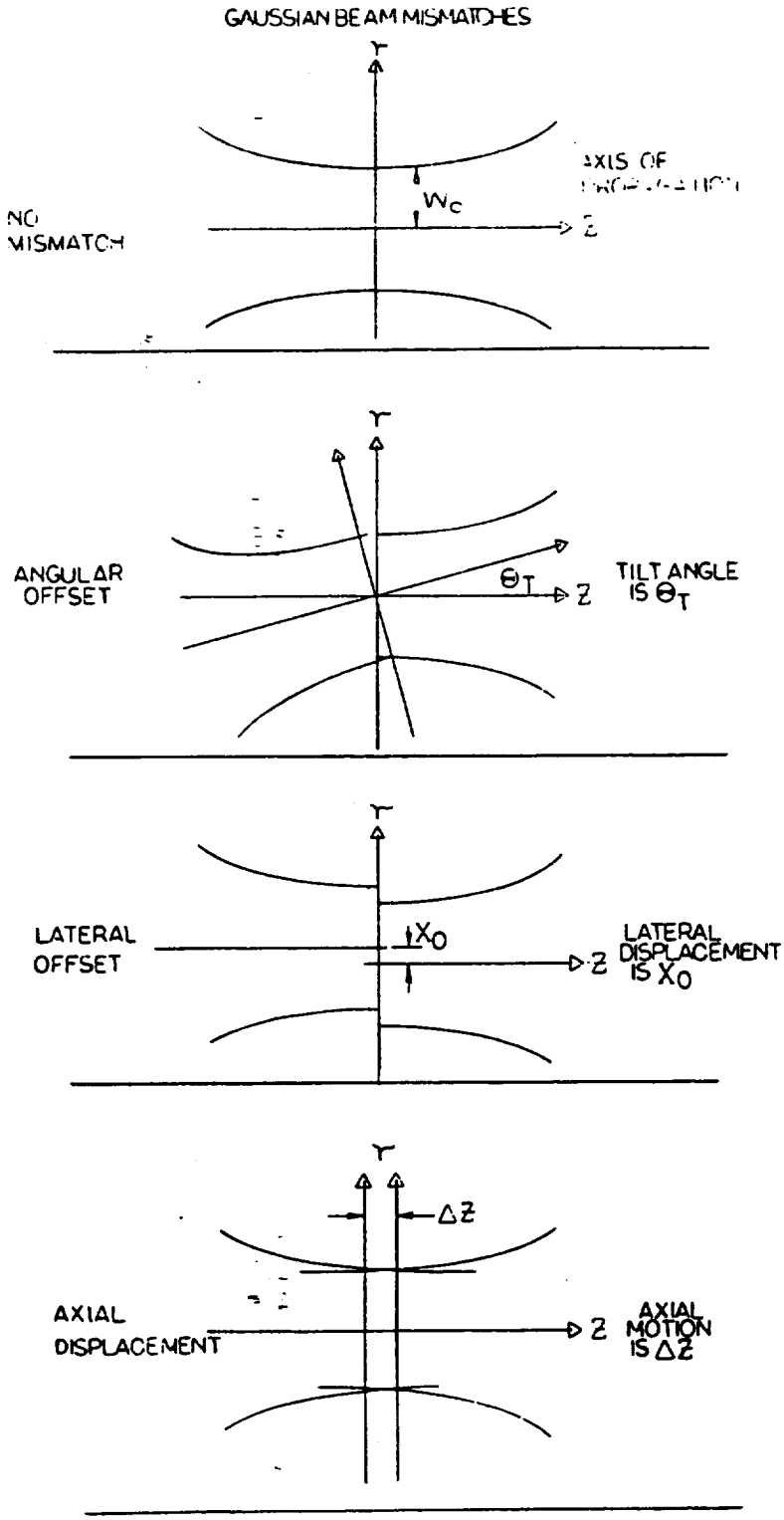
GAUSSIAN BEAM MISMATCHES
NO MISMATCH
W_c
Z
ANGULAR OFFSET
Θ_T
Z
TILT ANGLE IS Θ_T
LATERAL OFFSET
X_0
Z
LATERAL DISPLACEMENT IS X_0
ΔZ
AXIAL DISPLACEMENT
Z
AXIAL MOTION IS ΔZ

Fig. 8

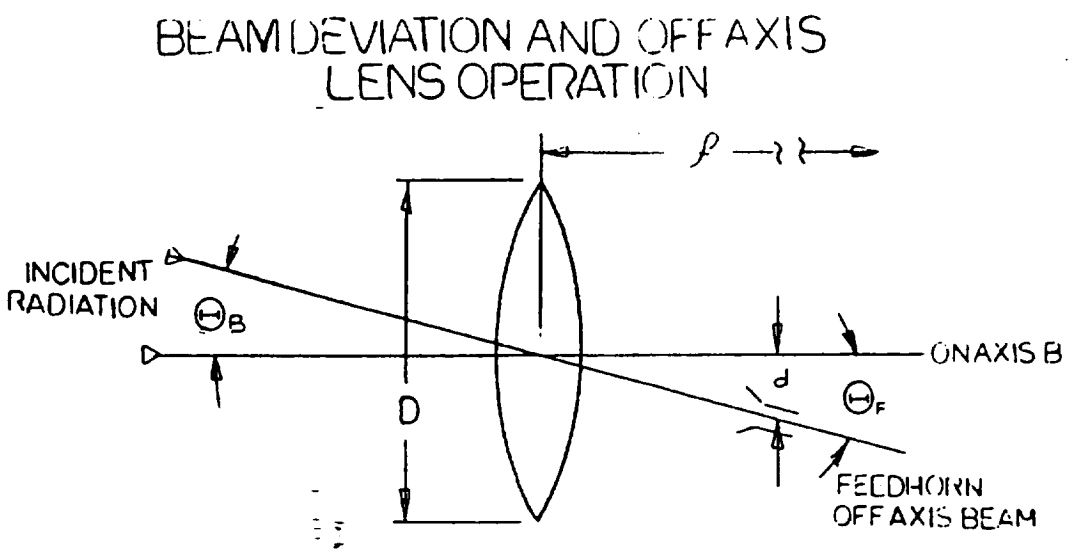
BEAM DEVIATION AND OFF AXIS LENS OPERATION
f
INCIDENT RADIATION
ΘB
ONAXIS B
D
d
ΘF
FEEDHORN OFF AXIS BEAM

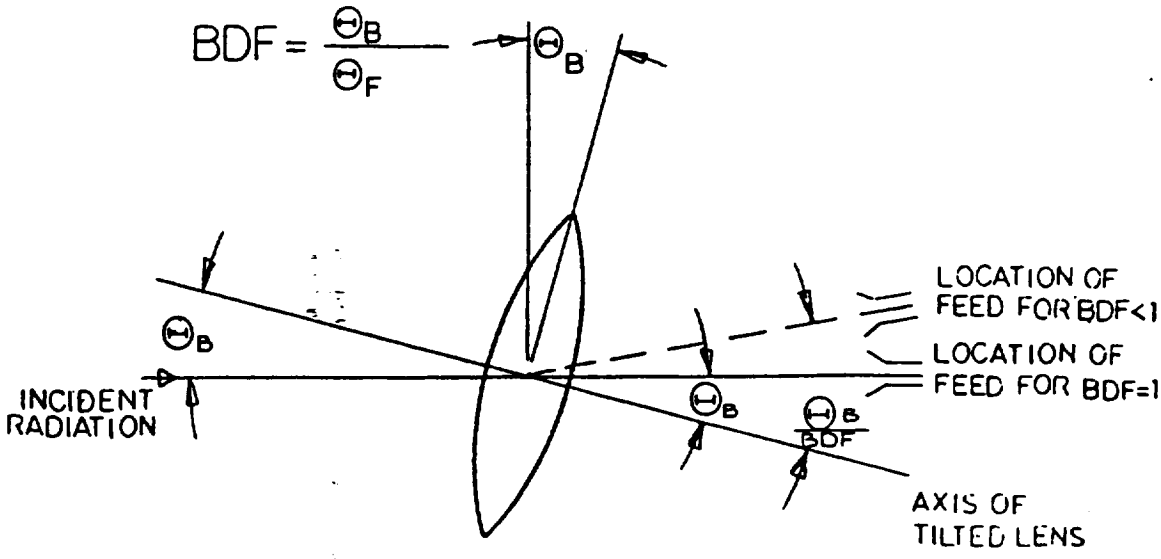
BDF = ΘB / ΘF
ΘB
ΘB
LOCATION OF FEED FOR BDF<1
LOCATION OF FEED FOR BDF=1
INCIDENT RADIATION
ΘB
ΘB / BDF
AXIS OF TILTED LENS

Figure 9

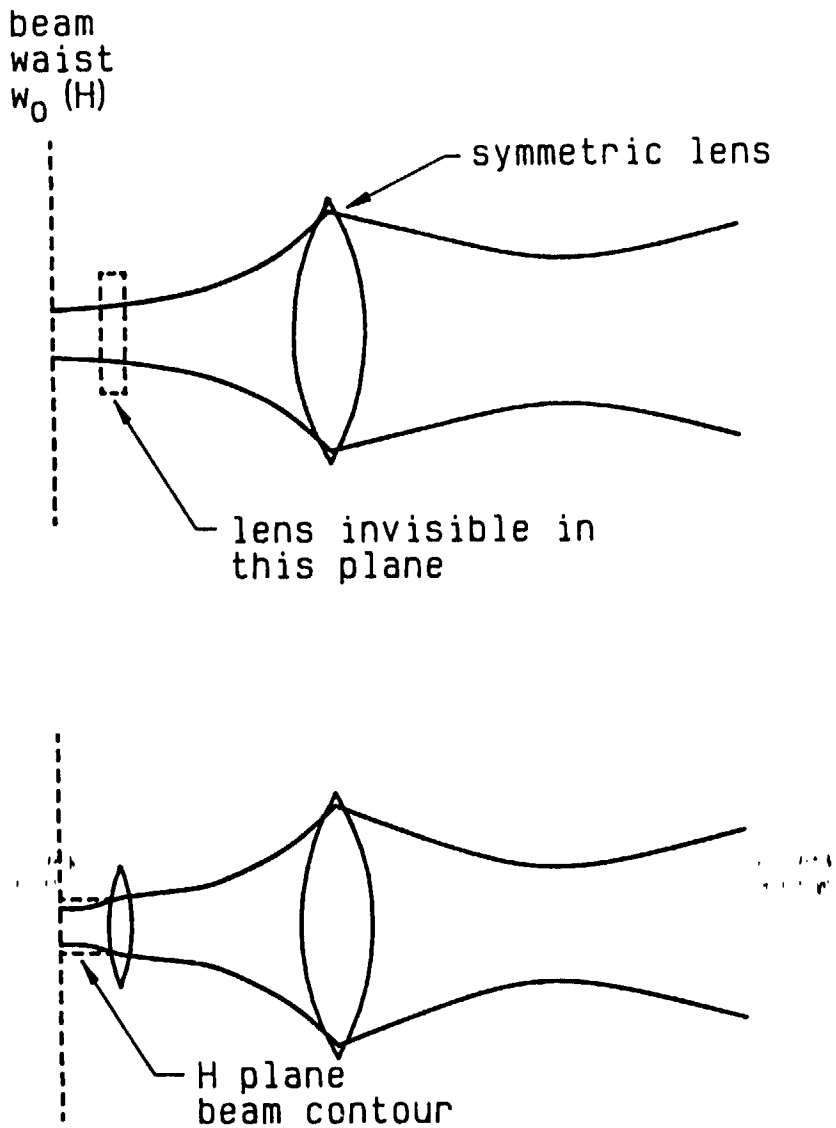
beam
waist
w_0 (H)
symmetric lens
lens invisible in
this plane
H plane
beam contour
beam
waist
w_0 (E) = w_0 (H) /1.15

Fig. 10

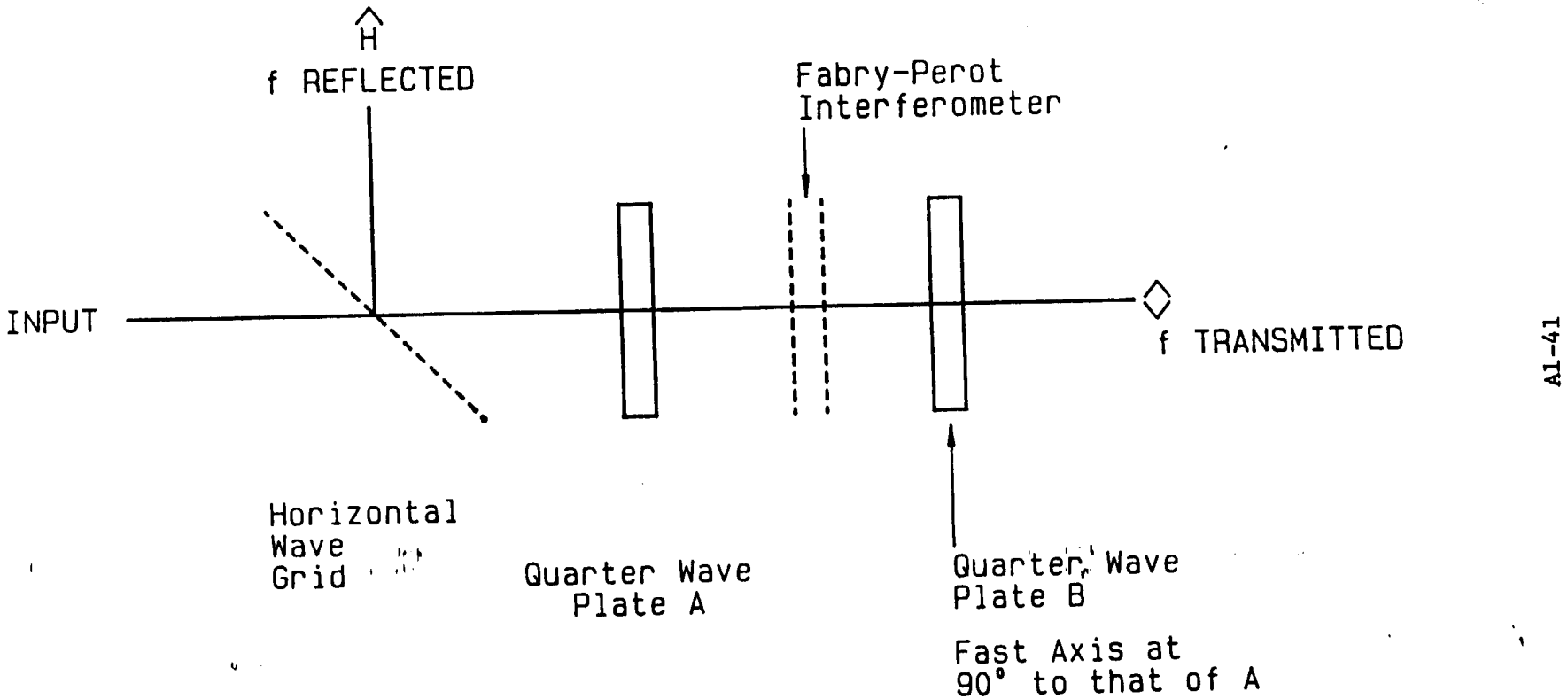
H
f REFLECTED
Fabry-Perot
Interferometer
INPUT
f TRANSMITTED
Horizontal
Wave
Grid
Quarter Wave
Plate A
Quarter Wave
Plate B
Fast Axis at
90° to that of A

A1-41

Fig. 11

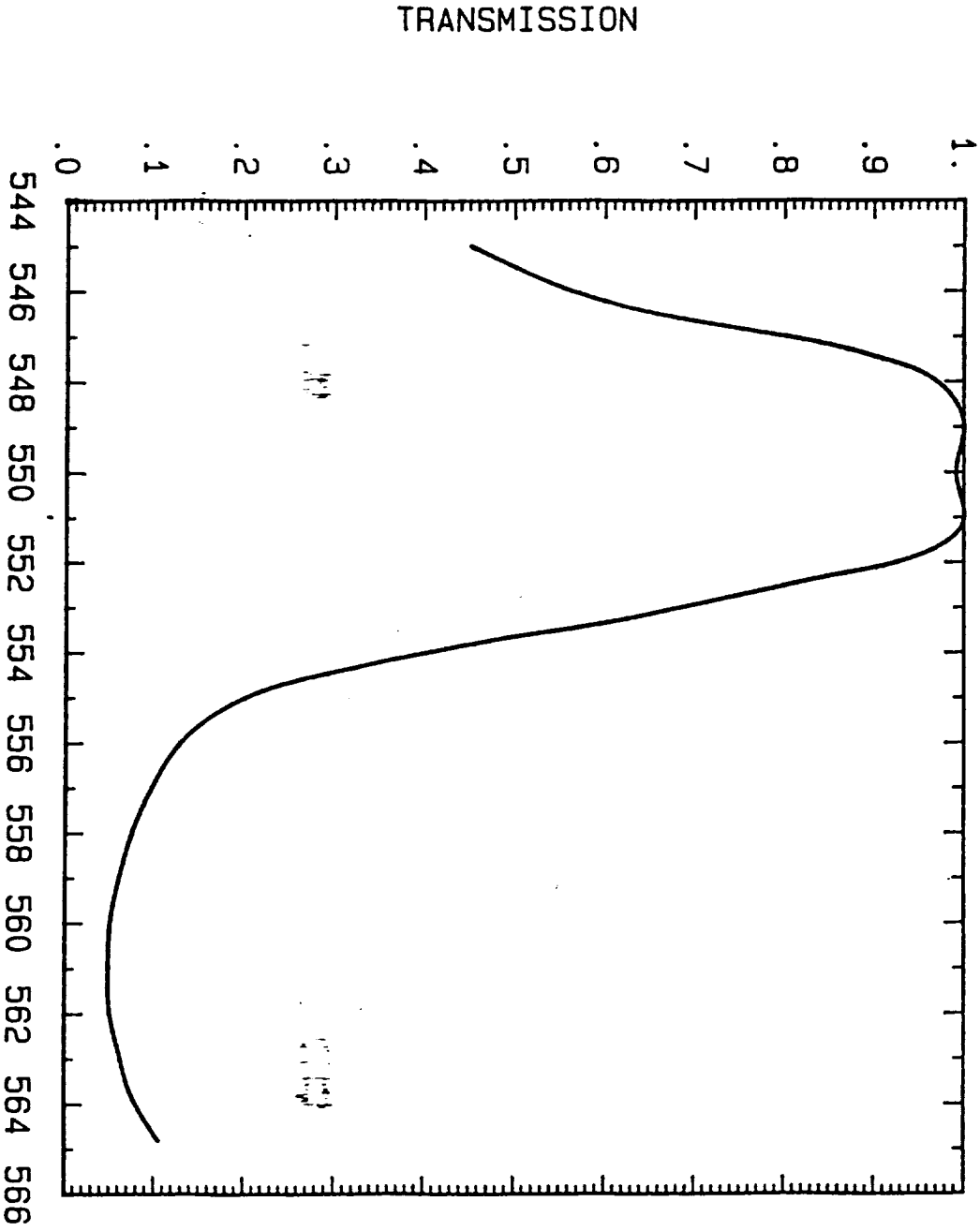
TRANSMISSION
DOUBLE FPI
d slabs = .125cm spacing = 1.0cm n = 3.5
0 .1 .2 .3 .4 .5 .6 .7 .8 .9 1.
544 546 548 550 552 554 556 558 560 562 564 566
FREQUENCY (GHz)

Fig. 12

APPENDIX 2

Gaussian Beam Transformation with Cylindrical Lenses

PAUL F. GOLDSMITH, SENIOR MEMBER, IEEE

Abstract—**We develop formulas for Gaussian beam transformation with fixed total distance between beamwaists, and consider the use of cylindrical lenses or mirrors to produce beams which are not symmetric about the axis of propagation. For antenna feeds, it is necessary that the beam waists for both planes perpendicular to the axis of propagation be coincident. This requirement is analyzed, and appropriate transformation formulas obtained. The far-field patterns of a scalar feed horn cylindrical lens combination operating at a frequency of 94 GHz have been measured and found to be in quite good agreement with the elliptical patterns predicted by the transformation formulas.**

I. Introduction

Fundamental mode Gaussian beams are used in open resonators [1], beam waveguides, and a wide variety of quasi-optical components [2]. These systems generally employ a beam which is symmetric about the axis of propagation. However, since the beam parameters in the two coordinates perpendicular to the axis of propagation are independent, we do have the possibility of creating asymmetric beams, which are useful for illumination of special types of antennas as well as in imaging applications. In Section II we derive expressions for Gaussian beam transformation which may be employed in a wide variety of situations. We consider explicitly the case with fixed total separation between the beamwaists, and obtain relations for the case of producing a beam with waists for both axes perpendicular to the direction of propagation located at the same position along the propagation axis. In Section III we discuss the use of cylindrical lenses for the production of asymmetric beams. A scalar feed horn is a high efficiency Gaussian beam launcher, and can be used together with a cylindrical lens to produce an asymmetric beam waist. In Section IV the measurements of the radiation pattern of such a combination are presented and compared with theory, and the use of cylindrical optics to symmetrize the patterns of asymmetric feed horns is discussed.

Manuscript received July 14, 1985; revised November 1, 1985.

The author is with the Millitech Corporation, P.O. Box 109, South Deerfield, MA 01373, and with the Department of Physics and Astronomy, University of Massachusetts, Amherst, MA 01033

IEEE Log Number 8407363

II. Transformation of Gaussian Beams by Thin Lenses

A. General Formulas

The effect of a thin lens on a Gaussian beam is assumed to be a change in the radius of curvature of the beam without any effect on the beam size. From this assumption it is possible to derive basic Gaussian beam transformation formulas [3], [4], which relate the input and output waists and distances (shown in Fig. 1) produced by a lens of focal length f operating at wavelength. By convention, we consider a beam traveling from left to right. The input distance d_1 is defined to be positive if the input waist is located to the left of the lens, while the output distance is defined to be positive when the output waist is located to the right of the lens. In many cases, we have two beamwaists having given waist radii which we wish to match to each other. In this situation, the basic imaging equations can be recast into the following expressions [3] for the input and output distances:

$$d_1 = f \pm \left(\frac{w_{01}}{w_{02}}\right)\left[f^2 - f_0^2\right]^{1/2} \tag{1a}$$

$$d_2 = f \pm \left(\frac{w_{02}}{w_{01}}\right)\left[f^2 - f_0^2\right]^{1/2} \tag{1b}$$

$$f_0 = \pi w_{01} w_{02}/\lambda \tag{1c}$$

where it is assumed that $|f| \geq f_0$, and the same sign is to be used for calculation of both of the distances. The two possible solutions are a reflection of the independence of the output waist size of a beam transformed by a focusing element on the sign of the quantity $d_1/f - 1$.

Equations (1) still do not determine the input and output distances as f remains a free parameter.

B. Fixed Waist Separation

The value of the focal length can be essentially determined if the total distance between the waists is specified, a situation that is often of practical importance. We define

$$d = d_1 + d_2 \tag{2}$$

as the total distance between the input and output waists, and define the system magnification

$$M = w_{02}/w_{01} \tag{3}$$

0018-926X/86/0400-0603$01.00

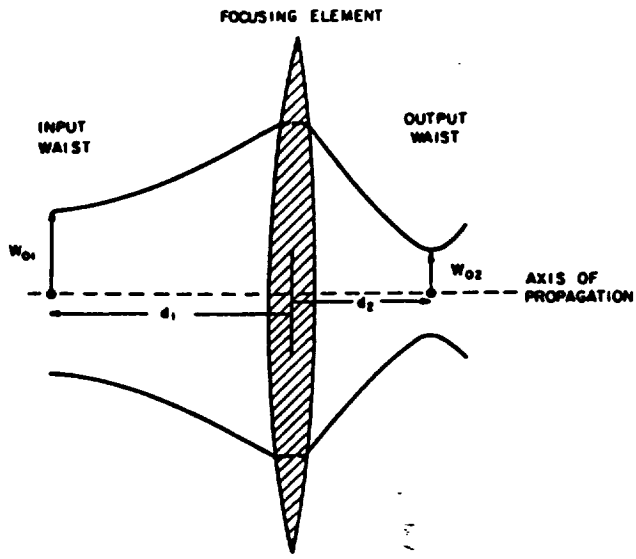

Fig. 1. Gaussian beam transformation by a focusing element. The waist radius is the distance, measured perpendicular to the axis of propagation in the plane where the beam has its minimum size, at which the electric field strength has fallen to $1/e$ of its on-axis value.

The expression for the total waist separation then becomes

$$d = 2f \pm (M + 1/M)[f^2 - f_0^2]^{1/2}, \tag{4}$$

again with $|f| \geq f_0$. For any $|f| > f_0$ we have a pair of solutions for d given a particular M. For $f > f_0$ both members of the pair have $d > 0$ or else one has $d > 0$ and the other $d < 0$. In the case $f < 0$, both solutions have $d < 0$ or else they have opposite signs.

Equation (4) can be solved for the required focal length as a function of the total waist separation, yielding

$$f = \frac{\pm[(M - 1/M)^2 f_0^2 + d^2]^{1/2}(M + 1/M) - 2d}{(M - 1/M)^2} \tag{5a}$$

for $M \neq 1$, and

$$f = \frac{d}{4} + \frac{f_0^2}{d} \tag{5b}$$

for $M = 1$. Equation (5a) is shown in graphical form in Fig. 2. The expressions relating the input and output distances in the case of fixed total waist separation are

$$d_1 = \frac{d - f(1 - M^2)}{(1 + M^2)} \quad d_2 = \frac{M^2 d + f(1 - M^2)}{(1 + M^2)} \tag{6a}$$

and the ratio of these distances is given by

$$\frac{d_2}{d_1} = \frac{M^2 d + f(1 - M^2)}{d - f(1 - M^2)}. \tag{6b}$$

Equation (5a) gives two values of f for a particular f_0, M, and d. The pair always have opposite signs, and always satisfy the condition $|f| \geq f_0$. Substituting $1/M$ for M has no effect on the value of f required, but can be seen to interchange d_1 and d_2 in (6).

C. Zero Waist Separation

The condition $d = 0$ results in (5a) taking the form

$$f = \pm \frac{(M^2 + 1)}{(M^2 - 1)} f_0 \tag{7a}$$

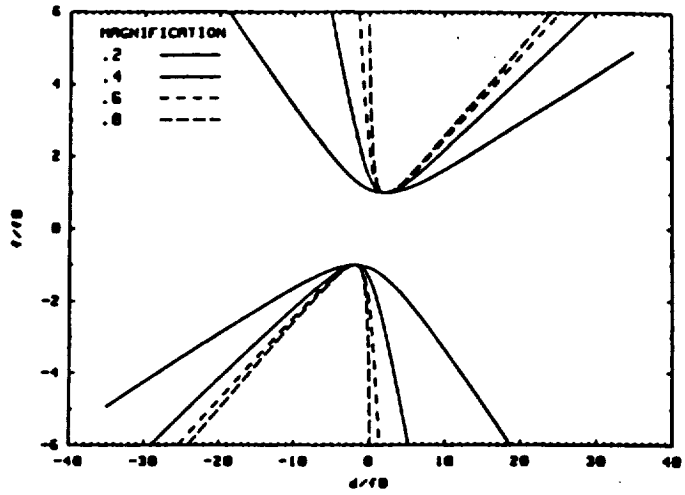

Fig. 2. Values of lens focal length f, expressed in units of f_0 (1c), as a function of total waist separation d (again in units of f_0) and system magnification M (3). Note that a curve for a particular M also applies for magnification M^{-1}.

with

$$d_1 = \pm f_0 \quad d_2 = \mp f_0. \tag{7b}$$

Both signs produce valid solutions, but only for the solutions with $f > 0$ for $M > 1$ and $f < 0$ for $M < 1$ do we have access to the input waist, as would be necessary in order to have a feed horn located there, for example. The other solutions have an input waist with negative distance, which can be used in conjunction with a beam waveguide.

III. Cylindrical Lens Use

A cylindrical lens is curved only in a single plane; consequently, it affects the Gaussian beam parameters only in that plane and has no effect on the beam radius or radius of curvature in the perpendicular plane. The reflective analog, the cylindrical mirror, has been used in a number of beam waveguide systems [5]–[7], but generally with mirrors in pairs acting to maintain a symmetric field distribution. Use of a cylindrical lens in a Gaussian beam system will in general result in the production of an asymmetric field distribution, but the locations of the waists for the plane unaffected by the lens and for the plane in which the beam has been transformed will be different. Their separation can be calculated, for example, using (4).

One application of an asymmetric Gaussian beam such as that produced by a cylindrical lens or mirror is the illumination of an elliptical antenna. The waists for both planes should have the same location, and, if the incident beam is symmetric, the value of M required will be the ratio of major to minor diameters, assuming that the input beam is designed to properly illuminate a hypothetical symmetric antenna having diameter equal to the major diameter of the elliptical antenna. If the input beam has the larger waist radius appropriate for illuminating a smaller antenna of diameter equal to the minor diameter of the elliptical antenna, the required value of M will be the inverse of that given above and hence will be less than unity.

Consider the situation in which we wish to use a cylindrical lens to modify the output of a feedhorn having a symmetric radiation pattern (and hence equal waist radii) to illuminate an elliptical antenna. We can, as described above, use the lens with M greater than or less than one, depending on whether the feed horn pattern matches the small or large dimension of the antenna. In either case, as indicated by (7b), the input distance is equal to f_0.

Equation (7) defines the element focal length and the input and output distances required to obtain a given magnification. If we are interested in the performance of a given cylindrical lens with a particular input waist, we can express f_0 in terms of the parameters of the input waist alone as

$$f_0 = M\left(\frac{\pi w_{01}^2}{\lambda}\right) = Mz_{c1} \tag{8}$$

and we see that

$$f = \frac{M(M^2+1)}{(M^2-1)} z_{c1}. \tag{9}$$

This is shown graphically in Fig. 3; the inverse equation giving M as a function of f is not particularly illuminating and results can be obtained graphically or numerically.

IV. Measurements

We have carried out a series of measurements at a frequency of 94 GHz (λ = 0.319 cm) to study Gaussian beam transformation with a cylindrical lens. The input beam was provided by a scalar feed horn; the horn, lens, and beams are shown schematically in Fig. 4. As shown by many measurements and analyzed specifically in terms of Gaussian modes [8], these devices produce highly symmetric beams with approximately 98 percent of the radiated power in the lowest Gaussian mode. The radiation pattern of the feed horn used is shown in Fig. 5(a); the waist radius is 0.51 cm. A fused silica planoconvex cylindrical lens having a focal length of 10 cm was used to produce an asymmetric beamwaist. The lens was antireflection coated using quarter wavelength thick dielectric layers on both surfaces. We see from Fig. 3 or (9) and (7) that there are two values of input distance for which d is equal to 0, each having a certain magnification: d_1 = 3.8 cm produces M = 1.5 and d_1 = 8.2 cm produces M = 3.2. Patterns for these input distances are shown in Figs. 5(b) and 5(c), respectively. The patterns were obtained by rotating the horn lens combination about the expected waist location; the receiving horn was at a distance of 1.5 m, approximately six times the confocal distance for the larger beamwaist, given by M^2z_{c1}.

The ratio of major to minor widths of the pattern in Fig. 5(b) is within a few percent of the expected value of 1.5; it is also apparent that the larger angular size is essentially unchanged from that of the feed horn. The pattern produced by the lens at a distance of 8.2 cm from the input waist (Fig. 5(c)) is less perfectly Gaussian and has an ellipticity of approximately 3.0. The difference between this value and that of 3.2 expected, as well as the slight reduction in the large angular extent of the pattern, may be a result of the truncation of the beam by the cylindrical lens (cf. [9]). At a distance of 8.2 cm from the feed horn beamwaist, the clear diameter of the lens produces a truncation at the -11 dB level. Measurements to verify the location of the beamwaist have not been carried out.

A second use of cylindrical optics is to correct the asymmetry present in the patterns of certain types of feed horns. For example, smooth-walled conical feed horns offer reasonably good performance, and are relatively inexpensive. However, the asymmetry of the TE_{11} mode defining the aperture illumination results in a pattern with E-plane beamwidth typically 25 percent narrower than that of the H-plane [10]–[12]. The main lobe of the pattern of a small aperture phase error conical horn can be modeled in terms of a Guassian beam having H-plane waist radius equal to 0.31 times the aperture diameter, and E-plane waist 1.25 times larger. A cylindrical corrector is thus designed with a magnification of 1.25, in order to produce a symmetric beam. The difference in the location of the E- and H-plane phase centers for the conical feed [13] is not a

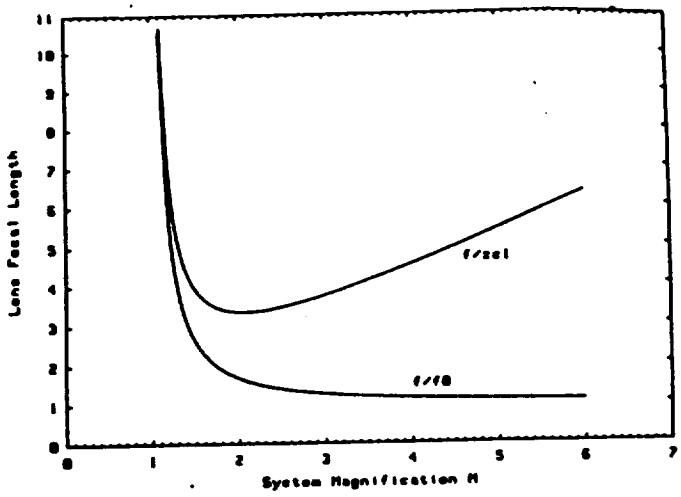

Fig. 3. Lens focal length for Gaussian beam transformation with zero separation between input and output waists, as a function of system magnification. The two curves give the lens focal length in terms of the system parameter f_0 (1c), and the confocal distance of the input waist, z_{c1} (8).

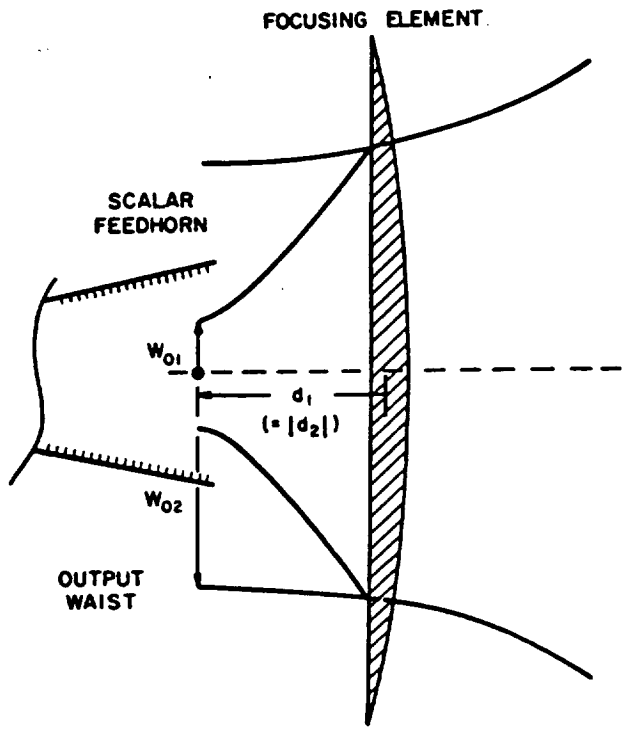

Fig. 4. Schematic view of scalar feed horn and cylindrical lens used in zero waist separation configuration. The feed horn beamwaist is located behind the horn aperture as discussed by Wylde [8].

fundamental problem for pattern correction since only the H-plane beam is being modified. For optimum results as a point feed the cylindrical corrector would not be designed for d exactly zero, but having the small value required to bring the phase centers for the two principal planes into coincidence. Using a cylindrical lens-conical horn combination, we have verified that good pattern symmetry is obtained to a level 12 dB below the peak. The cylindrical lens leaves the sidelobes present in the E-plane pattern largely unchanged.

V. Conclusion

We have demonstrated the ability of cylindrical lenses to produce asymmetric Gaussian beams. The standard Gaussian beam imaging

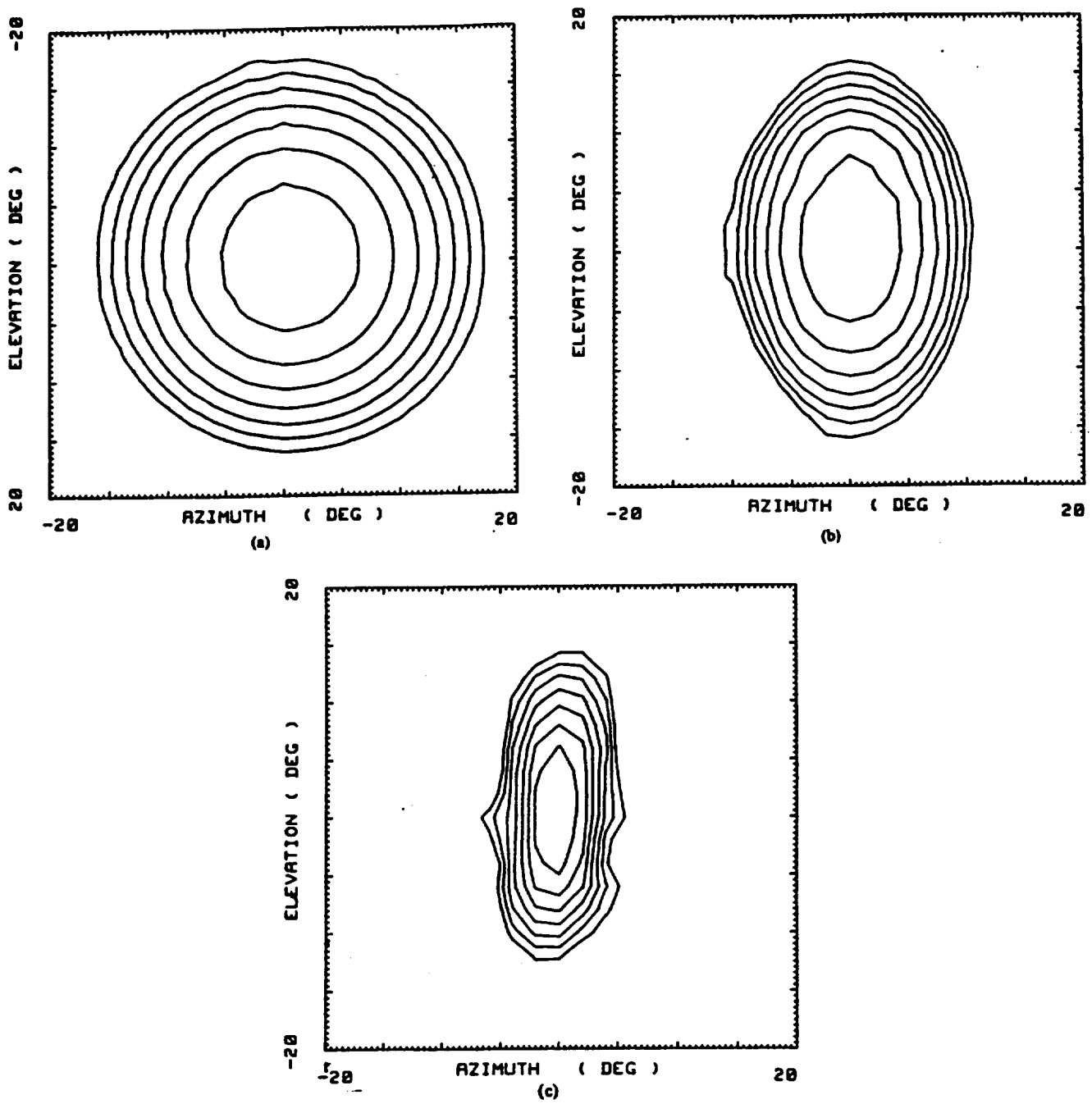

Fig. 5. (a) Radiation patterns of scalar feed horn. (b) Pattern with f = 10 cm cylindrical lens at distance of 3.8 cm from feed horn beamwaist. (c) Pattern with same lens at distance 8.2 cm from feed horn waist. In each panel, the innermost contour is 3 dB below the maximum response, and successive contours are at 3 dB intervals.

formulas have been extended to allow calculation of lens parameters for fixed distance between input and output waists. The situation of having the waists located at the same distance along the axis of propagation leads to particularly simple expressions which are convenient for using a cylindrical lens to modify the pattern of a feed horn used to illuminate an elliptical antenna.

Gaussian beam imaging calculations can also be used to design correctors for feed horns having asymmetric but reasonably Gaussian patterns, such as smooth-walled conical feed horns. Other uses include relatively efficient illumination of a linear array of antennas. The approach studied here can be employed with reflective cylindrical optics as well as with lenses, in a variety of situations.

ACKNOWLEDGMENT

The author expresses his thanks to E. L. Moore for carrying out the pattern measurements, to J. Kapitzky for computational assistance, and to a referee for useful suggestions.

REFERENCES

[1] M. Tsuji, H. Shigesawa, and K. Takiyama, "Open-resonator method for sumbillimeter wave dielectric measurements," in *Proc. Ninth Int. Conf. IR&MM Waves*, Takarazuka, 1984, pp. 372-373.

[2] P. F. Goldsmith, "Quasi-optical techniques at millimeter and submillimeter wavelengths," in *Infrared and Millimeter Waves*, vol. 6, K. J. Button, Ed. New York: Academic, pp. 272-343, 1982.

[3] H. Kogelnik and T. Li, "Laser beams and resonators," *Proc. IEEE*, vol. 54, pp. 1312-1329, 1966.
[4] T. S. Chu, "Geometrical representation of Gaussian beam propagation," *Bell Syst. Tech. J.*, vol. 45, pp. 287-299, 1966.
[5] J. A. Arnaud, D. C. Hogg, and J. T. Ruscio, "Focusing of 52 GHz beams by cylindrical mirrors," *IEEE Trans. Microwave Theory Tech.*, vol. MTT-20, pp. 344-345, 1972.
[6] J. T. Ruscio, "Focusing of 104 GHz beams by cylindrical mirrors," *IEEE Trans. Microwave Theory Tech.*, vol. MTT-21, pp. 154-155, 1973.
[7] J. A. Arnaud and J. T. Ruscio, "Guidance of 104 GHz beams by cylindrical mirrors," *IEEE Trans. Microwave Theory Tech.*, vol. MTT-23, pp. 377-379, 1975.
[8] R. J. Wylde, "Optics and corrugated feed horns," *Proc. Inst. Elec. Eng.*, vol. 131, pt. H, pp. 258-262, 1984.
[9] P. Belland and J. P. Crenn, "Changes in the characteristics of a Gaussian beam weakly diffracted by a circular aperture," *Appl. Opt.*, vol. 21, pp. 522-527, 1982.
[10] M. G. Schorr and F. J. Beck, "Electromagnetic field of the conical horn," *J. Appl. Phys.*, vol. 21, pp. 795-801, 1950.
[11] A. P. King, "The radiation characteristics of conical horn antennas," *Proc. IRE*, vol. 38, pp. 249-251, 1950.
[12] M. K. Hamid, "Diffraction by a conical horn," *IEEE Trans. Antennas Propagat.*, vol. AP-16, pp. 520-528, 1968.
[13] I. Ohtera and H. Ujiie, "Nomographs for phase centers of conical corrugated and TE_{11} mode horns," *IEEE Trans. Antennas Propagat.*, vol. AP-23, pp. 858-859, 1975.

Multilayer Approximation for Plane Wave Propagation in a Layered Medium

KOHEI HONGO, SENIOR MEMBER, IEEE, AND YASUAKI UEHARA

Abstract—**Linear profile multilayer approximation for computing reflection or transmission coefficients of plane wave by a layered medium, which is formal extension of standard staircase stratification method, is studied theoretically and numerically. The problem is reduced to evaluate 2 × 2 matrix product whose elements include the Bessel functions of order ± 1/3 and ± 2/3. The polynomial approximation for the Bessel function is constructed by applying modified Chebyshev method to facilitate the numerical calculation.**

I. Introduction

Wave propagation in inhomogeneous media has attracted a great deal of attention because it is applicable to several branches of physical science, especially to acoustics, electromagnetics, and optics. Many of these problems can be analyzed in terms of a scalar wave equation, but an exact solution of this wave equation is restricted to few special profiles so that we must rely on approximate techniques. An excellent review of the approximate analytical methods has been given in [1]. A detailed discussion of the application of the so-called staircase stratification method to planar structures has been given in [2], and an application to circular waveguide was proposed in [3]. Recently [4], a method for which the solution corresponding to the actual index profile of the guide is approximated by means of a combination of analytically solvable solutions was proposed.

In this communication, we study a numerical procedure of linear profile approximation (LPA) in which the dielectric profile or equivalent dielectric profile in each subsection is approximated by linear profile. To facilitate the numerical calculation using this method, the polynomial approximation for the Bessel function of order ± 1/3 and ± 2/3 is constructed by using modified Chebyshev approximation. The method is applied to a few simple problems having a planar structure, and the results are compared with those obtained by other methods. Though the application of the present method is limited to planar structures, computing time can be reduced considerably compared to conventional staircase stratification method.

Manuscript received October 4, 1985; revised November 16, 1985.

The authors are with the Faculty of Engineering, Shizuoka University, Hamamatsu 432, Japan.

IEEE Log Number 8407356.

II. Linear Profile Approximation

Consider a layered medium whose permittivity varies along the z-coordinate in the region $0 < z < z_n$ and is otherwise constant, as shown in Fig. 1. The problem is to determine reflected and transmitted wave when a plane wave is incident from the bottom side. For simplicity the incident wave is assumed to have no variation along the y-coordinate; hence, the problem is two-dimensional. In this case there exist two independent plane wave solutions, which are specified from E_y (transverse electric (TE) wave) and H_y (transverse magnetic (TM) wave), respectively. E_y and H_y are obtained from the solutions of second-order differential equation

$$\frac{d^2F}{dz^2} + k_0^2 \epsilon_{eff}(z) F = 0 \tag{1}$$

where

(a) TE wave; $F = E_y$, $\epsilon_{eff} = \epsilon(z) - \sin^2 \theta_i$

(b) TM wave; $F = \sqrt{\epsilon(z)}\, H_y$ (2)

$$\epsilon_{eff} = \epsilon(z) - \sin^2 \theta_i + k_0^{-2} \left\{ \frac{1}{2} \frac{\epsilon''(z)}{\epsilon(z)} - \frac{4}{3} \left(\frac{\epsilon'(z)}{\epsilon(z)} \right)^2 \right\} \tag{3}$$

where $k_0 = \omega\sqrt{\epsilon_0 \mu_0}$ is the wavenumber in free space. In a subsection $z_l < z < z_{l+1}$, $\epsilon_{eff}(z)$ is approximated by the linear profile

$$\epsilon_{eff}^L(z) = a_l z + b_l \tag{4}$$

where a_l and b_l are coefficients. Firstly, $\epsilon_{eff}(z)$ is approximated by a parabolic curve $\epsilon_p(z)$ passing through three points $\epsilon_l = \epsilon_{eff}(z_l)$, $\epsilon_m = \epsilon_{eff}([z_l + z_{l+1}]/2)$ and ϵ_{l+1}. The coefficient a_l is assumed to be $a_l = (\epsilon_{l+1} - \epsilon_l)/(z_{l+1} - z_l)$ and b_l is determined such that the integrated values of the integrals with integrands $\epsilon_p(z)$ and $\epsilon_{eff}^L(z)$ in the subsection (z_l, z_{l+1}) become equal. Then $\epsilon_{eff}(z)$ is given by

$$\epsilon_{eff}(z) = \frac{\epsilon_{l+1} - \epsilon_l}{z_{l+1} - z_l}(z - z_l) + \frac{2}{3}\epsilon_m + \frac{1}{6}(\epsilon_l + \epsilon_{l+1}). \tag{5}$$

For TE wave, if $\epsilon(z)$ is parabolic profile, $\epsilon_{eff}(z)$ also becomes parabolic. A numerical computation was conducted to verify that such choice a_l and b_l, as in (5), was effective.

Substituting (4) into (1), F can be expressed in terms of Bessel functions of order ± 1/3. Following the same procedure as in staircase approximation [2], the relation between the tangential components of electromagnetic fields at $z = z_l$, (E_l, H_l) and at $z = z_{l+1}$, (E_{l+1}, H_{l+1}), are expressed as

$$\begin{bmatrix} E_{l+1} \\ H_{l+1} \end{bmatrix} = M_l \begin{bmatrix} A_l & jB_l \\ jC_l & D_l \end{bmatrix} \begin{bmatrix} E_l \\ H_l \end{bmatrix} \tag{6}$$

where $A_l \sim D_l$ and M_l are given as follows.

0018-926X/86/0400-0607$01.00

APPENDIX 3

National Technical Systems

Test Report No. 20749-86D

No. of Pages 12

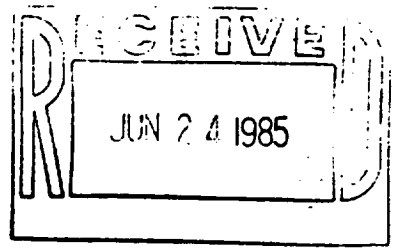

REPORT OF TEST

FOR

RANDOM VIBRATION TESTING
FOUR MILLIMETER WAVE COMPONENTS

MILLITECH CORPORATION
SOUTH DEERFIELD RESEARCH PARK
P.O. BOX 109
SOUTH DEERFIELD, MA 01373

Purchase Order No. 3683

Prepared by: Irene Dickinson Date 6/18/85
Irene Dickinson, Technical Writer
NTS/Acton
533 Main Street, Acton, MA 01720

Reviewed & Approved by: Marcel E. Casaubon Date 6/14/85
Marcel E. Casaubon, Project Engineer
NTS/Acton

ID/po:303

National Technical Systems

ADMINISTRATIVE DATA

1.0 PURPOSE OF TEST: To subject the test items to random vibration testing

2.0 MANUFACTURER: Millitech Corporation

3.0 MANUFACTURER'S TYPE OR MODEL NO.: Four millimeter wave components:
One (1) P/N MUW-10F S/N 39;
One (1) P/N P1;
One (1) MU2W20 S/N 5;
One (1) Tripler

4.0 DRAWING, SPECIFICATION OR EXHIBIT: Customer specification

5.0 QUANTITY OF ITEMS TESTED: One each of the above

6.0 SECURITY CLASSIFICATION OF ITEMS: Unclassified

7.0 DATE TEST COMPLETED: 11 June 1985

8.0 TEST CONDUCTED BY: C. Forbes

9.0 DISPOSITION OF SPECIMENS: Returned to Millitech Corporation

10.0 ABSTRACT: The test items successfully completed testing. For specified data, refer to results herein.

National Technical Systems

1.0 RANDOM VIBRATION TESTING

1.1 Requirements

The test items shall be subjected to random vibration testing in accordance with Millitech Corporation Purchase Order No. 3683.

1.2 Procedures

The test items were mounted on a six-inch fixture plate, provided by Millitech, that was secured to the moveable table of the Ling A300 vibration system.

The test items were vibrated in each of three mutually perpendicular axes at the following levels:

20 Hz - 50 Hz @ 9 dB/octave
50 Hz - 300 Hz @ .15 g^2/Hz
300 Hz - 2 KHz @ -3 dB/octave
3 minutes per axis

Visicorder data was retained by Millitech representative, Mr. David Fein.

National Technical Systems

1.0 RANDOM VIBRATION TESTING (continued)

1.2 Procedures (continued)

Test 1

Z axis (vertical)
Random
3 minutes
Operating

Test 2

X axis
Random
3 minutes
Operating

Test 3

Y axis
Random
3 minutes
Operating

1.3 Results

The test items successfully completed random vibration testing. There was no evidence of physical damage or deterioration to the test items as a result of testing.

National Technical Systems

2.0 TEST EQUIPMENT LIST

TEST EQUIPMENT LIST

Test Report # 20749-86D
Page 2-2

NAME	MFR.	MODEL	SER.NO.	RANGE	ACCURACY	INV.#	CAL FREQ.
Accelerometer	PCB	302A	1821	1 Hz to 5 KHz	±5%	AC437	6 months
Amplifier Exciter	Ling	MPA-16 A300	167 59	5 Hz to 5 KHz 7500 lbs force 1" P/P disp.	±2%	PE314	6 months
Digital Controller	Time Data	TDV-20		70 dB voltage DC to 6 KHz	±1 dB	PE392	1 year
Power Supply	PCB	483A04	872	4 Channel Gain: X1	±2%	PE401	6 months
Visicorder	Honey- well	1858T- 79HG	3840- ME79	18 Channel Main Frame .1 in/sec to 160 in/sec	N/A	RE352	6 months

National Technical Systems

3.0 TEST PLOTS

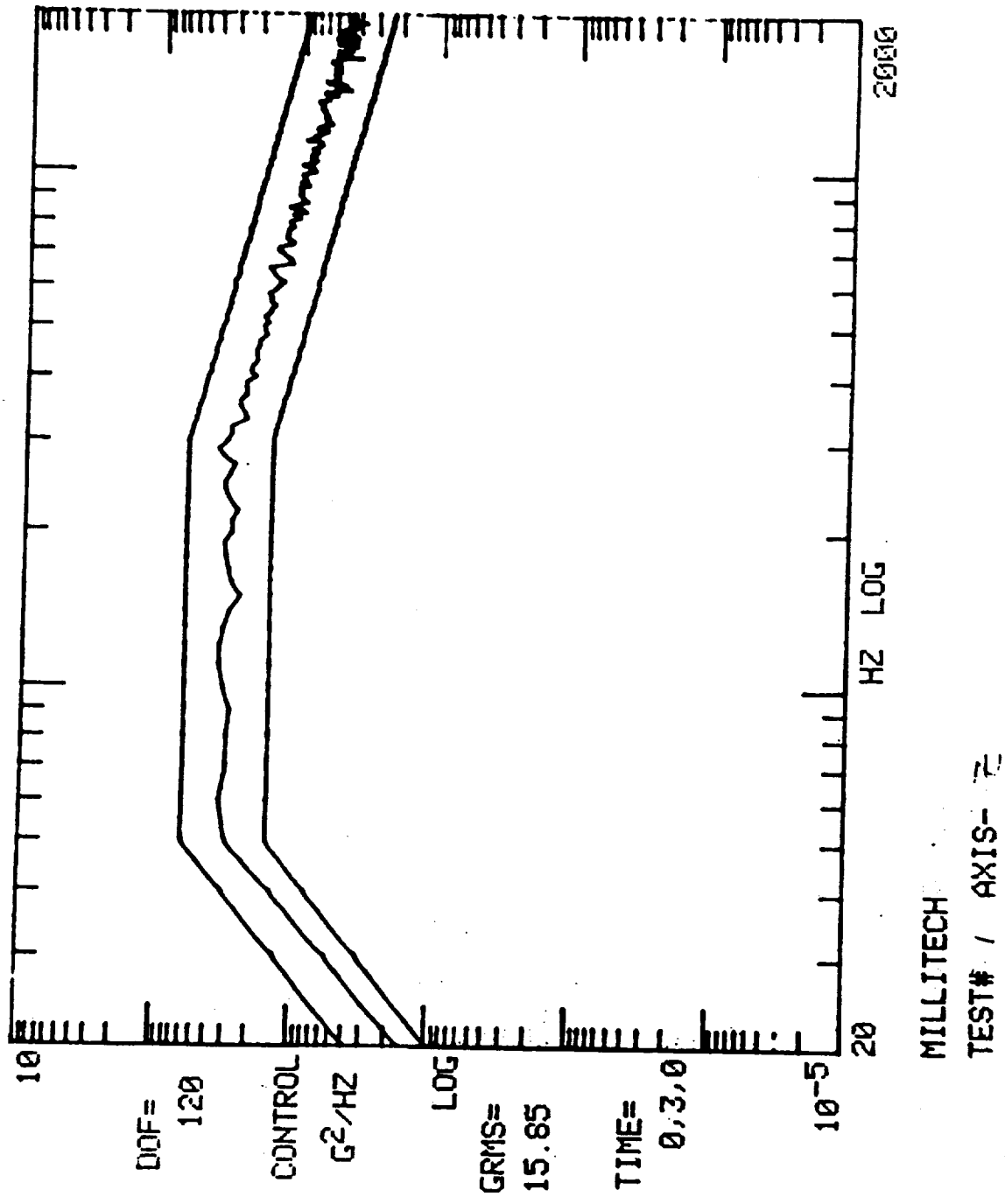
10
20
2000
10⁻⁵
HZ LOG
MILLITECH
TEST# / AXIS- Z
DOF=
120
CONTROL
G²/HZ
LOG
GRMS=
15.85
TIME=
0,3,0

3-2

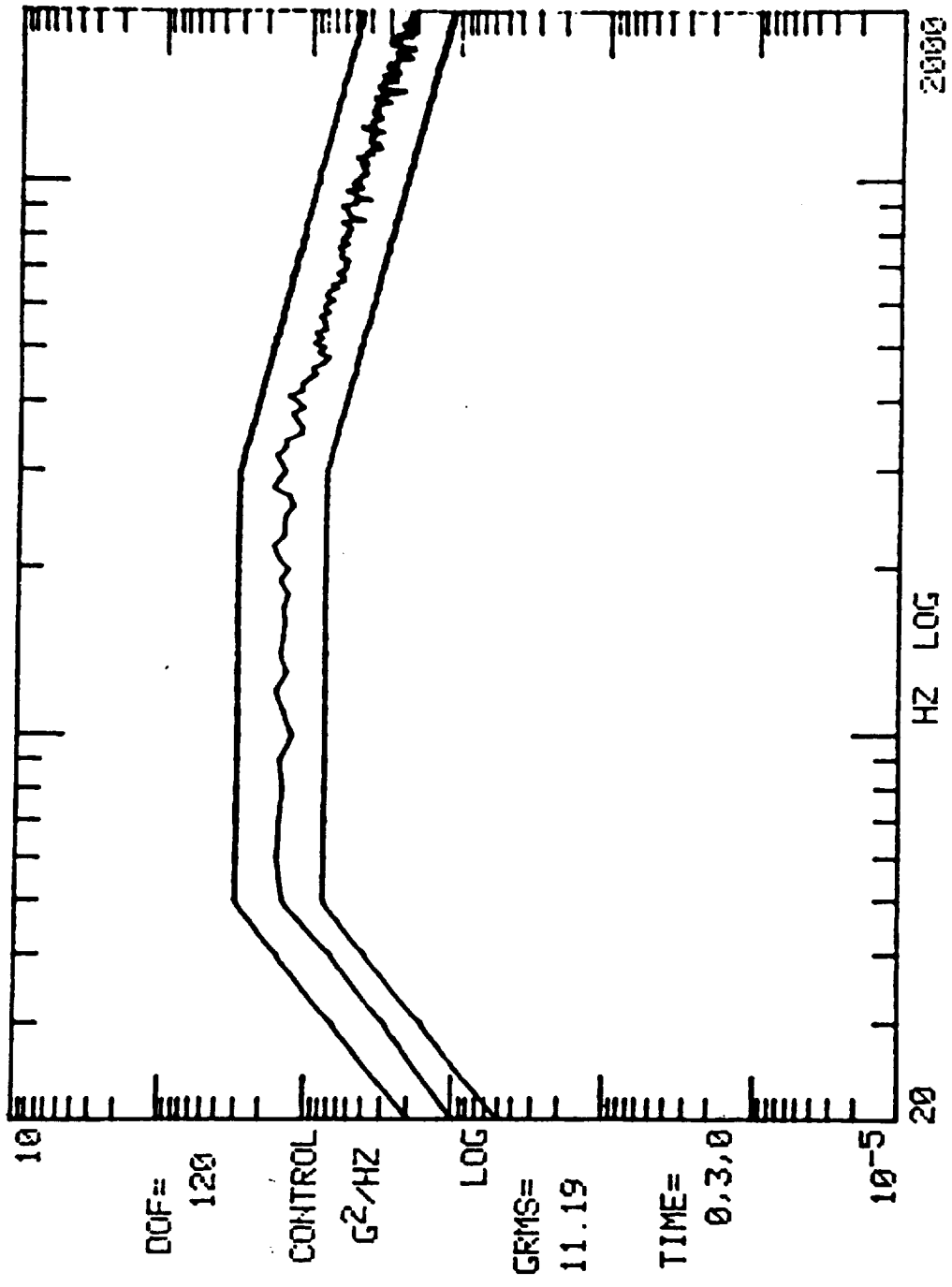
MILLITECH #20749 6-11-85
TEST# 2 AXIS- X
HZ LOG
20
2000
10
10⁻⁵
DOF=
120
CONTROL
G²/HZ
LOG
GRMS=
11.19
TIME=
0,3,0

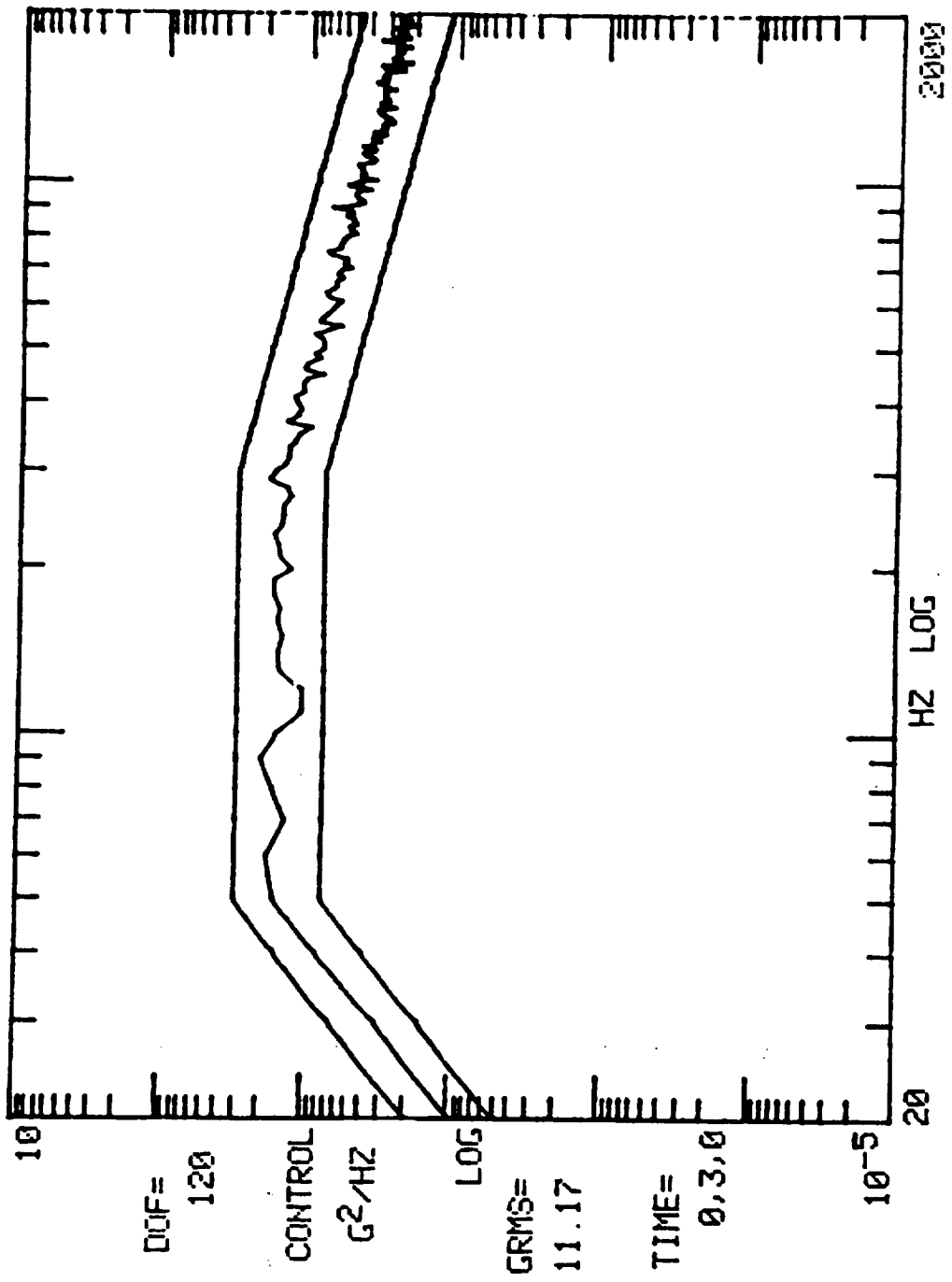
MILLITECH #20749 6-11-85
TEST# 3 AXIS- Y
HZ LOG
10
20
2000
10^{-5}
DOF= 120
CONTROL
G^2/HZ
LOG
GRMS= 11.17
TIME= 0,3,0

3-4

National Technical Systems

4.0 PHOTOGRAPHS

National Technical Systems

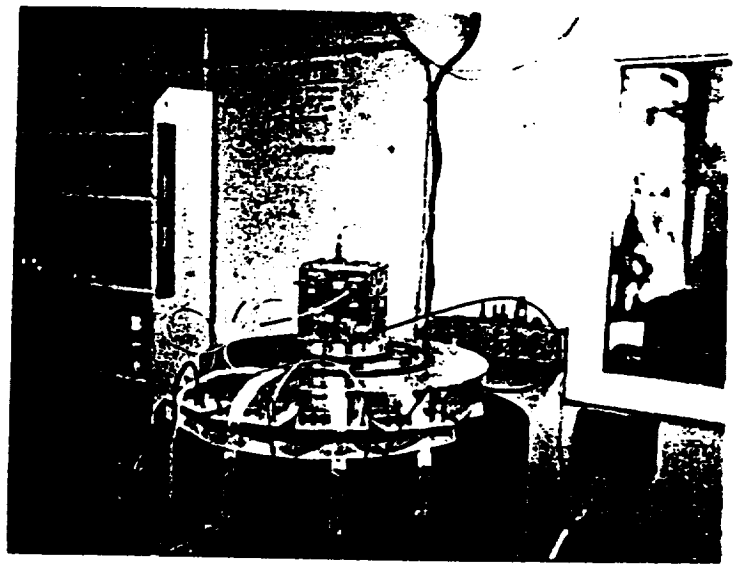

TEST SETUP

X AXIS

Report No. 20749-86D

Page No. 4-2

National Technical Systems

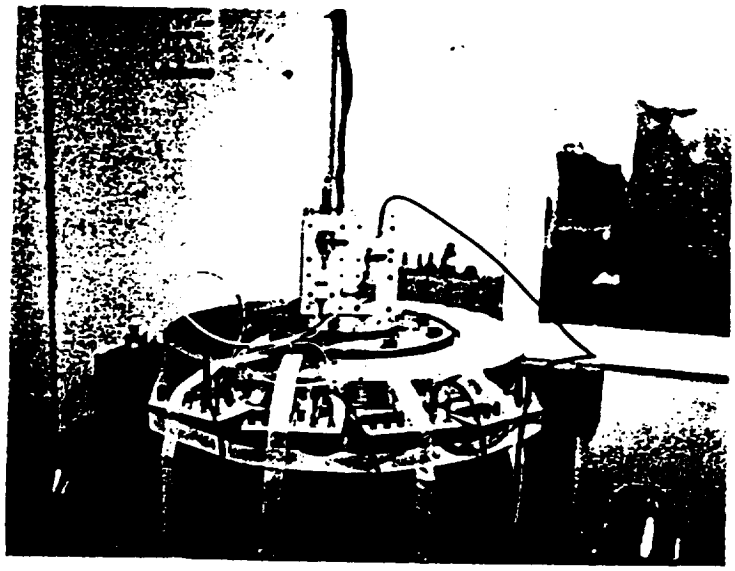

TEST SETUP

Y AXIS

Report No. 20749-86D

Page No. 4-3

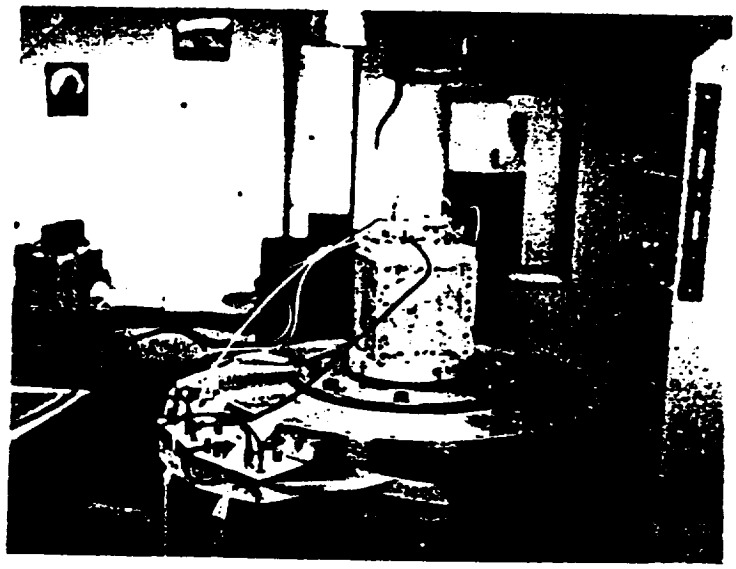

TEST SETUP

Z AXIS

NOTES:

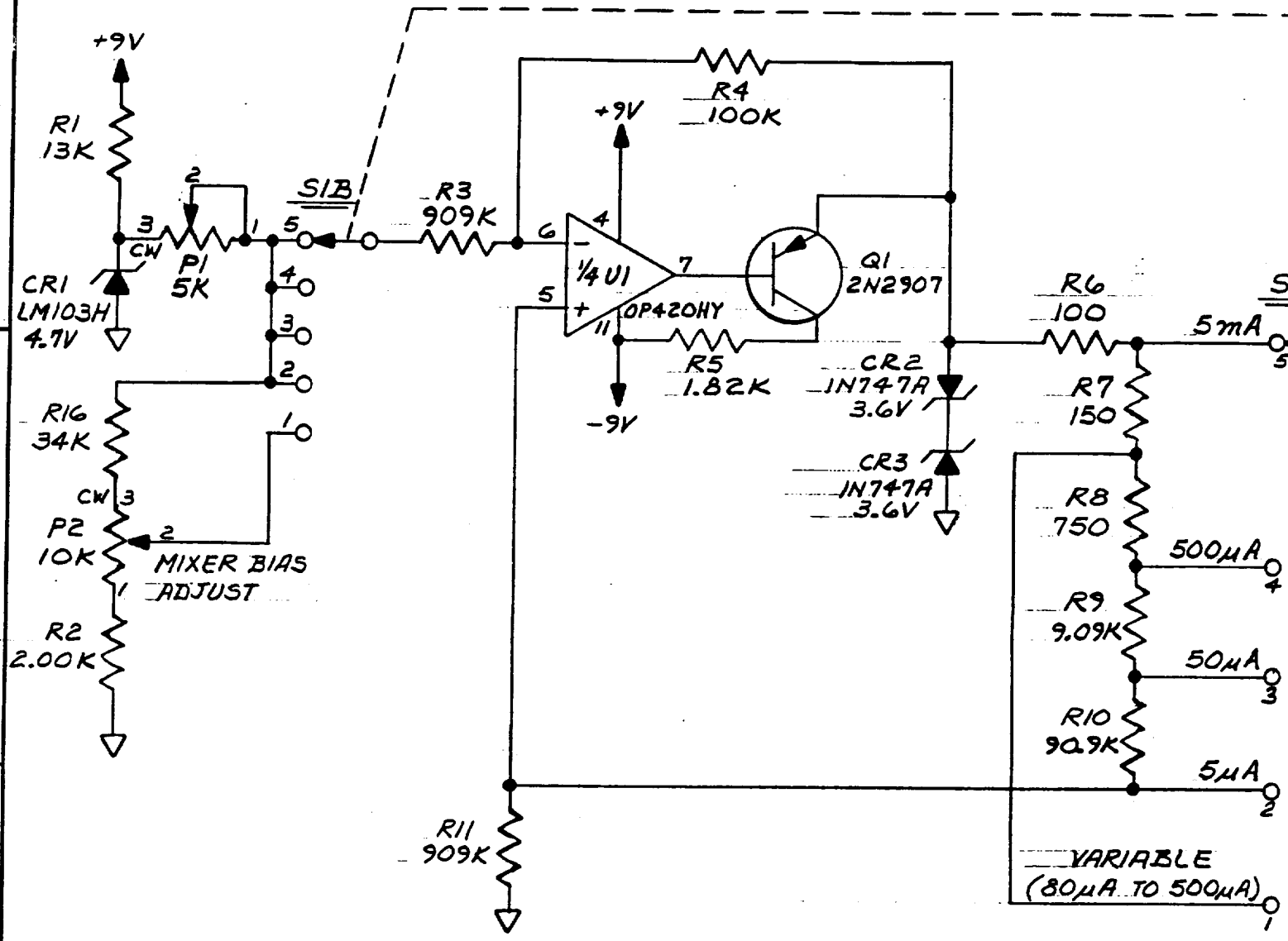

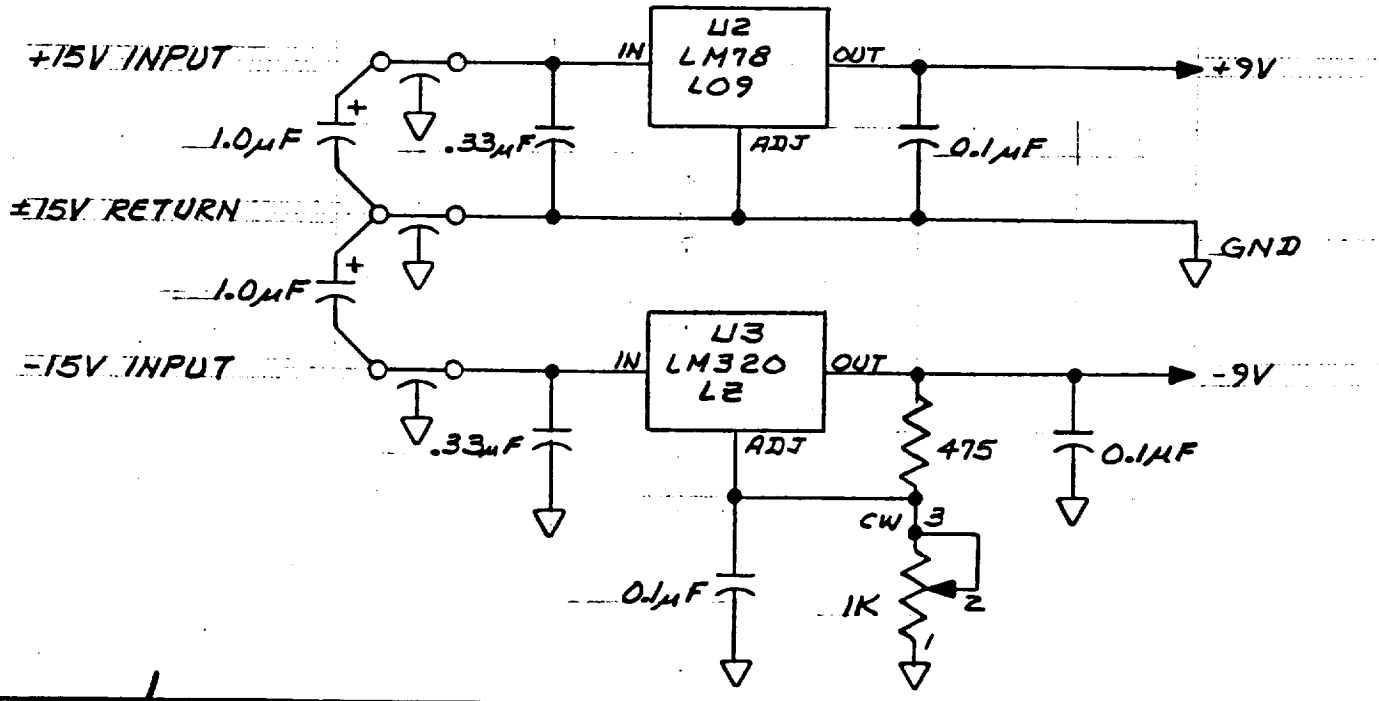

BRUNING 40-107 2 6/125

OLDOUT FRAME

4

3

REVISION				
ZONE	LETTER	DESCRIPTION	DATE	APPROVED

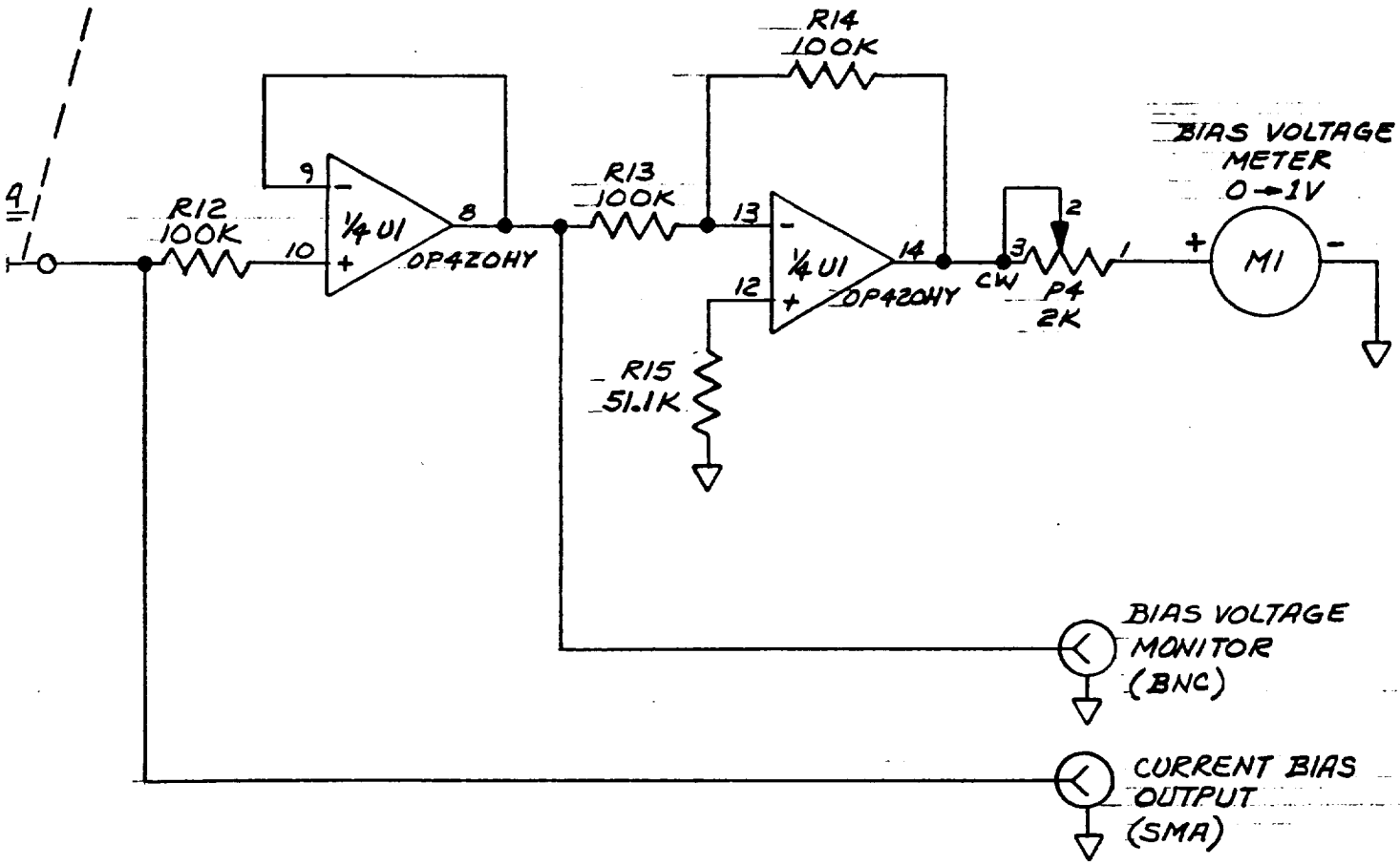

NOTE:

ALL RESISTOR VALUES ARE IN OHMS, 1/4 W, METAL FILM, ±1%

UNLESS OTHERWISE SPECIFIED ALL DIMENSIONS ARE IN INCHES AND TOLERANCES ARE:

.XX = ± .01
.XXX = ± .005
.XXXX = ± .0005

FRACTIONS = ± 1/64
ANGLES = ± 0°30'
SURFACE FINISH = 63 RMS
BREAK ALL SHARP EDGES .015 MAX

MATERIAL & CONDITION

FINISH REQ'D

millitech®

Millimeter and Submillimeter Components, Instruments and Subsystems

APPENDIX 4

DWG. BY	G. WINSLOW	7/8/86
CHK'D BY	J LaBARGE	7/29/86
DRAFT/DOC.		
DESIGN		
PROJ. MAN.		
E. ENGR.		
M. ENGR.		
MANUFACT.		
Q. CONTROL		

TITLE: MIXER BIAS SUPPLY SCHEM.
A125 RADIOMETER

PART NO. —

SERIES IDENT. B | DWG. NO. 800122 | REV. —

SCALE — | PHOTO REDUCT. — | SHT. 1 OF 1

APPENDIX 5 - OPERATING INSTRUCTIONS FOR SNM-02

1.0 METER OPERATION INSTRUCTIONS

The Millitech signal-to-noise ratio meter requires that a suitable chopper with TTL output be connected to the front panel BNC jack, and set such that the chopper blade indicates the correct input to the receiver or device under test. A rear panel 5 Volt DC BNC jack is provided to power the chopper's optical switch.

The phase of the TTL output is unimportant as long as it indicates the correct position. For example, when the blade fully interrupts the receiver beam, the TTL output should be at the halfway point.

Now, switching the mode switch to the total power position and hand rotating the chopper wheel, the meter should indicate some two different levels as the chopper passes through the receiver beam. In addition, the LED above the phase switch should change as the chopper is rotated.

Turning on the chopper and switching the mode switch to SWITCHED should yield a positive indication on the front panel meter. If the meter is pegged in the negative direction, simply reverse the position of the PHASE switch.

Switching to the SWITCHED/TOTAL position, a positive 3/4 full scale meter reading should be obtained. If the meter reading is too low or too high, adjust the RANGE either upwards or downwards respectively until the desired reading is obtained. The Y factor can now be computed via the above formula or maximized by tuning the receiver parameters and peaking the meter.

1.1 METER CALIBRATION

Meter calibration is performed with the detector normally used, a sensitive DC voltmeter and the chopper.

Input Offset Adjustment Trim: While the meter is on and connected to the detector, short the input to the detector and measure the voltage at U1 pin 9. Adjust R1 until the meter reads zero volts.

Range Input and Output Offset Adjustment Trim: While the meter is on and connected to the shorted detector, turn on the chopper. Measuring the voltage at U3 Pin 9, and setting RANGE switch to 40, adjust R2 (input offset) for zero Volts. Next set the RANGE switch to 1 and adjust R3 (output offset) for zero Volts. Repeat these adjustments alternately until changing the RANGE switch produces little or no output change.

2.0 LOOP ADJUSTMENT AND TROUBLESHOOTING

Loop adjustment is fairly straightforward. The lock box contains four adjustments, two of which it should not be necessary to change unless the Gunn oscillator is replaced or retuned mechanically, and a third that requires adjustment only for lock detection malfunctions. The fourth is the loop DC offset adjustment which requires only a meter or preferably an oscilloscope to set providing the loop is locked properly.

Instruments required for adjustment or repair:

1. 0.01 to 1 GHz spectrum analyzer
2. 100 MHz bandwith oscilloscope
3. 100 MHz frequency counter

Some familiarity with phase-lock loop operation is extremely helpful if not required before attempting to replace or repair major components of the loop.

Offset Adjustment: The loop DC offset adjustment can be made by first removing the lock box cover and locating R18 on the phase lock filter board. This is a 100 KΩ potentiometer located near U3. With the frequency of the loop tuned for 92.6 GHz (center), there should be about +3.5 Volts DC here. This point is adjusted so that a ninety degree phase offset occurs at the lock indicator or quadrature phase detector. This state can be discerned by slowly rotating the pot in either direction until the lock indicator is extinguished. Now turning the pot in the opposite direction, count how many turns in the opposite direction it takes before the lamp extinguishes again. Divide the number of turns by two and return the pot that number of turns back in the first direction. Proper loop operation should be verified by attaching a spectrum analyser to the IF minitor port and comparing the spectrum found there to that in Figure 1, and Figure 2.

VCO Turn-on Threshold: Since the VCO has a minimum turn-on voltage and for proper loop operation the IF must always be within certain frequency limits, a threshold adjustment or minimum VCO output voltage adjustment is provided. This consists of a comparator whose input is the Gunn voltage and whose output drives the offset of the loop filter amplifier. If the Gunn voltage drops below a preset level, the comparator drives the loop offset such that the loop is steered back towards lock. This offset adjustment is provided for by R26, a 100 KΩ potentiometer, located on the phase lock filter board.

First the lowest loop voltage must be measured. This is done by setting the loop frequency to its lowest point. Now measure and record the voltage at pin 6 of U4. After first removing the lock box cover, locate R26. This is a potentiometer located near U4. While measuring the voltage at pin 5 of U4, set the voltage to just below the previously measured voltage at pin 6 of U4 by about 0.5 Volts. With the original VCO installed, this voltage is approximately 6.6 VDC. Proper loop operation should be verified by attaching a spectrum analyzer to the IF monitor port and comparing the spectrum found there to that in Figure 1.

Caution: Over-reduction of this adjustment may cause the loop to oscillate.

Sideband Kick-in Threshold: If the loop detects that it is on the far side of the opposite sideband (>20 MHz beyond opposite sideband), another circuit provides a slight offset adjustment through U1 that steers the loop back towards the proper sideband. This adjustment is made through R19, a 100 KΩ potentiometer located on the phase lock filter board.

After first removing the lock box cover, locate R19 near U4. Set the voltage at pin 12 of U1 by adjusting R19 to approximately +7.7 Volts DC. Test for proper operation by switching the reference input from the synthesizer on and off. The loop should lock up and the lock indicator light should be on. If not, check the IF monitor port with a spectrum analyzer to verify that the 20 MHz IF signal is present. A slight adjustment of R19 while examining the loop IF with the spectrum analyzer should bring the loop back into lock. Proper loop operation should be verified by attaching a spectrum analyzer to the IF monitor port and comparing the spectrum found there to that in Figure 1.

Caution: Over-reduction of this adjustment will cause the loop to oscillate.

Lock Indicator Threshold Adjust: This adjustment is preset and should not need further adjustment. If needed, it is performed by locating R15 on the Phase Detector/Divider board, Millitech drawing number #800086. This board is mounted in the lock box on the opposite side of the phase lock filter board. This adjustment consists of setting the voltage U7 pin 2 equal to +3.5 to +3.6 VDC. After this adjustment the lock indicator should respond correctly to the state of the loop. Proper loop operation should be verified by attaching a spectrum analyzer to the IF monitor port and comparing the spectrum found there to that in Figure 1. This adjustment is preset and should not need further adjustment.

FIGURE 1

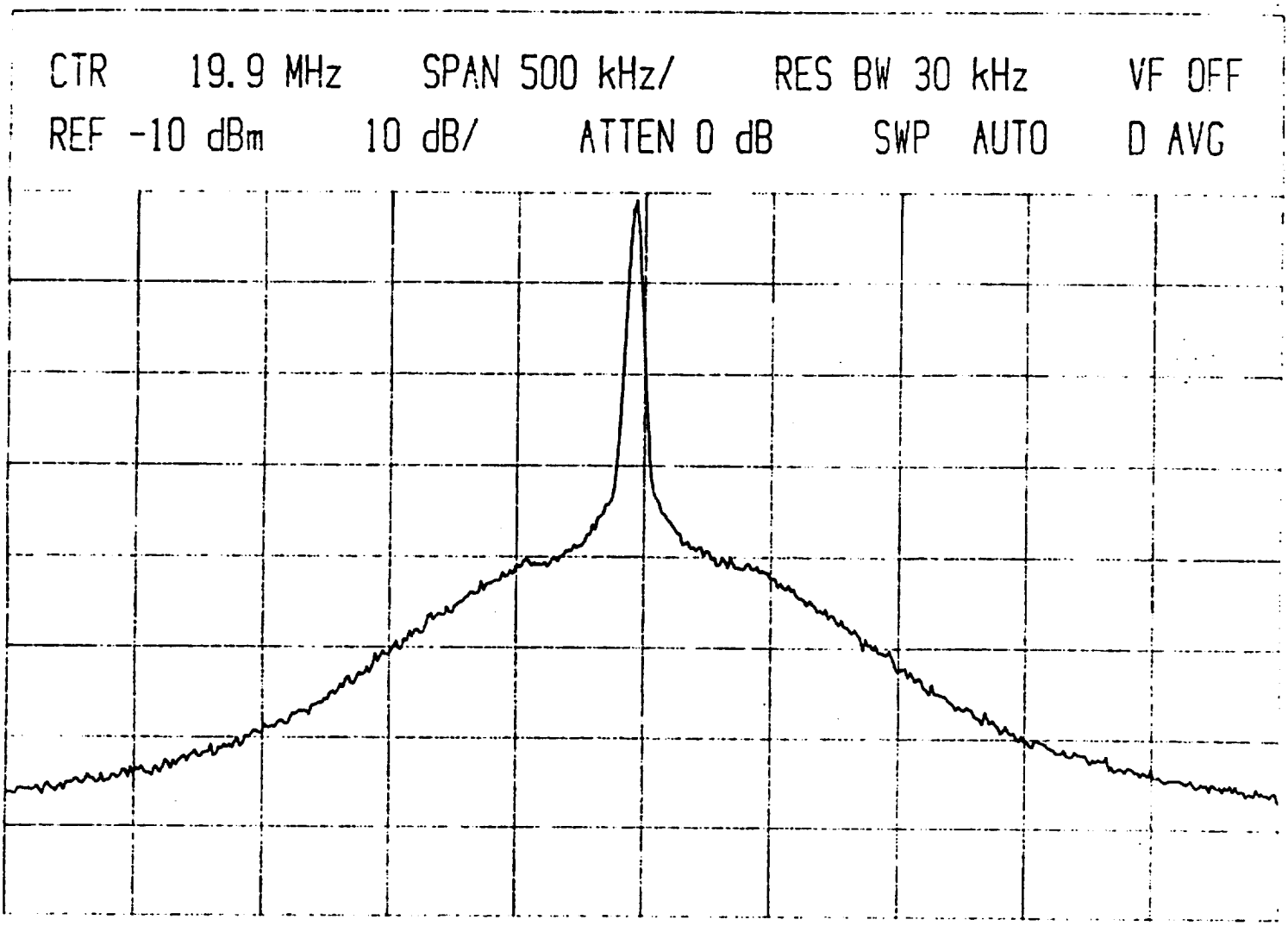

FIGURE 2